Master Thesis

Phonon lasing with intrinsic Kerr-nonlinearity & Numerical implementation of homodyne detection

Manuel Grimm
June 1, 2016

Department of Physics, University of Basel
Klingelbergstrasse 82, 4056 Basel, Switzerland

Supervisors: Dr. N. Lörch
Prof. Dr. C. Bruder

Contents

Part I
Phonon lasing with intrinsic Kerr-nonlinearity

1 Introduction to optomechanics

The field of optomechanics studies the interaction between optical and mechanical degrees of freedom. It has been known for a long time that light can exert forces on objects via radiation pressure. Johannes Kepler postulated this in the 17th century after noticing that the dust tails of comets always point away from the sun. Experimentally the radiation pressure was verified in the beginning of the 20th century [1].

In quantum mechanics the radiation pressure exerted on a reflective surface is explained by photons transferring their momentum. For single photons the effect on macroscopic objects is small. In the nano- or micrometer range these interactions become more important. But even for large objects the radiation pressure might play an important role for precision measurements, especially if the laser power is large. This is for example the case in the LIGO project, which was recently able to detect gravitational waves [2]. Other experimental realizations of radiation pressure coupling include cold atom clouds, mechanical cantilevers, vibrating microtoroids and membranes. Some of these setups are illustrated in Fig. 1.0.1. The dimensions of these systems vary over a wide range with masses from 10^{-20} kg to several kg and span several orders of magnitude in size [3]. While we will focus on the coupling via radiation pressure, there are other possible interactions worth exploring such as optical gradient and dipole forces [4].

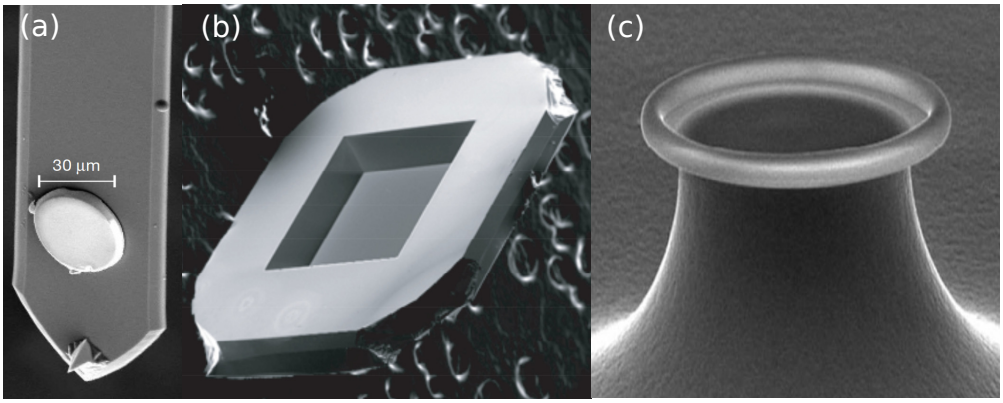

Figure 1.0.1: Experimental setups in optomechanics: (a) Tip of a cantilever with attached mirror [5], (b) SiN_3 membrane on a silicon chip [6], (c) Toroid microcavity on a chip [7].

In Fig. 1.0.2 we schematically illustrate a typical experimental setup in optomechanics. Since the momentum transfer due to a single photon is small, a cavity is used. The cavity resonantly amplifies the light intensity and therefore the effective coupling strength. The end-mirror is freely movable which might be achieved by mounting it on a cantilever. The radiation pressure moves the cantilever. This changes the cavity length and thereby its resonance frequency. In turn the intensity of the light is changed and hence the radiation pressure, which creates a feedback loop known as dynamical back-action. In this setup the cavity resonance frequency depends on the oscillator position. This kind of coupling is called dispersive. We note that there are other possible couplings which we do not consider in this master thesis such as dissipative coupling,

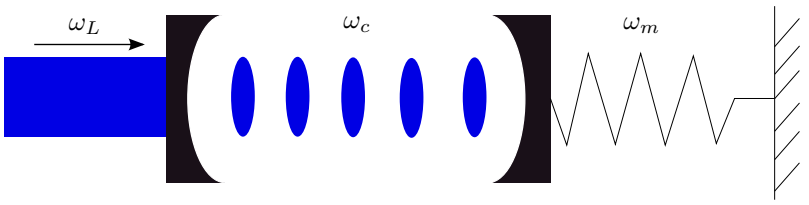

Figure 1.0.2: Schematic illustration of a typical experimental setup in optomechanics. ω_L is the driving frequency, ω_c is the cavity frequency and ω_m is the mechanical frequency.

where the position of the oscillator modulates the cavity linewidth [8].

A wealth of interesting effects can be seen in optomechanical experiments even in the most simple setup. One consequence of the dynamical back-action is the optical spring effect. The force gradient of the radiation pressure changes the mechanical frequency. If the driving laser is red-detuned, i.e. if its frequency is lower than the cavity resonance frequency, the mechanical oscillator will be spring softened. On the other hand we find spring hardening for blue-detuned lasers whose frequencies are higher than the cavity frequency.

Another interesting effect is the optical damping. A red-detuned laser will induce further damping to the oscillator and cool it. With additional cryogenic cooling it is even possible to reach the quantum ground state of the mechanical oscillator [9, 10]. By measuring the phase shift of the output light one can detect the position of the oscillator. This allows active feedback control [11].

On the other hand driving on the blue sideband creates negative damping. For large laser powers this effect can dominate the intrinsic mechanical damping. Any amplitude oscillation will grow exponentially due to the overall negative damping. At large amplitudes nonlinear effects kick in and the oscillator exhibits periodic self-oscillations. This effect is similar to a laser above the lasing threshold. The simple picture of a laser consists of a medium of two-level systems inside a resonator. Population inversion of the medium is achieved via pumping. Incoming light induces spontaneous absorption and emission. Since the two-level systems are population inverted, the emission is larger than the absorption. This leads to amplification of the light inside the cavity. The cavity decay rate as well as the rate of spontaneous emission and absorption determine the amplitude of the light. In optomechanics the roles of pump, gain medium and resonator are assumed by the driving laser, the cavity and the mechanical oscillator, respectively [12].

Optomechanical setups can be used to create non-classical states of both light and mechanics [13, 14]. These are crucial for quantum information processing [15] and testing the fundamentals of quantum mechanics such as the collapse of states [16] and Bell's theorem [17]. On both sidebands mechanical squeezed states have been realized [18]. For strong mechanical anharmonicity, stabilization of mechanical Fock states on the blue sideband has been proposed [19] but not yet realized.

For weak anharmonicity, driving on the blue sideband leads to laser-like mechanical states. In the first part of this master thesis we derive a semi-classical description of these self-oscillations for large mechanical amplitudes, where the intrinsic anharmonicity is the system's dominant nonlinearity. We derive conditions for which a Fano factor smaller than one is possible. This corresponds to sub-Poissonian phonon statistics which is a non-classical feature [20].

This part of the master thesis is organized as follows: We briefly review the derivation of the linearized optomechanical Hamiltonian and introduce the quantum phase space distributions in

Section 2. In Section 3 we couple a bosonic mechanical mode with intrinsic Kerr-nonlinearity to a driven cavity mode. We study the steady-state of this system, in particular the amplitude distribution of the mechanical oscillator. Furthermore we show that non-classical mechanical states with a Fano factor smaller than one can be achieved in the zero temperature limit. In Section 4 the Kerr Hamiltonian is derived as a rotating wave approximation of the Duffing Hamiltonian. In Section 5 we consider two systems. First we couple the oscillator to two independent cavities driven by a red- and a blue-detuned laser, respectively. Then we study the case of one cavity driven by two lasers with different frequencies. In Section 6 we conclude with a summary of the results and an outlook.

2 Theory of optomechanics

In this section we derive the linearized optomechanical Hamiltonian following the review by Aspelmayer, Kippenberg and Marquardt [3]. Furthermore we introduce quantum phase space distributions following "Introductory Quantum Optics" by C. Gerry and P. Knight [21] as well as "Quantum Noise" by C. Gardiner and P. Zoller [22].

2.1 Linearized optomechanics

We want to model the optomechanical system of a driven cavity coupled to a mechanical resonator. We consider the simplest implementation which consists of a movable end-mirror that modulates the cavity frequency. A schematic setup is illustrated in Fig. 1.0.2. In our description we only use the optical mode closest to the driving laser frequency. We couple this cavity mode to a bosonic mechanical mode. We model both the mechanical and the cavity mode as harmonic oscillators, i.e.

$$H_c' = \omega_c a^\dagger a, \quad H_m = \omega_m b^\dagger b, \tag{2.1.1}$$

where H_c' and H_m denote the cavity and mechanical Hamiltonian. The operators $a^\dagger, a$ and $b^\dagger, b$ represent the creation and annihilation operators of the optical cavity and the mechanical oscillator, respectively. Note that we write H_c' since we have not yet introduced the driving. We will later change into a rotating frame which will transform our Hamiltonian.

Since we have a movable end-mirror, the cavity frequency is a function of the displacement x

$$\omega_c(x) \approx \omega_c + x\frac{\partial \omega_c(x)}{\partial x} + ... \tag{2.1.2}$$

Higher order terms can be neglected for the systems of interest here.

The linear term in x gives rise to the interaction between cavity and mechanical oscillator. We use the relation $x = x_0(b + b^\dagger)$ where x_0 is the zero point fluctuation of the oscillator. With the definition of the optomechanical single-photon coupling strength $g_0 = -\frac{\partial \omega_c(x)}{\partial x} x_0$ we find the interaction Hamiltonian

$$H_{\text{int}} = -g_0 a^\dagger a(b + b^\dagger). \tag{2.1.3}$$

The cavity is driven by a laser with frequency ω_L. The driving Hamiltonian can be written as

$$H'_{\text{drive}} = E\left(ae^{i\omega_L t} + a^\dagger e^{-i\omega_L t}\right), \tag{2.1.4}$$

where E is the driving amplitude. We can get rid of the time dependency of the Hamiltonian by changing into a rotating frame, i.e. by applying the unitary transformation $U = e^{i\omega_L a^\dagger a t}$ to our (total) Hamiltonian which will transform according to

$$H_{\text{new}} = UH_{\text{old}}U^\dagger + i\frac{\partial U}{\partial t}U^\dagger. \tag{2.1.5}$$

We can write the effects of this transformation as H_c' changing to H_c and H'_{drive} to H_{drive} with

$$H_c = -\Delta a^\dagger a, \quad H_{\text{drive}} = \Omega\left(a + a^\dagger\right). \tag{2.1.6}$$

Here we defined the cavity detuning $\Delta = \omega_L - \omega_c$. Positive detuning Δ corresponds to blue-detuning and negative Δ to red-detuning.

Note that the interaction Hamiltonian in Eq. (2.1.3) is nonlinear which means it contains products of more than two creation and annihilation operators. Since linear systems are easier to solve analytically, we wish to make an approximation by linearizing this Hamiltonian. We split a into an average and fluctuating term $a = \langle a \rangle + \delta a$. Then we insert this into our Hamiltonian

and neglect terms $\sim \delta a^\dagger \delta a$, assuming that the expectation value of the fluctuations δa is much smaller than the average amplitude $\langle a \rangle$. This is satisfied for large driving amplitude Ω. The arising term $-g_0 |\langle a \rangle|^2 (b + b^\dagger)$ in the interaction Hamiltonian is the average radiation pressure force. We can omit this term and the driving Hamiltonian after introducing a small shift δx to the displacement of the oscillator position x. In the Hamiltonian this is done by changing into a displaced frame with $b \to b_c + b$, where the complex-valued number b_c is known as the DC-shift. This also leads to a small shift in the detuning $\Delta \to \bar{\Delta} = \Delta + \frac{g_0}{x_0}\delta x$. Unless declared otherwise we will still write Δ instead of $\bar{\Delta}$ in the rest of this thesis. We want to emphasize again that the driving Hamiltonian gets cancelled out by the introduced displacement δx.

We can assume without loss of generality that $\langle a \rangle = \sqrt{\bar{n}_c}$ is real-valued, where $\bar{n}_c$ is the average photon number in the cavity. Otherwise we could redefine $a \to a e^{i\phi}$ such that $\langle a \rangle$ is a real number. We define the effective optomechanical coupling strength

$$g = g_0 \sqrt{\bar{n}_c}. \tag{2.1.7}$$

Rewriting δa as a, we arrive at the linearized optomechanical Hamiltonian

$$H = H_c + H_m + H_{\mathrm{int-lin}} = -\Delta a^\dagger a + \omega_m b^\dagger b - g(a + a^\dagger)(b + b^\dagger), \tag{2.1.8}$$

where $H_{\mathrm{int-lin}} = -g(a + a^\dagger)(b + b^\dagger)$ is the linearized interaction Hamiltonian. The coupling to the cavity induces damping Γ_{opt} and a frequency shift $\delta\omega$ in the mechanical oscillator. If we include dissipation of the light with photon amplitude decay rate κ they can be derived as [3]

$$\begin{aligned} \delta\omega =& g^2 \left(\frac{\Delta - \omega_m}{(\Delta - \omega_m)^2 + \kappa^2} + \frac{\Delta + \omega_m}{(\Delta + \omega_m)^2 + \kappa^2} \right), \\ \Gamma_{\mathrm{opt}} =& g^2 \kappa \left(\frac{1}{(\Delta + \omega_m)^2 + \kappa^2} - \frac{1}{(\Delta - \omega_m)^2 + \kappa^2} \right). \end{aligned} \tag{2.1.9}$$

For red-detuned lasers ($\Delta < 0$) the optically induced damping is positive and leads to cooling of the oscillator. For blue-detuned lasers ($\Delta > 0$) the damping is negative. If this effect is larger than the intrinsic mechanical damping, mechanical oscillations will grow exponentially until nonlinear effects kick in. These can lead to laser-like self-oscillations which cannot described by the linearized treatment.

2.2 Phase space distributions

We have derived the linearized optomechanical Hamiltonian. We will use it to study an optomechanical system with intrinsic Kerr-nonlinearity in the following section. The evolution of the system is described by its master equation, which is an equation of motion for the density operator. Any physical observable can be found with this density matrix. For our purpose it is more convenient to express the density operator in terms of a phase space distribution which is a (quasi-)probability distribution in the phase space. We review the three commonly used phase space distributions following the textbook of C. Gerry, P. Knight [21] and introduce the (Husimi) Q function, the (Glauber-Sudarshan) P function and the Wigner function. In the end of this section we generalize these distributions using an s-parametrized function.

The Q function describes the density operator in terms of the coherent states $|\alpha\rangle$. These are given by

$$|\alpha\rangle = e^{-\frac{1}{2}|\alpha|^2} \sum_{n=0}^{\infty} \frac{\alpha^n}{\sqrt{n!}} |n\rangle = e^{-\frac{1}{2}|\alpha|^2} \sum_{n=0}^{\infty} \frac{\alpha^n (a^\dagger)^n}{\sqrt{n!}} |0\rangle, \tag{2.2.1}$$

where $|0\rangle$ is the vacuum state and α can be any complex number. $a^\dagger$ is the creation operator of the system. The coherent states are eigenfunctions of the annihilation operator a satisfying

$$a|\alpha\rangle = \alpha |\alpha\rangle, \quad \langle\alpha| a^\dagger = \alpha^* \langle\alpha|. \tag{2.2.2}$$

The Q function is defined in terms of diagonal elements of the density operator with respect to the coherent states

$$Q(\alpha) = \frac{1}{\pi} \langle\alpha| \rho |\alpha\rangle = \frac{1}{\pi} \mathrm{Tr} \left[\rho |\alpha\rangle \langle\alpha|\right]. \tag{2.2.3}$$

It is normalized with

$$\int \mathrm{d}^2\alpha \; Q(\alpha) = \mathrm{Tr}\left[\frac{1}{\pi} \int \mathrm{d}^2\alpha \, |\alpha\rangle \langle\alpha| \, \rho\right] = \mathrm{Tr}[\rho] = 1. \tag{2.2.4}$$

The Q function can be used to find the expectation value of a function $g_{(A)}(a, a^\dagger)$ of anti-normally ordered annihilation and creation operators $a, a^\dagger$. The expectation value is calculated by replacing the operators $a, a^\dagger$ with the complex numbers α, α^* and averaging over the distribution $Q(\alpha)$. Using the eigenvalue relation in Eq. (2.2.2) it can be shown that

$$\langle g_{(A)}(a, a^\dagger)\rangle = \int \mathrm{d}^2\alpha Q(\alpha) g_{(A)}(\alpha, \alpha^*) \equiv \langle g_{(A)}(\alpha, \alpha^*)\rangle_Q . \tag{2.2.5}$$

Here and in the following of this thesis $\langle \, \rangle$ denotes the expectation value with respect to the density matrix and $\langle \, \rangle_\sigma$ with respect to the phase space distribution σ.

The Q function is positive for any α as it is defined as the square of a norm. In fact it is bounded by $0 \leq Q(\alpha) \leq \frac{1}{\pi}$. Since the Q function is also normalized and can be used as a weight function to calculate expectation values, we can interpret it as a probability distribution in the phase space spanned by α, α^*.

Another commonly used phase space distribution is the P function. We define it by the relation

$$\rho = \int \mathrm{d}^2\alpha P(\alpha) \, |\alpha\rangle \langle\alpha| . \tag{2.2.6}$$

The P function is normalized

$$\int \mathrm{d}^2\alpha P(\alpha) = \mathrm{Tr}\left[\int \mathrm{d}^2\alpha P(\alpha) \, |\alpha\rangle \langle\alpha|\right] = \mathrm{Tr}[\rho] = 1 \tag{2.2.7}$$

and is explicitly calculated with

$$P(\alpha) = \frac{e^{|\alpha|^2}}{\pi^2} \int \mathrm{d}^2\beta e^{|\beta|^2} \langle -\beta| \, \rho \, |\beta\rangle \, e^{\beta^*\alpha - \beta\alpha^*}. \tag{2.2.8}$$

The P function can be used to find expectation values of a normally ordered function $g_{(N)}(a, a^\dagger)$ of annihilation and creation operators $a, a^\dagger$. Similar to the Q function we find

$$\langle g_{(N)}(a, a^\dagger)\rangle = \int \mathrm{d}^2\alpha P(\alpha) g_{(N)}(\alpha, \alpha^*) \equiv \langle g_{(N)}(\alpha, \alpha^*)\rangle_P . \tag{2.2.9}$$

Note that although the P function is normalized, it is not necessarily strictly positive. Therefore we cannot talk about a probability distribution in the usual sense. Nevertheless it shares enough similarities with one that we call it a quasi-probability distribution.

The third phase space distribution that we will consider is the Wigner function. It is historically defined as

$$W(x, p) = \frac{1}{2\pi} \int \mathrm{d}y \, \langle x + \frac{y}{2}| \, \rho \, |x - \frac{y}{2}\rangle \, e^{-ipy}. \tag{2.2.10}$$

We have introduced the most common phase space distributions independently, but they can be defined in a more general framework via the characteristic functions. A (classical) probability

distribution $p(x)$ can be fully characterized by its characteristic function $C(k) = \langle e^{ikx} \rangle$. The two are related by a Fourier transform

$$C(k) = \int \mathrm{d}x e^{ikx} p(x), \quad p(x) = \frac{1}{2\pi} \int \mathrm{d}k e^{-ikx} C(k). \tag{2.2.11}$$

In analogy we introduce three kinds of quantum-mechanical characteristic functions for $\lambda \in \mathbb{C}$: the normally ordered (C_N), the anti-normally ordered (C_A) and the symmetric (C_W) characteristic functions

$$C_N(\lambda) = \mathrm{Tr}[\rho e^{\lambda a^\dagger} e^{-\lambda^* a}], \quad C_A(\lambda) = \mathrm{Tr}[\rho e^{-\lambda a^\dagger} e^{\lambda^* a}], \quad C_W(\lambda) = \mathrm{Tr}[\rho e^{\lambda a^\dagger - \lambda^* a}]. \tag{2.2.12}$$

Using the Baker-Campbell-Hausdorff formula it can be shown that these characteristic functions are related by

$$C_W(\lambda) = C_N(\lambda) e^{-\frac{1}{2}|\lambda|^2} = C_A e^{\frac{1}{2}|\lambda|^2}. \tag{2.2.13}$$

Similar to classical probability distributions we find our phase space distributions via a Fourier transform, but in this case we have to use the Fourier transform in the complex plane

$$\begin{aligned}
Q(\alpha) &= \frac{1}{\pi^2} \int \mathrm{d}^2\lambda e^{\lambda^*\alpha - \lambda\alpha^*} C_A(\lambda), \quad C_A(\lambda) = \int \mathrm{d}^2\alpha e^{\lambda\alpha^* - \lambda^*\alpha} Q(\alpha), \\
P(\alpha) &= \frac{1}{\pi^2} \int \mathrm{d}^2\lambda e^{\lambda^*\alpha - \lambda\alpha^*} C_N(\lambda), \quad C_N(\lambda) = \int \mathrm{d}^2\alpha e^{\lambda\alpha^* - \lambda^*\alpha} P(\alpha), \\
W(\alpha) &= \frac{1}{\pi^2} \int \mathrm{d}^2\lambda e^{\lambda^*\alpha - \lambda\alpha^*} C_W(\lambda), \quad C_W(\lambda) = \int \mathrm{d}^2\alpha e^{\lambda\alpha^* - \lambda^*\alpha} W(\alpha).
\end{aligned} \tag{2.2.14}$$

This definition of the Wigner function is equivalent to the definition in Eq. (2.2.10). The Wigner function can be used to calculate expectation values of a symmetrically ordered function $g_{(W)}(a, a^\dagger)$ of annihilation and creation operators $a, a^\dagger$, i.e. $g_{(W)}(a, a^\dagger) = g_{(W)}(a^\dagger, a)$. We find

$$\langle g_{(W)}(a, a^\dagger) \rangle = \int \mathrm{d}^2\alpha W(\alpha) g_{(W)}(\alpha, \alpha^*) \equiv \langle g_{(W)}(\alpha, \alpha^*) \rangle_W . \tag{2.2.15}$$

Phase space distributions can not only be used to calculate expectation values but also to differentiate between classical and non-classical quantum states. A negative Wigner function for example implies non-classical states.

The three introduced characteristic functions and phase space distributions can be generalized by the s-parametrized characteristic function $C(\lambda, s)$ and phase space distribution $\sigma(\alpha, s)$ with $s \in [-1, 1]$ [23]

$$C(\lambda, s) = \mathrm{Tr}\left[\rho e^{\lambda a^\dagger - \lambda^* a + s|\lambda|^2/2}\right], \quad \sigma(\alpha, s) = \frac{1}{\pi^2} \int \mathrm{d}^2\lambda e^{\lambda^*\alpha - \lambda\alpha^*} C(\lambda, s). \tag{2.2.16}$$

For $s = -1$ we recover the Q function, for $s = 1$ the P function and for $s = 0$ the Wigner function.

3 One laser

We introduced the linearized optomechanical Hamiltonian and phase space distributions. In this section we add an intrinsic mechanical Kerr-nonlinearity to the optomechanical system. The mechanical part will show self-oscillations which we describe in the large amplitude limit. We derive equations of motion for the cavity and mechanical variables of the phase space distribution. We then adiabatically eliminate the oscillator variable to solve the optical part of the problem. We find effective drift and diffusion terms for the mechanical amplitude. Using this we derive conditions under which the mechanical steady-state shows number squeezing. In our approach we use a method similar to the papers of D. A. Rodrigues and A. D. Armour [24, 25].

3.1 Equations of motion

We consider a simple optomechanical setup with intrinsic Kerr-nonlinearity K. Its Hamiltonian is given by

$$H_K = K(b^\dagger b)^2. \tag{3.1.1}$$

Figure 3.1.1 schematically shows our system. In total it is described by the Hamiltonian

$$H = H_c + H_m + H_{\text{int}-\text{lin}} + H_K = -\Delta a^\dagger a + \omega_m b^\dagger b - g(a + a^\dagger)(b + b^\dagger) + K(b^\dagger b)^2. \tag{3.1.2}$$

Note that the shift δx that we mentioned in Section 2.1 will have a negligible effect on the Kerr Hamiltonian H_K for large amplitudes of b, which is the limit we are interested in. We assume H_K to be unchanged.

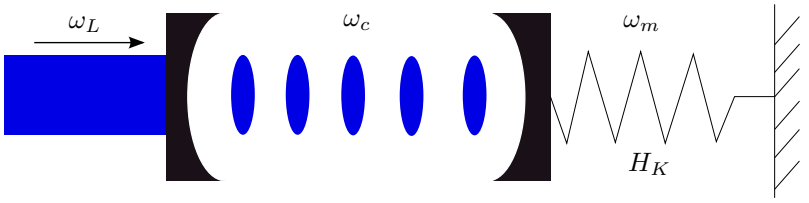

Figure 3.1.1: Schematic illustration of the optomechanical setup with Kerr Hamiltonian H_K. ω_L is the driving frequency, ω_c is the cavity frequency and ω_m is the mechanical frequency.

The oscillator and cavity are coupled to the environment which induces dissipation to our system. We model this by coupling the oscillator to a bath of harmonic oscillators at temperature T. The cavity is coupled to a separate bath of harmonic oscillators. For large optical frequencies $\hbar\omega_c \gg k_B T$ we can neglect the temperature of the optical bath. This leads to the master equation in Lindblad form [26]

$$\dot{\rho} = -i[H, \rho] + \mathcal{L}_m\rho + \mathcal{L}_c\rho, \tag{3.1.3}$$

with the dissipators

$$\begin{aligned} \mathcal{L}_m\rho &= -\Gamma_m(\bar{n} + 1)(b^\dagger b\rho + \rho b^\dagger b - 2b\rho b^\dagger) - \Gamma_m\bar{n}(bb^\dagger\rho + \rho bb^\dagger - 2b^\dagger\rho b), \\ \mathcal{L}_c\rho &= -\kappa(a^\dagger a\rho + \rho a^\dagger a - 2a\rho a^\dagger). \end{aligned} \tag{3.1.4}$$

Here κ denotes the photon amplitude decay rate of the cavity and Γ_m the mechanical damping. $\bar{n} = \left(e^{\hbar\omega_m/k_B T} - 1\right)^{-1}$ is the mean phonon number at frequency ω_m in the bath.

For our purpose we find it more convenient to work with phase space distributions as introduced in Section 2.2 than with operators. This is why we transform the master equation (3.1.3) into a partial differential equation for the s-parametrized phase space distribution σ. We use the translation rules [27]

$$\begin{aligned} b\rho &\to (\beta + q\partial_{\beta^*})\sigma, & b^\dagger\rho &\to (\beta^* - p\partial_\beta)\sigma, \\ \rho b &\to (\beta - p\partial_{\beta^*})\sigma, & \rho b^\dagger &\to (\beta^* + q\partial_\beta)\sigma, \end{aligned} \tag{3.1.5}$$

where $p = \frac{s+1}{2}$, $q = 1 - p$ and $s \in [-1, 1]$ is the parametrization. The complex derivatives are defined as $\partial_\beta = \frac{1}{2}(\partial_x - i\partial_y)$, $\partial_{\beta^*} = \frac{1}{2}(\partial_x + i\partial_y)$, where x and y are the real and imaginary part of β, respectively. The phase space distribution σ is expressed via complex numbers. We have two modes, i.e. two pairs of commuting annihilation and creation operators $a, a^\dagger$ and $b, b^\dagger$ for which we write α, α^* and β, β^*, respectively. The translation rules in Eq. (3.1.5) apply to both. The master equation (3.1.3) can then be written as the partial differential equation

$$\begin{aligned} \partial_t\sigma = &\big[i\Delta(\partial_{\alpha^*}\alpha^* - \partial_\alpha\alpha) - i\omega_m(\partial_{\beta^*}\beta^* - \partial_\beta\beta) + ig\big((\beta + \beta^*)(\partial_{\alpha^*} - \partial_\alpha) \\ &+ (\alpha + \alpha^*)(\partial_{\beta^*} - \partial_\beta) + (q^2 - p^2)\partial_{\alpha^*}\partial_{\beta^*} + (p^2 - q^2)\partial_\alpha\partial_\beta\big) \\ &+ \Gamma_m(\partial_\beta\beta + \partial_{\beta^*} + 2(\bar{n} + pq + q^2)\partial_\beta\partial_{\beta^*}) \\ &+ \kappa(\partial_\alpha\alpha + \partial_{\alpha^*}\alpha^* + \partial_\alpha\partial_{\alpha^*}) \\ &- iK\big(\partial_\beta(-2|\beta|^2\beta + (3p - q)\beta) + (p - q)\partial_\beta + \frac{1}{2}pq\partial_\beta^2\partial_{\beta^*}\beta - \text{h.c.}\big)\big]\sigma. \end{aligned} \tag{3.1.6}$$

Our goal is to find equations of motion for α and β. For this purpose we derive a Fokker-Planck type equation which can then be expressed as Langevin equations.

Note that the equation of motion (3.1.6) is reminiscent of a Fokker-Planck equation but contains third-order derivatives in β, β^*. We will neglect these terms in a truncated Kramers-Moyal expansion [28]. This approximation is valid for large system sizes which would in our case correspond to large mechanical amplitudes, i.e. large energies of the mechanical oscillator.

Neglecting the third-order derivatives Eq. (3.1.6) simplifies for $p = q = \frac{1}{2}$ since the mixed derivatives $\partial_\alpha\partial_\beta, \partial_{\alpha^*}\partial_{\beta^*}$ vanish. This corresponds to the parametrization $s = 0$ in which case the phase space distribution is the Wigner function. We find an equation of motion for the Wigner function $W(\alpha, \beta)$

$$\begin{aligned} \partial_t W = &\big[i\Delta(\partial_{\alpha^*}\alpha^* - \partial_\alpha\alpha) - i\omega_m(\partial_{\beta^*}\beta^* - \partial_\beta\beta) + ig\big((\beta + \beta^*)(\partial_{\alpha^*} - \partial_\alpha) + (\alpha + \alpha^*)(\partial_{\beta^*} - \partial_\beta)\big) \\ &+ \Gamma_m(\partial_\beta\beta + \partial_{\beta^*}\beta^* + (2\bar{n} + 1)\partial_\beta\partial_{\beta^*}) + \kappa(\partial_\alpha\alpha + \partial_{\alpha^*}\alpha^* + \partial_\alpha\partial_{\alpha^*}) \\ &- iK\big(\partial_{\beta^*}(2|\beta|^2\beta^* - \beta^*) - \partial_\beta(2|\beta|^2\beta - \beta)\big)\big]W. \end{aligned} \tag{3.1.7}$$

We can rewrite this equation in the form of a quasi Fokker-Planck equation

$$\partial_t W = \big(-\sum_i \partial_{y_i} A_i + \frac{1}{2}\sum_{i,j} \partial_{y_i}\partial_{y_j} D_{i,j}\big)W, \tag{3.1.8}$$

where we defined a vector of random variables $\vec{y}$

$$\vec{y} = \begin{pmatrix} \alpha \\ \alpha^* \\ \beta \\ \beta^* \end{pmatrix}, \tag{3.1.9}$$

the drift vector $\vec{A}$

$$\vec{A} = \begin{pmatrix} (i\Delta - \kappa)\alpha + ig(\beta + \beta^*) \\ (-i\Delta - \kappa)\alpha^* - ig(\beta + \beta*) \\ ig(\alpha + \alpha^*) - \big(i\omega_m + iK(2|\beta|^2 - 1) + \Gamma_m\big)\beta \\ -ig(\alpha + \alpha^*) + \big(i\omega_m + iK(2|\beta|^2 - 1) - \Gamma_m)\beta^* \end{pmatrix}, \tag{3.1.10}$$

and the diffusion matrix D

$$D = \begin{pmatrix} 0 & \kappa & 0 & 0 \\ \kappa & 0 & 0 & 0 \\ 0 & 0 & 0 & \Gamma_m(2\bar{n} + 1) \\ 0 & 0 & \Gamma_m(2\bar{n} + 1) & 0 \end{pmatrix}. \tag{3.1.11}$$

Note that strictly speaking this is not a Fokker-Planck equation since our diffusion matrix D is not positive definite. If we were to use position and momentum variables we would get a real Fokker-Planck equation. Nevertheless we can find a corresponding Langevin equation by decomposing the diffusion matrix into $D = BB^T$ [29]. In our case it is given by

$$B = \frac{1}{\sqrt{2}} \begin{pmatrix} i\sqrt{\kappa} & \sqrt{\kappa} & 0 & 0 \\ -i\sqrt{\kappa} & \sqrt{\kappa} & 0 & 0 \\ 0 & 0 & i\sqrt{\Gamma_m(2\bar{n} + 1)} & \sqrt{\Gamma_m(2\bar{n} + 1)} \\ 0 & 0 & -i\sqrt{\Gamma_m(2\bar{n} + 1)} & \sqrt{\Gamma_m(2\bar{n} + 1).} \end{pmatrix}. \tag{3.1.12}$$

The Langevin equation takes the form

$$\partial_t \vec{y} = \vec{A} + B\vec{E}(t), \tag{3.1.13}$$

with the Gaussian white-noise process $\vec{E}(t)$ satisfying

$$\langle E_i(t) \rangle = 0, \quad \langle E_i(t) E_j(t') \rangle = \delta_{ij}\delta(t - t'). \tag{3.1.14}$$

The diffusion term B in Eq. (3.1.12) couples the noise terms E_1, E_2 and E_3, E_4. To simplify our equations of motion we define the complex stochastic force terms

$$\begin{aligned} \eta_\alpha(t) &= \frac{1}{\sqrt{2}}(E_2(t) + iE_1(t)), \quad \eta_{\alpha^*(t)} = \frac{1}{\sqrt{2}}(E_2(t) - iE_1(t)), \\ \eta_\beta(t) &= \frac{1}{\sqrt{2}}(E_4(t) + iE_3(t)), \quad \eta_{\beta^*(t)} = \frac{1}{\sqrt{2}}(E_4(t) - iE_3(t)). \end{aligned} \tag{3.1.15}$$

Note that $\eta_{\alpha^{(*)}}, \eta_{\beta^{(*)}}$ are complex white-noise processes with the correlations

$$\langle \eta_i(t)\eta_{i^*}(t') \rangle = \delta(t - t'), \quad \langle \eta_i(t) \rangle = \langle \eta_{i^*(t)} \rangle = \langle \eta_i(t)\eta_i(t') \rangle = \langle \eta_i(t)\eta_{j^*}(t') \rangle = 0, \tag{3.1.16}$$

where $i = \alpha, \beta$ and $i \neq j$. With these definitions we find the Langevin equations for α and β

$$\begin{aligned} \dot{\alpha} &= (i\Delta - \kappa)\alpha + ig(\beta + \beta^*) + \sqrt{\kappa}\eta_\alpha, \\ \dot{\beta} &= \big(- i\omega_m - iK(2|\beta|^2 - 1) - \Gamma_m\big)\beta + ig(\alpha + \alpha^*) + \sqrt{\Gamma_m(2\bar{n} + 1)}\eta_\beta. \end{aligned} \tag{3.1.17}$$

The equations of motion for α^*, β^* can be derived from Eq. (3.1.17) by complex conjugation.

3.2 Adiabatic elimination

We have found equations of motion for the cavity and the resonator variables α, β. In this subsection we solve for α by using adiabatic elimination. Furthermore we derive equations of motion for the mechanical amplitude and phase.

To find an analytical expression for α we have to make assumptions about the parameters. We assume the cavity decay rate to be much larger than the interaction strength and the mechanical damping, i.e. $\kappa \gg g, \Gamma_m$. We make the further assumption that the mechanical frequency is much larger than the interaction strength $\omega_m \gg g$. These are realistic assumptions that can be achieved in typical optomechanical experiments. We choose the general ansatz for β

$$\beta = Be^{-i\phi}e^{-i\omega_m(B)t} \quad \text{with} \quad \omega_m(B) = \omega_m + 2KB^2 - K, \tag{3.2.1}$$

where $\phi(t)$ and $B(t)$ are real numbers describing the phase and amplitude of the oscillator. Because of the factor $-iK(2|\beta|^2 - 1)$ in the equation of motion (3.1.17), we choose an amplitude dependent frequency $\omega_m(B)$ in the ansatz. We predict that β rotates approximately with $\omega_m(B)$ since the mechanical frequency is much larger than the interaction strength. In this case the phase $\phi(t)$ will be a slowly varying function in time compared to α. The amplitude B will also vary slowly on the time scale of α because $\kappa \gg g, \Gamma_m$, i.e. neither the mechanical damping nor the interaction will change the amplitude fast compared to α. We can then solve for α by adiabatic elimination, i.e. by assuming B and ϕ to be constant on the relevant time scale of α. We do this by using the Fourier transform defined as

$$\mathcal{F}[f(t)] = \int \mathrm{d}t e^{-i\omega t} f(t), \quad \mathcal{F}^{-1}[g(\omega)] = \frac{1}{2\pi}\int \mathrm{d}\omega e^{i\omega t} g(\omega). \tag{3.2.2}$$

We write $\alpha(t) = \frac{1}{2\pi}\int \mathrm{d}\omega e^{i\omega t}\alpha(\omega)$ and $\eta_\alpha(t) = \frac{1}{2\pi}\int \mathrm{d}\omega e^{i\omega t}\eta_\alpha(\omega)$ in the equation of motion (3.1.17) and apply the Fourier transform $\mathcal{F}$. Using the relation $\mathcal{F}\left[\mathcal{F}^{-1}1[f(\omega)]\right] = f(\omega)$ as well as $\int \mathrm{d}t e^{-i\omega t} = 2\pi\delta(\omega)$ we find

$$\alpha(\omega) = \frac{ig2\pi B\left(e^{-i\phi}\delta(\omega + \omega_m(B)) + e^{i\phi}\delta(\omega - \omega_m(B))\right)}{i\omega - i\Delta + \kappa} + \frac{\sqrt{\kappa}\eta_\alpha(\omega)}{i\omega - i\Delta + \kappa}. \tag{3.2.3}$$

Similarly $\alpha^*(\omega)$ can either be solved for by using its equation of motion or with the relation $\alpha^*(\omega) = (\alpha(-\omega))^*$. Note that we write an explicit frequency dependency on $\alpha(\omega)$ to distinguish it from $\alpha(t) \equiv \alpha$. With the inverse Fourier transform of Eq. (3.2.3) we arrive at

$$\begin{aligned}\alpha &= igB\left(\frac{e^{-i\phi}e^{-i\omega_m(B)t}}{-i\omega_m(B) - i\Delta + \kappa} + \frac{e^{i\phi}e^{i\omega_m(B)t}}{i\omega_m(B) - i\Delta + \kappa}\right) + \mathcal{F}^{-1}\left[\frac{\sqrt{\kappa}\eta_\alpha(\omega)}{i\omega - i\Delta + \kappa}\right] \\ &= ig\left(\frac{\beta}{-i\omega_m(B) - i\Delta + \kappa} + \frac{\beta^*}{i\omega_m(B) - i\Delta + \kappa}\right) + \mathcal{F}^{-1}\left[\frac{\sqrt{\kappa}\eta_\alpha(\omega)}{i\omega - i\Delta + \kappa}\right].\end{aligned} \tag{3.2.4}$$

We have found a description for the optical variable α. Now we have to find a solution to the mechanical part β. We insert Eq. (3.2.4) into the equation of motion for β but neglect the terms $\sim \beta^*$ in a rotating wave approximation. The idea behind this is changing into a rotating frame with frequency $\omega_m(B)$. The terms $\sim \beta$ will then be approximately constant in time since $\phi(t)$ varies slowly. The terms $\sim \beta^*$ on the other hand will rotate with frequency $2\omega_m(B)$. We can neglect these terms since they will average out on a reasonable time scale. This is known as the rotating wave approximation [30]. We find the equation of motion

$$\begin{aligned}\dot{\beta} =& -(i\omega_m(B) + i\delta\omega + \Gamma_m + \Gamma_{\mathrm{opt}})\beta + \sqrt{\Gamma_m(2\bar{n}+1)}\eta_\beta \\ &+ ig\left(\mathcal{F}^{-1}\left[\frac{\sqrt{\kappa}\eta_\alpha(\omega)}{i\omega - i\Delta + \kappa}\right] + \mathcal{F}^{-1}\left[\frac{\sqrt{\kappa}\eta_{\alpha^*}(\omega)}{i\omega + i\Delta + \kappa}\right]\right),\end{aligned} \tag{3.2.5}$$

where we defined the optically induced damping

$$\Gamma_{\text{opt}} = g^2\kappa\left(\frac{1}{(\Delta+\omega_m(B))^2+\kappa^2}-\frac{1}{(\Delta-\omega_m(B))^2+\kappa^2}\right), \tag{3.2.6}$$

and the frequency shift

$$\delta\omega = g^2\left(\frac{\omega_m(B)+\Delta}{(\Delta+\omega_m(B))^2+\kappa^2}+\frac{\Delta-\omega_m(B)}{(\Delta-\omega_m(B))^2+\kappa^2}\right). \tag{3.2.7}$$

Both terms are real-valued. Note that compared to the standard linearized optomechanical Hamiltonian (see Eq. (2.1.9)) the optically induced damping and frequency shift are now amplitude dependent via the frequency $\omega_m(B) = \omega_m + 2KB^2 - K$. For blue-detuned lasers ($\Delta > 0$) we find negative damping. We illustrate this in Fig. 3.2.1 for the parameters $\kappa/\omega_m = 0.1$, $g/\omega_m = 0.01$, $K/\omega_m = 0.01$.

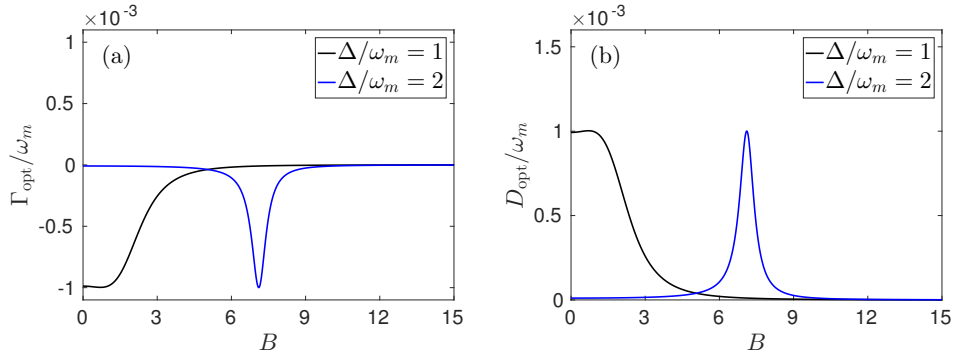

Figure 3.2.1: Optically induced damping (a) and diffusion (b) as a function of the amplitude B. The used parameters are $\kappa/\omega_m = 0.1$, $g/\omega_m = 0.01$, $K/\omega_m = 0.01$. We choose a large detuning $\Delta/\omega_m = 2$ to illustrate the Lorentzian-like peak.

We find the equations of motion for the amplitude and phase by inserting the ansatz for β into Eq. (3.2.5). We follow the notation from [24] and introduce a term relating to the amplitude diffusion

$$\begin{aligned}\eta_T^- =& \frac{\sqrt{\Gamma_m(2\bar{n}+1)}}{2}\left(\eta_\beta e^{i\phi}e^{i\omega_m(B)t}+\eta_{\beta^*}e^{-i\phi}e^{-i\omega_m(B)t}\right)\\ &+\frac{ig}{2}\left(\mathcal{F}^{-1}\left[\frac{\sqrt{\kappa}\eta_\alpha(\omega)}{i\omega-i\Delta+\kappa}\right]+\mathcal{F}^{-1}\left[\frac{\sqrt{\kappa}\eta_{\alpha^*}(\omega)}{i\omega+i\Delta+\kappa}\right]\right)\left(e^{i\phi}e^{i\omega_m(B)t}-e^{-i\phi}e^{-i\omega_m(B)t}\right).\end{aligned} \tag{3.2.8}$$

With this we find the equation of motion for the amplitude by taking the radial part of Eq. (3.2.5)

$$\dot{B} = -(\Gamma_m+\Gamma_{\text{opt}})B+\eta_T^- \equiv F_B. \tag{3.2.9}$$

The equation of motion for the phase is found by taking the angular part. We arrive at

$$B\dot{\phi} = 2K(B^2-B_0^2)B+\delta\omega B+\eta_T^+ \equiv BF_\phi, \tag{3.2.10}$$

where we defined a term related to the phase diffusion

$$\begin{aligned}\eta_T^+ =& i\frac{\sqrt{\Gamma_m(2\bar{n}+1)}}{2}\left(\eta_\beta e^{i\phi}e^{i\omega_m(B)t}-\eta_{\beta^*}e^{-i\phi}e^{-i\omega_m(B)t}\right)\\ &-\frac{g}{2}\left(\mathcal{F}^{-1}\left[\sqrt{\kappa}\frac{\eta_\alpha(\omega)}{i\omega-i\tilde{\Delta}+\kappa}\right]+\mathcal{F}^{-1}\left[\frac{\sqrt{\kappa}\eta_{\alpha^*}(\omega)}{i\omega+i\tilde{\Delta}+\kappa}\right]\right)\left(e^{i\phi}e^{i\omega_m(B)t}+e^{-i\phi}e^{-i\omega_m(B)t}\right).\end{aligned} \tag{3.2.11}$$

We introduced the symbols F_B and F_ϕ which denote the Langevin forces for the amplitude and the phase, respectively. They are explicitly defined as

$$\begin{aligned} F_B &= -(\Gamma_m + \Gamma_{\text{opt}})B + \eta_T^-, \\ F_\phi &= \frac{1}{B}\left(2K(B^2 - B_0^2)B + \delta\omega B + \eta_T^+\right). \end{aligned} \tag{3.2.12}$$

3.3 Amplitude drift and diffusion

In the last subsection we have found equations of motion for α and β. We solved for α by adiabatic elimination making a slowly varying ansatz for β. Furthermore we found equations of motion for the amplitude and phase of the mechanical oscillator. Our next goal is to simplify the amplitude equation (3.2.9). We do this by finding an approximate Fokker-Planck equation for the joint probability distribution $W(B, \phi)$ of B and ϕ. We will see that the radial part is independent of the phase which allows us to write down a Langevin equation for the amplitude independent of the phase. We can then describe the properties of the amplitude without considering the phase.

Our coupled Langevin equations (3.2.9), (3.2.10) can be rewritten as a Fokker-Planck equation according to [31]

$$\begin{aligned} \partial_t W = &- \partial_B A_B W - \partial_\phi A_\phi W \\ &+ \frac{1}{2}\partial_B^2 D_{B,B} W + \frac{1}{2}\partial_B\partial_\phi D_{B,\phi} W + \frac{1}{2}\partial_\phi\partial_B D_{\phi,B} W + \frac{1}{2}\partial_\phi^2 D_{\phi,\phi} W. \end{aligned} \tag{3.3.1}$$

Here we defined the drift terms

$$\begin{aligned} A_B &= \langle F_B\rangle + \int_{-\infty}^{0} \mathrm{d}\tau \,\langle \partial_B F_B(t), F_B(t+\tau)\rangle + \int_{-\infty}^{0} \mathrm{d}\tau \,\langle \partial_\phi F_B(t), F_B(t+\tau)\rangle\,, \\ A_\phi &= \langle F_\phi\rangle + \int_{-\infty}^{0} \mathrm{d}\tau \,\langle \partial_\phi F_B(t), F_B(t+\tau)\rangle + \int_{-\infty}^{0} \mathrm{d}\tau \,\langle \partial_\phi F_\phi(t), F_B(t+\tau)\rangle) \end{aligned} \tag{3.3.2}$$

and the diffusion terms

$$\begin{aligned} D_{B,B} &= 2\int_{-\infty}^{0} \mathrm{d}\tau \,\langle F_B(t), F_B(t+\tau)\rangle\,, \quad D_{B,\phi} = 2\int_{-\infty}^{0} \mathrm{d}\tau \,\langle F_B(t), F_\phi(t+\tau)\rangle\,, \\ D_{\phi,B} &= 2\int_{-\infty}^{0} \mathrm{d}\tau \,\langle F_\phi(t), F_B(t+\tau)\rangle\,, \quad D_{\phi,\phi} = 2\int_{-\infty}^{0} \mathrm{d}\tau \,\langle F_\phi(t), F_\phi(t+\tau)\rangle\,, \end{aligned} \tag{3.3.3}$$

where $\langle A, B\rangle = \langle AB\rangle - \langle A\rangle\langle B\rangle$ denotes the covariance function. F_B and F_ϕ are the Langevin forces defined in Eq. (3.2.12). Note that B and ϕ are treated as deterministic variables in this approach.

For a stationary process, i.e. a process whose autocorrelation function depends only on the time difference, the covariance functions will be even in time. We can then change the upper limit of the integration interval to infinity if we include a factor $\frac{1}{2}$. For the following calculations we use the drift terms

$$\begin{aligned} A_B &= \langle F_B\rangle + \frac{1}{2}\int \mathrm{d}\tau \,\langle \partial_B F_B(t), F_B(t+\tau)\rangle + \frac{1}{2}\int \mathrm{d}\tau \,\langle \partial_\phi F_B(t), F_B(t+\tau)\rangle\,, \\ A_\phi &= \langle F_\phi\rangle + \frac{1}{2}\int \mathrm{d}\tau \,\langle \partial_\phi F_B(t), F_B(t+\tau)\rangle + \frac{1}{2}\int \mathrm{d}\tau \,\langle \partial_\phi F_\phi(t), F_B(t+\tau)\rangle) \end{aligned} \tag{3.3.4}$$

and the diffusion terms

$$\begin{aligned} D_{B,B} &= \int \mathrm{d}\tau \left\langle F_B(t), F_B(t+\tau)\right\rangle, \quad D_{B,\phi} = \int \mathrm{d}\tau \left\langle F_B(t), F_\phi(t+\tau)\right\rangle, \\ D_{\phi,B} &= \int \mathrm{d}\tau \left\langle F_\phi(t), F_B(t+\tau)\right\rangle, \quad D_{\phi,\phi} = \int \mathrm{d}\tau \left\langle F_\phi(t), F_\phi(t+\tau)\right\rangle. \end{aligned} \tag{3.3.5}$$

Let us first derive the amplitude diffusion term $D_{B,B}$. As mentioned before we will see that the radial part is independent of the phase. We therefore write $D_B \equiv D_{B,B}$ for the amplitude diffusion, i.e.

$$D_B = \int \mathrm{d}\tau \left\langle F_B(t), F_B(t+\tau)\right\rangle. \tag{3.3.6}$$

In this treatment the Langevin force F_B consist of a deterministic part $-(\Gamma_m + \Gamma_{\mathrm{opt}})B$ and the stochastic term η_T^-. The expectation value of a deterministic function is given by itself, i.e. the covariance vanishes

$$\langle(\Gamma_m + \Gamma_{\mathrm{opt}})B(t), (\Gamma_m + \Gamma_{\mathrm{opt}})B(t+\tau)\rangle = 0. \tag{3.3.7}$$

Furthermore the covariance of a deterministic function G and a random function H with mean value 0 vanishes, i.e. $\langle G, H\rangle = 0$ or for our amplitude equation

$$\langle -(\Gamma_m + \Gamma_{\mathrm{opt}})B, \eta_T^-\rangle = 0. \tag{3.3.8}$$

Therefore the only contributing term to the amplitude diffusion is determined by the covariance $\langle \eta_T^-(t), \eta_T^-(t+\tau)\rangle$. We split the term $\eta_T^- \equiv \eta_{T,\mathrm{mech}}^- + \eta_{T,\mathrm{opt}}^-$ into a mechanical and an optical part

$$\begin{aligned} \eta_{T,\mathrm{mech}}^- &= \frac{\sqrt{\Gamma_m(2\bar{n}+1)}}{2}\left(\eta_\beta e^{i\phi}e^{i\omega_m(B)t} + \eta_{\beta^*}e^{-i\phi}e^{-i\omega_m(B)t}\right), \\ \eta_{T,\mathrm{opt}}^- &= \frac{ig}{2}\left(\mathcal{F}^{-1}\left[\frac{\sqrt{\kappa}\eta_\alpha(\omega)}{i\omega - i\Delta + \kappa}\right] + \mathcal{F}^{-1}\left[\frac{\sqrt{\kappa}\eta_{\alpha^*}(\omega)}{i\omega + i\Delta + \kappa}\right]\right)\left(e^{i\phi}e^{i\omega_m(B)t} - e^{-i\phi}e^{-i\omega_m(B)t}\right). \end{aligned} \tag{3.3.9}$$

Since $\eta_{\alpha^{(*)}}, \eta_{\beta^{(*)}}$ are independent noise processes (see Eq. (3.1.16)) there is no mixed contribution to the amplitude diffusion, i.e.

$$\langle \eta_{\alpha^{(*)}}(\omega), \eta_{\beta^{(*)}}(t)\rangle = \int \mathrm{d}t e^{-i\omega t'} \langle \eta_{\alpha^{(*)}}(t'), \eta_{\beta^{(*)}}(t)\rangle = 0. \tag{3.3.10}$$

We split the amplitude diffusion into an intrinsic mechanical part and an optically induced part

$$D_B = \frac{1}{2}D_m + \frac{1}{2}D_{\mathrm{opt}}. \tag{3.3.11}$$

The mechanical contribution to D_m is evaluated using the relation $\langle \eta_\beta(t), \eta_{\beta^*}(t')\rangle = \delta(t-t')$. We find

$$D_m = 2\int \mathrm{d}\tau \left\langle \eta_{T,\mathrm{mech}}^-(t), \eta_{T,\mathrm{mech}}^-(t+\tau)\right\rangle = \Gamma_m(2\bar{n}+1). \tag{3.3.12}$$

The optical part of the amplitude diffusion D_{opt} contains the covariance of Fourier transformed expressions. We use the relation

$$\langle \eta_\alpha(\omega)\eta_{\alpha^*}(\omega')\rangle = \int\int \mathrm{d}t\mathrm{d}t' \langle \eta_\alpha(t)\eta_{\alpha^*}(t)\rangle e^{-i\omega t}e^{-i\omega t'} = \int \mathrm{d}t e^{-it(\omega+\omega')} = 2\pi\delta(w+w'). \tag{3.3.13}$$

Similarly we find $\langle \eta_\alpha(\omega)\eta_\alpha(\omega')\rangle = \langle \eta_{\alpha^*}(\omega)\eta_{\alpha^*}(\omega')\rangle = 0$. With this we calculate the covariance of the Fourier transformed expressions

$$\begin{aligned}
&\langle\left(\mathcal{F}^{-1}\left[\frac{\sqrt{\kappa}\eta_\alpha(\omega)}{i\omega - i\Delta + \kappa}\right](t) + \mathcal{F}^{-1}\left[\frac{\sqrt{\kappa}\eta_{\alpha^*}(\omega)}{i\omega + i\Delta + \kappa}\right](t)\right), \\
&\left(\mathcal{F}^{-1}\left[\frac{\sqrt{\kappa}\eta_\alpha(\omega')}{i\omega' - i\Delta + \kappa}\right](t+\tau) + \mathcal{F}^{-1}\left[\frac{\sqrt{\kappa}\eta_{\alpha^*}(\omega')}{i\omega' + i\Delta + \kappa}\right](t+\tau)\right)\rangle \\
&= \frac{\kappa}{2\pi}\int \mathrm{d}\omega \left(\frac{1}{(\Delta-\omega)^2+\kappa^2} + \frac{1}{(\Delta+\omega)^2+\kappa^2}\right) e^{-i\omega\tau} \\
&= \frac{1}{2} e^{-k|\tau|}\left(e^{i\Delta\tau} + e^{-i\Delta\tau}\right),
\end{aligned} \tag{3.3.14}$$

where we solved the integral in the second line via the residue theorem resulting in

$$\int \mathrm{d}x \frac{1}{x^2+a^2} e^{-ikx} = \frac{\pi}{a} e^{-a|k|}. \tag{3.3.15}$$

Here a and k are real numbers. We find D_{opt} by including the prefactors of the Fourier transformed expressions in Eq. (3.3.9) and integrating over τ. The integrand, i.e. the covariance given in Eq. (3.3.14), decays on the time scale $\tau_{\mathrm{corr}} = 1/\kappa$. In the last subsection we argued that B and ϕ are slowly varying on the time scale of α assuming that $\omega_m \gg g$. Since $1/\kappa$ is the time scale on which the amplitude $|\alpha|$ changes, we can assume that B and ϕ are constant in time for the integration. We find

$$\begin{aligned}
D_{\mathrm{opt}} = -\frac{g^2}{4}\int \mathrm{d}\tau e^{-\kappa|\tau|}\big(&e^{i\omega_m(B)(2t+\tau)}e^{2i\phi} - e^{-i\omega_m(B)\tau} \\
&- e^{i\omega_m(B)\tau} + e^{-i\omega_m(B)(2t+\tau)}e^{-2i\phi}\big)\big(e^{i\Delta\tau} + e^{-i\Delta\tau}\big).
\end{aligned} \tag{3.3.16}$$

We perform a rotating wave approximation and neglect the fast rotating terms $\sim e^{\pm 2i\omega_m(B)t}$ which results in

$$D_{\mathrm{opt}} = \frac{g^2}{4}\int_{-\infty}^{\infty} \mathrm{d}\tau e^{-\kappa|\tau|}\big(e^{-i\omega_m(B)\tau} + e^{+i\omega_m(B)\tau}\big)\big(e^{i\Delta\tau} + e^{-i\Delta\tau}\big). \tag{3.3.17}$$

We split the integral into intervals for negative and positive τ since $|\tau| = \mathrm{sign}(\tau)\tau$, i.e.

$$\int_{-\infty}^{\infty} \mathrm{d}\tau e^{-\kappa|\tau|}... = \int_{-\infty}^{0} \mathrm{d}\tau e^{\kappa\tau}... + \int_{0}^{\infty} \mathrm{d}\tau e^{-\kappa\tau}... \ . \tag{3.3.18}$$

After the integration we find the optical part of the amplitude diffusion

$$D_{\mathrm{opt}} = g^2\kappa\left(\frac{1}{(\Delta+\omega_m(B))^2+\kappa^2} + \frac{1}{(\Delta-\omega_m(B))^2+\kappa^2}\right). \tag{3.3.19}$$

We arrive at the amplitude diffusion

$$\begin{aligned}
D_B &= \frac{1}{2}(D_m + D_{\mathrm{opt}}) \\
&= \frac{1}{2}\Gamma_m(2\bar{n}+1) + \frac{g^2\kappa}{2}\left(\frac{1}{(\Delta+\omega_m(B))^2+\kappa^2} + \frac{1}{(\Delta-\omega_m(B))^2+\kappa^2}\right).
\end{aligned} \tag{3.3.20}$$

Now we have to find an expression for the amplitude drift A_B, which we defined in Eq. (3.3.4) as

$$A_B = \langle F_B \rangle + \frac{1}{2}\int \mathrm{d}\tau \, \langle \partial_B F_B(t), F_B(t+\tau)\rangle + \frac{1}{2}\int \mathrm{d}\tau \, \langle \partial_\phi F_B(t), F_B(t+\tau)\rangle \,. \tag{3.3.21}$$

We remember that only the stochastic terms contribute to the covariance. Since the mechanical noise process $\eta^-_{T,\mathrm{mech}}$ is δ-correlated and we showed that the optical process $\eta^-_{T,\mathrm{opt}}$ has a correlation time of $1/\kappa$, we will again assume B, ϕ to be constant in time. The mechanical contribution to the third term is zero, i.e.

$$\langle \eta^-_{T,\mathrm{mech}}(t), \eta^-_{T,\mathrm{mech}}(t+\tau)\rangle = i\phi\frac{\Gamma_m(2\bar{n}+1)}{2}\big(\langle \eta_\beta(t), \eta_{\beta^*}(t+\tau)\rangle - \langle \eta_{\beta^*}(t+\tau), \eta_\beta(t)\rangle\big) = 0, \tag{3.3.22}$$

where we used that $\eta_\beta, \eta_{\beta^*}$ are complex white-noise processes. Note that the optical part of η^-_T is only phase dependent in the exponent. Similar to Eq. (3.3.16) we find the optical contribution to be

$$\begin{aligned}\int \mathrm{d}\tau \, \langle \eta^-_{T,\mathrm{opt}}(t), \eta^-_{T,\mathrm{opt}}(t+\tau)\rangle =& i\frac{g^2}{8}\int \mathrm{d}\tau e^{-\kappa|\tau|}\big(e^{i\omega_m(B)(2t+\tau)}e^{i\phi} - e^{-i\omega_m(B)\tau} \\ &+ e^{i\omega_m(B)\tau} + e^{-i\omega_m(B)(2t+\tau)}e^{-i\phi}\big)\big(e^{i\Delta\tau} + e^{-i\Delta\tau}\big),\end{aligned} \tag{3.3.23}$$

where the second and third term cancel after the integration. The terms $\sim e^{\pm 2i\omega_m(B)t}$ can again be neglected in a rotating wave approximation. Therefore the third term of the amplitude drift in Eq. (3.3.21) is zero. A similar calculation shows that the second term vanishes too. We find our amplitude drift

$$A_B = \langle F_B \rangle = -(\Gamma_m + \Gamma_{\mathrm{opt}})B. \tag{3.3.24}$$

Let us now take a look at the diffusion terms $D_{B,\phi}, D_{\phi,B}$. To find $D_{B,\phi}$ we have to calculate the covariance $\langle F_B(t), F_\phi(t+\tau)\rangle$. The only contributions to this will be given by the stochastic parts, i.e. $\langle \eta^-_T(t), \eta^+_T(t+\tau)\rangle$. We divide $\eta^+_T \equiv \eta^+_{T,\mathrm{mech}} + \eta^+_{T,\mathrm{opt}}$ into a mechanical and an optical part

$$\begin{aligned}\eta^+_{T,\mathrm{mech}} &= i\frac{\sqrt{\Gamma_m(2\bar{n}+1)}}{2}\left(\eta_\beta e^{i\phi}e^{i\omega_m(B)t} - \eta_{\beta^*}e^{-i\phi}e^{-i\omega_m(B)t}\right), \\ \eta^+_{T,\mathrm{opt}} &= \frac{g}{2}\left(\mathcal{F}^{-1}\left[\sqrt{\kappa}\frac{\eta_\alpha(\omega)}{i\omega - i\Delta + \kappa}\right] + \mathcal{F}^{-1}\left[\frac{\sqrt{\kappa}\eta_{\alpha^*}(\omega)}{i\omega + i\Delta + \kappa}\right]\right)\left(e^{i\phi}e^{i\omega_m(B)t} + e^{-i\phi}e^{-i\omega_m(B)t}\right).\end{aligned} \tag{3.3.25}$$

Similar as for the drift the mechanical contribution to $D_{B,\phi}$ equals zero. The optical contribution will vanish after a rotating wave approximation just as we calculated for the drift term in Eq. (3.3.23). Therefore $D_{B,\phi} = 0$. The same argument holds for $D_{\phi,B}$, i.e. $D_{\phi,B} = 0$.

We can now write the Fokker-Planck equation for the joint probability distribution $W(B,\phi)$ in polar coordinates

$$\partial_t W = -\partial_B A_B W - \partial_\phi A_\phi W + \frac{1}{2}\partial_B^2 D_B W + \frac{1}{2}\partial_\phi^2 D_{\phi,\phi} W. \tag{3.3.26}$$

Since both A_B and D_B are independent of the phase, we can find a simplified equation of motion for the amplitude independent of the phase. Note that we did not explicitly derive the expressions A_ϕ and $D_{\phi,\phi}$ as they are not needed here.

The Langevin equation for B corresponding to Eq. (3.3.26) is

$$\dot{B} = -(\Gamma_m + \Gamma_{\mathrm{opt}})B + \sqrt{D_B}\eta_B, \tag{3.3.27}$$

where η_B is a Gaussian white-noise process. Since this equation is independent of the phase ϕ we can also write down a Fokker-Planck equation for the amplitude probability distribution W_B

$$\partial_t W_B = -\partial_B\big(-(\Gamma_m + \Gamma_{\text{opt}})BW_B\big) + \frac{1}{2}\partial_B^2 D_B W_B. \tag{3.3.28}$$

3.4 Steady-state solution for the amplitude

We have derived an effective equation of motion in the form of a Fokker-Planck equation for the amplitude B. We will now calculate its steady-state solution. If in the steady state $A_B W_B$ and $\partial_B D_B W_B$ vanish at $B = 0$ the analytical steady-state solution of the Fokker-Planck equation (3.3.28) can be written as [28]

$$W_B = \mathcal{N}\frac{1}{D_B}\exp\left(2\int_0^B \frac{A_{B'}}{D_{B'}}\mathrm{d}B'\right), \tag{3.4.1}$$

where $\mathcal{N}$ is a normalization constant. We apply this model only to the situation where a well-defined limit cycle forms, i.e. the amplitude distribution is strongly peaked around an average value B_0. Then the probability distribution W_B approximately vanishes at $B = 0$ and at infinity for B_0 large enough. Furthermore both the drift and diffusion are finite at $B = 0$ and go to zero for B going to infinity. Equation (3.4.1) is therefore the analytical solution for our steady-state.

We could calculate this solution explicitly but it is more intuitive to analyze the solution after the following approximations. The cente B_0 of the amplitude distribution is given by the non-trivial solution to the deterministic equation

$$A_B(B_0) = -(\Gamma_m + \Gamma_{\text{opt}}(B_0))B_0 = 0. \tag{3.4.2}$$

This is a fourth-order equation in B_0 as can be seen from the definition of the optical damping in Eq. (3.2.6). To find a simpler solution we assume $(\omega_m(B_0) - \Delta)^2 \ll (\omega_m(B_0) + \Delta)^2$ and approximate Γ_{opt} by dropping the non-resonant term, i.e.

$$\Gamma_{\text{opt}} = -\frac{g^2\kappa}{(\omega_m(B) - \Delta)^2 + \kappa^2}. \tag{3.4.3}$$

This is a good approximation for the parameters considered here ($\omega_m \gg \kappa \gg g, K \gg \Gamma_m$) as long as the mechanical damping is not too small. This can be explained by the fact that the two terms in the optical damping in Eq. (3.2.6) are similar to Lorentzian peaks with a maximum and minimum value of $\pm\frac{g^2}{\kappa}$, respectively. The resonant term has a (negative) peak at $\omega_m(B) = \Delta$, i.e. $B = \sqrt{\frac{\Delta-\omega_m+K}{2K}}$, and the non-resonant term has a (positive) peak at $\omega_m(B) = -\Delta$. The width of the peaks scales with κ. For $\Delta > 0$ we can neglect the non-resonant term compared to the resonant peak since $\omega_m(B) > 0$. This is valid as long as the fixpoint B_0 (see Eq. (3.4.2)) is not too far away from the peak of the resonant term in Eq. (3.4.3). This condition is satisfied for cooperativities $C \equiv \frac{g^2}{\kappa\Gamma_m}$ that are not too large. With this approximation we find the average amplitude in the steady state

$$B_0 = \sqrt{\frac{1}{2K}\left(\Delta - \omega_m + K + \kappa\sqrt{C-1}\right)}, \tag{3.4.4}$$

with the conditions $C = \frac{g^2}{\kappa\Gamma_m} \geq 1$ and $\Delta > -\omega_m + K + \kappa\sqrt{C-1}$. The amplitude B_0 scales inversely with K, i.e. B_0 is larger for small nonlinearities, as was expected. Furthermore B_0 scales with κ and C. The larger the detuning Δ, the larger the mean amplitude B_0 will be.

Note that for very large detunings this expression is not valid as the limit cycle will not start. This can be explained by the fact that our approximated optical damping in Eq. (3.4.3) is a Lorentzian-like distribution with a peak at $B = \sqrt{\frac{\Delta-\omega_m+K}{2K}}$. The optically induced damping is negligible for small amplitudes compared to Γ_m and the oscillator never reaches B_0.

Since in the semi-classical limit we only expect small fluctuations around the peak of the amplitude distribution, we now linearize the drift around B_0. Using $\Gamma_m + \Gamma_{\mathrm{opt}}(B_0) = 0$ we find

$$A_B(B) \approx A_B(B_0) + \left.\frac{\mathrm{d}A_B}{\mathrm{d}B}\right|_{B=B_0} \delta B = -\Gamma_L \delta B, \tag{3.4.5}$$

where we defined the amplitude fluctuation $\delta B = B - B_0$ and the linearized damping

$$\Gamma_L = B_0 \left.\frac{\mathrm{d}\Gamma_{\mathrm{opt}}}{\mathrm{d}B}\right|_{B=B_0}. \tag{3.4.6}$$

We assume that the diffusion is approximately constant at B_0 with $D_{B_0} \equiv D_B(B_0)$. The steady state solution Eq. (3.4.1) is then a Gaussian distribution with mean B_0 and variance $\sigma^2 = \frac{D_{B_0}}{2\Gamma_L}$ [24], i.e.

$$W_B \sim \exp\left(-\frac{1}{2}\frac{(\delta B)^2}{\sigma^2}\right). \tag{3.4.7}$$

Note that the same result is obtained by linearizing the Langevin equation (3.3.27), that is by writing $B = B_0 + \delta B$ and Γ_{opt} as a first-order Taylor expansion. For small fluctuations we can neglect the term $\sim \delta B^2$ and assume the diffusion to be approximately constant. We find

$$\delta\dot{B} = -\Gamma_L \delta B + \sqrt{D_{B_0}}\eta_B. \tag{3.4.8}$$

This is an Ornstein-Uhlenbeck process whose steady-state distribution is given by a Gaussian with mean zero and variance $\sigma^2 = \frac{D_{B_0}}{2\Gamma_L}$.

Just as in the case of the optically induced damping Γ_{opt} in Eq. (3.4.3), we can drop the non-resonant term in $D_{\mathrm{opt}}(B_0)$ if we assume $(\Delta - \omega_m(B_0))^2 \ll (\Delta + \omega_m(B_0))^2$. We approximate

$$D_{\mathrm{opt}}(B_0) = \frac{g^2\kappa}{(\omega_m(B_0) - \Delta)^2 + \kappa^2}. \tag{3.4.9}$$

With this simplified optical diffusion we find the steady-state variance

$$\sigma^2 = \frac{\bar{n}+1}{8} \frac{1}{1 - \frac{1}{C} + \frac{\Delta-\omega_m+K}{\kappa}\sqrt{\frac{1}{C} - \frac{1}{C^2}}}. \tag{3.4.10}$$

We compare these results to the numerical solution in Section 3.6.

3.5 Fano factor

We have described the amplitude of the mechanical oscillator in the Wigner representation. The steady-state amplitude distribution was approximated as a Gaussian peak. In this subsection we derive conditions under which the oscillator shows number squeezing and is therefore in a non-classical steady state. The Fano factor is defined as

$$F = \frac{\langle n^2\rangle - \langle n\rangle^2}{\langle n\rangle}, \tag{3.5.1}$$

where $n = b^\dagger b$ is the number operator of the mechanical oscillator. The Fano factor is the variance of the Fock states divided by the mean phonon number. For a coherent state, i.e. a highly classical state, the Fano factor will be 1. A Fano factor less than 1 implies sub-Poissonian phonon statistics and therefore number state squeezing [20].

As mentioned in Section 2.2 (see Eq. (2.2.15)) expectation values with respect to the Wigner function correspond to expectation values of functions of symmetrized creation and annihilation operators, e.g. $\langle B^2\rangle_W = \langle \beta^*\beta\rangle_W = \frac{1}{2}\langle b^\dagger b + b b^\dagger\rangle$. Using the bosonic commutation relations of $b, b^\dagger$ we find

$$\begin{aligned}\langle B^2\rangle_W &= \langle n\rangle + \frac{1}{2},\\ \langle B^4\rangle_W &= \langle n^2\rangle + \langle n\rangle + \frac{1}{2} = \langle n^2\rangle + \langle B^2\rangle_W,\end{aligned} \tag{3.5.2}$$

where the expectation values of the operators n, n^2 are with respect to the steady-state density matrix, and expectation values of B, B^2 are with respect to the corresponding Wigner function. The Fano factor can then be rewritten in terms of the amplitude B

$$F = \frac{\langle B^4\rangle_W - \left(\langle B^2\rangle_W\right)^2 - \frac{1}{4}}{\langle B^2\rangle_W - \frac{1}{2}} \approx \frac{\langle B^4\rangle_W - \left(\langle B^2\rangle_W\right)^2}{\langle B^2\rangle_W}, \tag{3.5.3}$$

where we assumed that the mean amplitude B_0 is large. The steady-state Wigner function W_B for the amplitude is a Gaussian with mean B_0 and variance σ^2. The moments of such a Gaussian random variable $B \sim \mathcal{N}(B_0, \sigma^2)$ are given by

$$\begin{aligned}\langle B^2\rangle_W &= B_0^2 + \sigma^2,\\ \langle B^4\rangle_W &= B_0^4 + 6B_0^2\sigma^2 + 3\sigma^4.\end{aligned} \tag{3.5.4}$$

In a well-defined limit cycle the condition $B_0^2 \gg \sigma^2$ is satisfied. We find an approximate Fano factor [24]

$$F = \frac{2\sigma^4 + 4B_0^2\sigma^2}{B_0^2 + \sigma^2} \approx \frac{4B_0^2\sigma^2}{B_0^2} = 4\sigma^2. \tag{3.5.5}$$

The Fano factor scales only with σ^2. Inserting the variance of the Gaussian distribution W_B we arrive at

$$F = \frac{\bar{n}+1}{2}\frac{1}{1 - \frac{1}{C} + \frac{\Delta-\omega_m+K}{\kappa}\sqrt{\frac{1}{C} - \frac{1}{C^2}}}. \tag{3.5.6}$$

In the limit of very large cooperativity $C \gg 1$ the Fano factor is

$$F = \frac{\bar{n}+1}{2}. \tag{3.5.7}$$

We find squeezed number states, i.e. non-classical states, for Fano factors smaller than one. For a given cooperativity we find the minimal Fano factor for large Δ and K and small κ. For realistic small nonlinearities $K \ll \omega_m, \kappa$ the Fano factor is approximately independent of K. F goes to zero and the mechanical system reaches a highly non-classical state for large detuning Δ and not too large cooperativity. As we already mentioned for the mean amplitude B_0 in Section 3.4, unfortunately we cannot raise Δ too high since then our limit cycle will not start. Nevertheless we can achieve a very small Fano factor in the zero temperature limit. We will compare this result in Section 3.6 with the numerical solution for different values of Δ and Γ_m.

At finite temperature the Fano factor scales with $\bar{n}+1$. This requires very low temperatures that could be achieved by cryogenic cooling. Another possibility is optomechanical sideband

cooling via radiation pressure. This is done with a red-detuned laser which induces positive optical damping to the resonator. One can even combine both methods and cool the mechanical oscillator close to its ground state [9, 10]. We will look at the case where the oscillator is driven by two lasers in Section 5. One laser is blue-detuned and one laser red-detuned for additional cooling.

3.6 Comparison with numerical results

We have derived the steady-state amplitude distribution and the Fano factor of the mechanical system. Let us now compare our analytical findings with the numerical solution to the master equation (3.1.3). The numerics were done using the QuTiP toolbox for Python [32]. We solved the master equation using three cavity states and 80 mechanical states where we truncated the Fock space around the expected mean value.

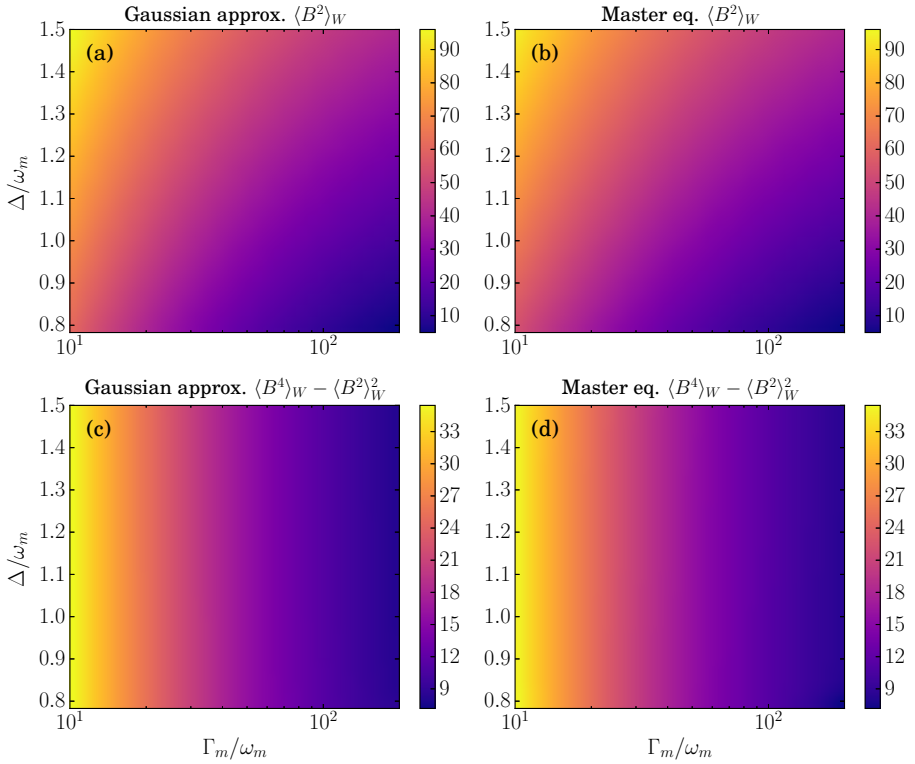

Figure 3.6.1: Mean $\langle B^2\rangle_W$ and variance $\langle B^4\rangle_W - \langle B^2\rangle_W^2$ as a function of the mechanical damping Γ_m/ω_m and detuning Δ/ω_m. We used the parameters $\kappa/\omega_m = 0.1$, $g/\omega_m = 0.01$, $K/\omega_m = 0.01$, $\bar{n} = 0$. (a) and (c) show the Gaussian approximation, while (b) and (d) show the numerical solution of the master equation.

In Fig. 3.6.1 we compare our Gaussian approximation of the mean $\langle B^2\rangle_W = B_0^2 + \sigma^2$ and variance $\mathrm{Var}(B^2) = \langle B^4\rangle_W - \langle B^2\rangle_W^2 = 4B_0^2\sigma^2 + 2\sigma^4$ in the steady-state with the numerical solution. As shown in Eq. (3.5.2), these expectation values correspond to $\langle B^2\rangle_W = \langle n\rangle + \frac{1}{2}$ and $\mathrm{Var}(B^2) = \langle n^2\rangle + \langle n\rangle + \frac{1}{2}$, respectively, where $n = b^\dagger b$ is the number operator for the mechanical Fock states. B_0 and σ^2 are given in Eqs. (3.4.4), (3.4.10). We plot the results as a function of the cavity detuning Δ/ω_m and mechanical damping Γ_m/ω_m. The temperature is assumed to be

zero, i.e. $\bar{n} = 0$. We used the decay rate $\kappa/\omega_m = 0.1$ and effective coupling $g/\omega_m = 0.01$ such that our assumption $g \ll \kappa \ll \omega_m$ is approximately satisfied. The Kerr-nonlinearity K is chosen to be equal to the effective coupling, i.e. $K/\omega_m = 0.01$. We use this value since this allows us to use less mechanical states. K might be on the high side of achievable nonlinearities but as we discussed the Fano factor is approximately independent of K for very small nonlinearities.

We find excellent agreement between numerics and the analytical model. The mean value $\langle B^2 \rangle_W$ of our approximation seems slightly shifted compared to the numerical solution for small Γ_m/ω_m and Δ/ω_m. This is more visible in Fig. 3.6.2(a), where we plotted the absolute error of the mean compared to the analytical solution. The error of around 10 percent for small Γ_m/ω_m and Δ/ω_m is explained by the fact that we dropped the non-resonant term in Γ_{opt}. Fig. 3.6.2(b) shows the absolute error of $\text{Var}(B^2)$. We find an error of around 20 percent for large Γ_m/ω_m and small Δ/ω_m. This is the limit of very small amplitudes where our model is no longer applicable.

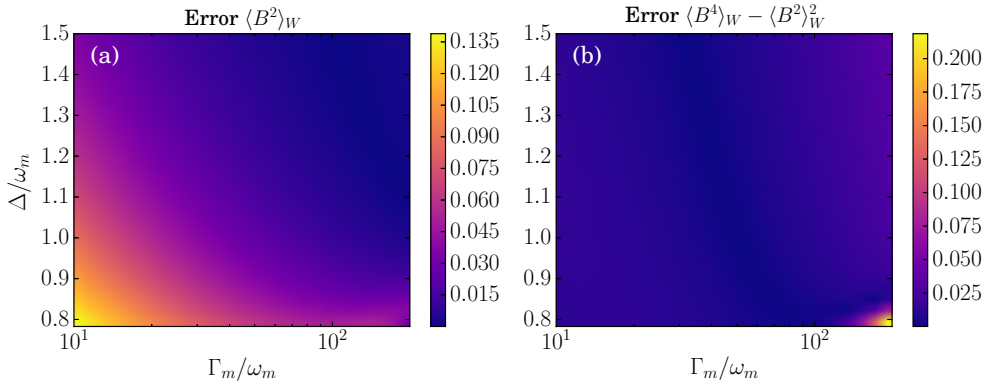

Figure 3.6.2: Relative error of the Gaussian approximated mean $\langle B^2 \rangle_W$ (a) and variance $\langle B^4 \rangle_W - \langle B^2 \rangle_W^2$ (b) as a function of the mechanical damping Γ_m/ω_m and detuning Δ/ω_m. We used the parameters $\kappa/\omega_m = 0.1$, $g/\omega_m = 0.01$, $K/\omega_m = 0.01$, $\bar{n} = 0$.

In Fig. 3.6.3 we show the numerical solution and our analytical approximation of the Fano factor as a function of detuning Δ/ω_m and mechanical damping Γ_m/ω_m for the same parameters as before. We plot the Fano factor up to one since this is the range where we find non-classical states. Note that we used the approximation in Eq. (3.5.5) for the analytical solution, i.e. $F = 4\sigma^2$. It is no surprise that we find very good agreement between the analytical model and numerics since the Fano factor is essentially the variance of B^2 divided by its mean. We see that a Fano factor smaller than one is achieved for a very wide set of parameters Δ/ω_m and Γ_m/ω_m.

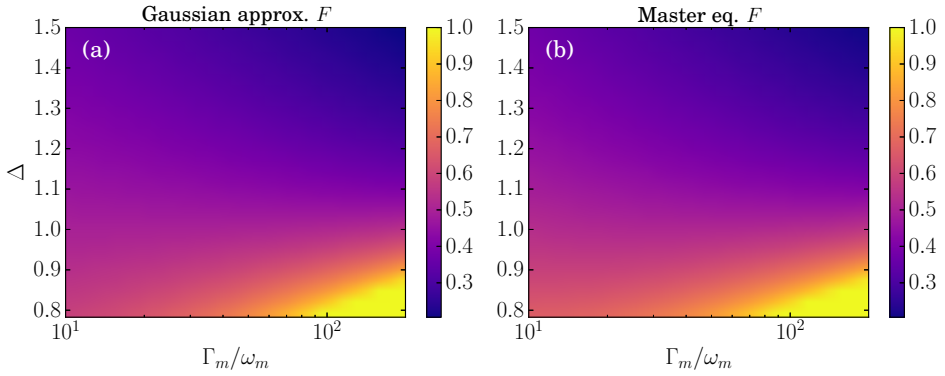

Figure 3.6.3: Fano factor F as a function of the mechanical damping Γ_m/ω_m and detuning Δ/ω_m. We used the parameters $\kappa/\omega_m = 0.1$, $g/\omega_m = 0.01$, $K/\omega_m = 0.01$, $\bar{n} = 0$. (a) shows the Gaussian approximation and (b) the numerical solution of the master equation. The Fano factor is only plotted from zero to one as this is the range where we find non-classical states.

4 Duffing oscillator

In the last section we studied the system composed of a mechanical oscillator with intrinsic mechanical Kerr-nonlinearity coupled to a driven cavity. In this section we want to illustrate that this Kerr-nonlinearity can be derived as a rotating wave approximation of a Duffing type nonlinearity.

For weak nonlinearity λ, the Hamiltonian of an uncoupled Duffing oscillator mode is given by [19]

$$H = \omega_m b^\dagger b + \frac{\lambda}{4}(b + b^\dagger)^4, \tag{4.0.1}$$

where $b, b^\dagger$ are the annihilation and creation operators, respectively. Such a nonlinearity might be an intrinsic property of the oscillator, e.g. if the stiffness of a spring does not exactly obey Hooke's law. There are many possible physical realizations of the Duffing oscillator such as suspended mechanical beams [33], nanowires [34] or nanotubes [35].

To find our Kerr Hamiltonian we change into a rotating frame with the unitary transformation $U = e^{i\omega b^\dagger b t}$. Using the bosonic commutation relations and neglecting the fast rotating terms $\sim e^{\pm 2i\omega b^\dagger b t}$ leads to the Hamiltonian

$$H = \left(\omega_m - \omega + \frac{3\lambda}{2}\right) b^\dagger b + \frac{3\lambda}{2}(b^\dagger b)^2. \tag{4.0.2}$$

We define the Kerr-nonlinearity $K = \frac{3\lambda}{2}$ and the frequency $\omega_m' = \omega_m + K$. Changing back into the non-rotating frame, we arrive at the Hamiltonian for the oscillator with Kerr-nonlinearity

$$H = \omega_m' b^\dagger b + K(b^\dagger b)^2. \tag{4.0.3}$$

The rotating wave approximation is only valid if the perturbation of the Duffing term is small compared to the Hamiltonian of the harmonic oscillator. In a mean-field approach we can introduce a small deviation operator d [36]

$$d = b^\dagger b - \langle b^\dagger b \rangle . \tag{4.0.4}$$

We can then neglect second-order terms in d which leads to

$$H = (\omega_m + K)d + 2K \langle b^\dagger b \rangle d. \tag{4.0.5}$$

Here we did not explicitly write the constant terms as they only contribute to a shift in the energy. The rotating wave approximation is valid for $K \ll \omega_m$ and $2K \langle b^\dagger b \rangle \ll \omega_m$. Note that in this regime we can write $\omega_m' \approx \omega_m$. For the system in the last section, i.e. a mechanical oscillator coupled to a driven cavity, we find the condition in the steady-state

$$2K \langle b^\dagger b \rangle \approx 2K \langle B^2 \rangle_W = \Delta - \omega_m + K + \kappa\sqrt{C-1} \ll \omega_m. \tag{4.0.6}$$

Previously we found the lowest Fano factor for large detuning Δ, but the rotating wave approximation is only valid up to $\Delta \approx \omega_m$. For small nonlinearity $K \ll \omega_m$ and Δ equal to the mechanical frequency, the condition simplifies to $\kappa\sqrt{C-1} \ll \omega_m$.

Let us now compare our analytical result with the numerical solution to the system with Duffing-nonlinearity. We used 50 mechanical and three cavity states, truncating the Fock space around the expected mean value. In Fig. 4.0.4 we plot the absolute error of the mean and variance of B^2 as a function of the cooperativity C and decay rate κ/ω_m. Note that we only show the relative error up to 30 percent. For the plots we used the (non-constant) coupling strength and nonlinearity $g = K = 0.1\kappa$ and zero temperature, i.e. $\bar{n} = 0$. As expected, the

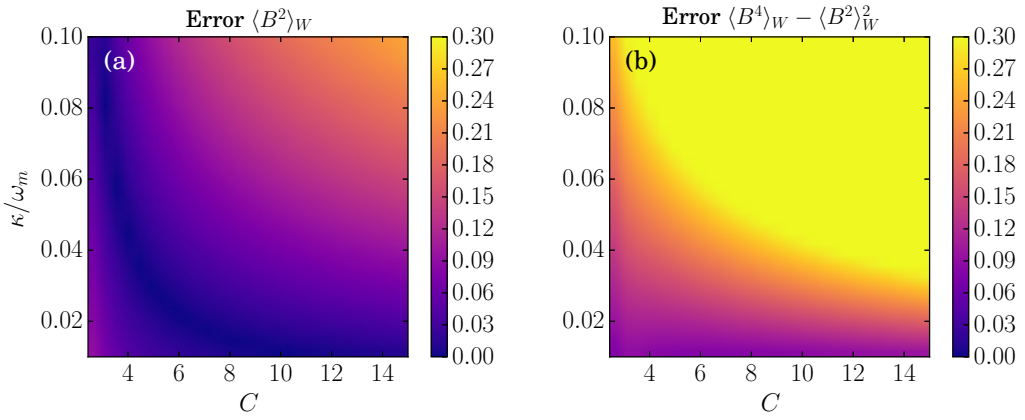

Figure 4.0.4: Comparison between the Kerr and Duffing Hamiltonian. We plot the relative error of the mean $\langle B^2\rangle_W$ (a) and the variance $\langle B^4\rangle_W - \langle B^2\rangle_W^2$ (b) as a function of the cooperativity C/ω_m and decay rate κ/ω_m. We used the parameters $\bar{n} = 0$, $g = K = 0.1\kappa$. The mechanical damping is given by $\Gamma_m = g^2/(\kappa C)$. We only plot the relative error up to 30 percent.

analytical result for the system with Kerr-nonlinearity agrees with the numerical result of the Duffing oscillator for small κ/ω_m and C.

In Fig. 4.0.5 we plot the Fano factor of each system. Again we find good agreement for small κ/ω_m and C. While the Fano factor is generally larger than in the case of Kerr-nonlinearity, we still find regions with non-classical states.

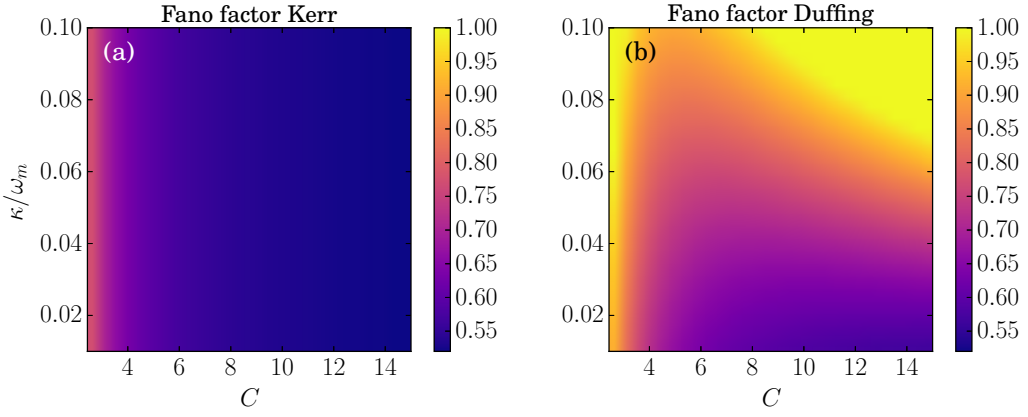

Figure 4.0.5: Fano factor of the Kerr (a) and Duffing (b) Hamiltonian as a function of the cooperativity C and decay rate κ. We used the parameters $\bar{n} = 0$, $g = K = 0.1\kappa$. The mechanical damping is given by $\Gamma_m = g^2/(\kappa C)$.

5 Two lasers

In Section 3 we coupled a bosonic oscillator mode with intrinsic Kerr-nonlinearity to a driven cavity. We found a steady-state solution for the mechanical amplitude and a description for the phase. Furthermore we derived an approximation of the mechanical oscillator's Fano factor. We showed that a Fano factor smaller than 1, which implies non-classical states, is achievable for a wide range of parameters. Unfortunately, the Fano factor scales with the temperature of the oscillator, i.e. with the mean phonon number $\bar{n}$ of the bath. Even for low temperatures this could lead to a Fano factor above 1. Therefore we suggest to use additional cooling. This can for example be done with cryogenic cooling or radiation pressure cooling, where the oscillator is cooled via optically induced damping from a red-detuned laser. This is why we now add a second laser to our system. Furthermore it turns out that the approximation of the Duffing-nonlinearity as a Kerr-nonlinearity in this system is satisfied even for large cooperativity, which is not the case for one cavity driven by one laser.

In this section we will look at two systems. First we couple two independent driven cavities, one red-detuned and one blue-detuned, to our mechanical oscillator with Kerr-nonlinearity. We will again derive an expression for the amplitude diffusion of the mechanical oscillator and find its steady-state solution.

In practice it might be easier to implement a system with only one cavity driven by two different lasers. This gives rise to new terms in the optically induced damping and diffusion.

5.1 Two independent cavities

Let us first couple a bosonic mechanical mode to two independent cavities c_1, c_2 driven by two different lasers. The first laser is assumed to be blue-detuned and the laser in the second cavity red-detuned, i.e. $\Delta_1 > 0 > \Delta_2$. The second laser will then induce (positive) mechanical damping and the first laser anti-damping. Figure 5.1.1 shows a schematic illustration of this system which we describe with the linearized optomechanical Hamiltonian with Kerr-nonlinearity

$$\begin{aligned} H &= H_m + H_K + \sum_{i=1,2} H_{c_i} + \sum_{i=1,2} H_{\mathrm{int}_i} \\ &= \omega_m b^\dagger b + K(b^\dagger b)^2 - \sum_{i=1,2} \Delta_i a_i^\dagger a_i - \sum_{i=1,2} g(a_i + a_i^\dagger)(b + b^\dagger), \end{aligned} \tag{5.1.1}$$

where $a_i, a_i^\dagger (i = 1, 2)$ denote the annihilation and creation operators of the two cavities. Note that since the two cavities are assumed to be independent, a_1 and a_2 operators commute with each other. Taking temperature into account, our system is described by the master equation

$$\dot{\rho} = -i[H, \rho] + \mathcal{L}_m \rho + \mathcal{L}_{c_1} \rho + \mathcal{L}_{c_2} \rho, \tag{5.1.2}$$

where the dissipators are defined in Eq. (3.1.4) with a_i instead of a for the cavity c_i. For simplicity we assume that both cavities have the same decay rate κ and coupling constant g. The following calculations could be done similarly if this were not the case.

Our goal is to find an expression for the amplitude diffusion. We follow the same approach as in Section 3. We rewrite the master equation as a partial differential equation for the Wigner function. After a system size expansion, i.e. neglecting the third-order derivatives, we can rewrite the quasi Fokker-Planck equation as Langevin equations for the optical and mechanical random variables:

$$\begin{aligned} \dot{\alpha}_1 &= (i\Delta_1 - \kappa)\alpha_1 + ig(\beta + \beta^*) + \sqrt{\kappa}\eta_{\alpha_1}, \\ \dot{\alpha}_2 &= (i\Delta_2 - \kappa)\alpha_2 + ig(\beta + \beta^*) + \sqrt{\kappa}\eta_{\alpha_2}, \\ \dot{\beta} &= \big(- i\omega_m - iK(2|\beta|^2 - 1) - \Gamma_m\big)\beta + ig(\alpha_1 + \alpha_1^*)\text{"} + ig(\alpha_2 + \alpha_2^*) + \sqrt{\Gamma_m(2\bar{n} + 1)}\eta_\beta. \end{aligned} \tag{5.1.3}$$

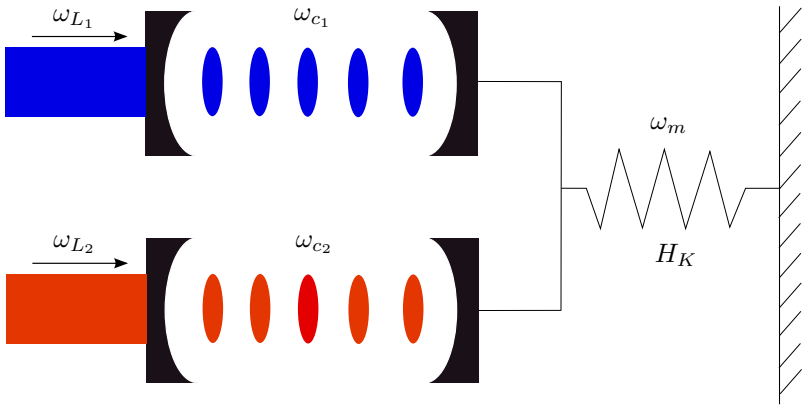

Figure 5.1.1: Schematic illustration of the optomechanical setup with Kerr Hamiltonian H_K. ω_{L_1}, ω_{L_2} are the driving frequencies, ω_{c_1}, ω_{c_2} are the cavity frequencies and ω_m is the mechanical frequency.

Here $\eta_{\alpha_1}, \eta_{\alpha_2}$ are independent complex white-noise processes. We make the same assumptions as in the last section, i.e. $\kappa \gg g, \Gamma_m$. Therefore we can again use the ansatz

$$\beta = Be^{-i\phi}e^{-i\omega_m(B)t} \quad \text{with} \quad \omega_m(B) = \omega_m + 2KB^2 - K. \tag{5.1.4}$$

We find solution to α_i $(i = 1, 2)$ by adiabatic elimination

$$\alpha_i = igB\left(\frac{e^{-i\phi}e^{-i\omega_m(B)t}}{-i\omega_m(B) - i\Delta_i + \kappa} + \frac{e^{i\phi}e^{i\omega_m(B)t}}{i\omega_m(B) - i\Delta_i + \kappa}\right) + \mathcal{F}^{-1}\left[\frac{\sqrt{\kappa}\eta_{\alpha_i}(\omega)}{i\omega - i\Delta_i + \kappa}\right]. \tag{5.1.5}$$

We insert this into the equation of motion for β and make a rotating wave approximation. Taking the radial (real) part of the resulting equation we find

$$\dot{B} = -(\Gamma_m + \Gamma_{\text{opt}})B + \eta_T^-, \tag{5.1.6}$$

where $\Gamma_{\text{opt}}, \eta_T^-$ are similar as in Eqs. (3.2.6), (3.2.8) but with contributions from cavity one and two

$$\Gamma_{\text{opt}} = g^2\kappa \sum_{i=1,2}\left(\frac{1}{(\Delta_i + \omega_m(B))^2 + \kappa^2} - \frac{1}{(\Delta_i - \omega_m(B))^2 + \kappa^2}\right). \tag{5.1.7}$$

The drift term is just the deterministic part of the equation of motion

$$A_B = -(\Gamma_m + \Gamma_{\text{opt}})B. \tag{5.1.8}$$

The effective amplitude diffusion is found the same way as in Section 3.3. Since η_{α_1} and η_{α_2} are independent complex white-noise processes, the amplitude diffusion will take the same form as in Eq. (3.3.20) but with contributions from both cavities

$$D_B = \frac{g^2\kappa}{2} \sum_{i=1,2}\left(\frac{1}{(\Delta_i + \omega_m(B))^2 + \kappa^2} + \frac{1}{(\Delta_i - \omega_m(B))^2 + \kappa^2}\right). \tag{5.1.9}$$

As an illustration we plot the optically induced damping and diffusion as a function of the amplitude in Fig. 5.1.2. We used the parameters $\kappa/\omega_m = 0.1$, $g/\omega_m = 0.01$, $K/\omega_m = 0.1$. The

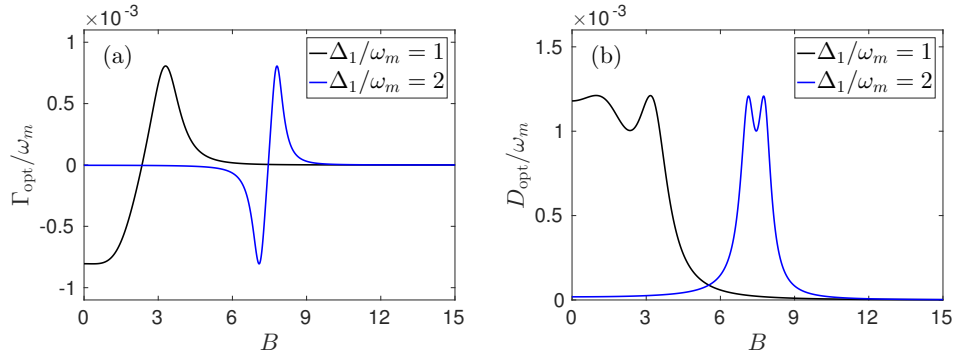

Figure 5.1.2: Optically induced damping (a) and diffusion (b) as a function of the amplitude B. The used parameters are $\kappa/\omega_m = 0.1$, $g/\omega_m = 0.01$, $K/\omega_m = 0.01$, $\Delta_2 = \Delta_1 - 2\kappa$. We choose a large detuning $\Delta_1/\omega_m = 2$ to illustrate the Lorentzian-like peaks.

detuning of the first laser is $\Delta_1/\omega_m = 1$ and $\Delta_1/\omega_m = 2$, respectively. The second laser is detuned by $\Delta_2 = -\Delta_1 - 2\kappa$.

We are interested in a limit cycle solution where the average amplitude B_0 is the non-zero solution to $A_B(B_0) = -(\Gamma_m + \Gamma_{\rm opt}(B_0))B_0 = 0$. We approximate the optically induced damping by dropping the non-resonant terms, i.e.

$$\Gamma_{\rm opt}(B_0) \approx g^2\kappa \left(\frac{-1}{(\omega_m(B_0) - \Delta_1)^2 + \kappa^2} + \frac{1}{(\omega_m(B_0) + \Delta_2)^2 + \kappa^2} \right). \tag{5.1.10}$$

As one can see from Eq. (5.1.10) we now have (positive) optically induced damping from cavity two. Assuming that this contribution is much larger than Γ_m at $B = B_0$, we can neglect the mechanical damping. This condition is satisfied for $C = \frac{g^2}{\kappa\Gamma_m} \gg 1$. We find the average amplitude

$$B_0 = \frac{1}{2}\sqrt{\frac{\Delta_1 - \Delta_2 - 2\omega_m + 2K}{K}}, \tag{5.1.11}$$

with the condition $\Delta_1 - \Delta_2 - 2\omega_m + 2K > 0$. The fixpoint B_0 is only stable if $|\Delta_1| < |\Delta_2|$ and therefore only then can we find a limit cycle. In the following part of this section we will assume this condition to be satisfied.

As in the last section we approximate the steady-state solution of the amplitude distribution as a Gaussian centered at B_0. This is done by assuming small amplitude fluctuations δB around B_0 and the diffusion to be approximately constant at B_0. We neglect the mechanically induced diffusion term $\frac{1}{2}\Gamma_m(2\bar{n}+1)$. This is valid for large cooperativity and small temperatures. In this limit we can also drop the non-resonant terms in the optically induced diffusion term $D_{\rm opt}(B_0)$

$$D_B(B_0) = \frac{g^2\kappa}{2}\left(\frac{1}{(\omega_m(B_0) - \Delta_1)^2 + \kappa^2} + \frac{1}{(\omega_m(B_0) + \Delta_2)^2 + \kappa^2} \right) \equiv \frac{1}{2} D_{\rm opt}(B_0). \tag{5.1.12}$$

With the definitions

$$\Delta_+ = \Delta_1 + \Delta_2, \qquad \Delta_- = \Delta_1 - \Delta_2 - 2\omega_m + 2K, \tag{5.1.13}$$

the variance of the Gaussian distribution is then given by

$$\begin{aligned} \sigma^2 &= \frac{D_{\rm opt}(B_0)}{4B_0 \left.\frac{d\Gamma_{\rm opt}}{dB}\right|_{B=B_0}} = -\frac{1}{16}\frac{(\Delta_1 + \Delta_2)^2 + 4\kappa^2}{(\Delta_1 - \Delta_2 - 2\omega_m + 2K)(\Delta_1 + \Delta_2)} \\ &= -\frac{1}{16}\frac{\Delta_+^2 + 4\kappa^2}{\Delta_+\Delta_-}. \end{aligned} \tag{5.1.14}$$

The Fano factor of the mechanical system can again be approximated as $F = 4\sigma^2$. With respect to $\Delta_+ = \Delta_1 + \Delta_2$ the variance is minimized for $\frac{\mathrm{d}\sigma^2}{\mathrm{d}\Delta_+} = 0$, i.e.

$$\Delta_1 + \Delta_2 = \pm 2\kappa. \tag{5.1.15}$$

Note that Δ_- is positive since this is the condition to find the fixpoint B_0. Δ_+ must therefore be negative, otherwise we would get a negative variance. This coincides with our earlier assumption $|\Delta_1| < |\Delta_2|$. Only then can we approximate the steady-state solution with a Gaussian distribution since otherwise we will not find a limit cycle. We therefore take the solution with the negative sign, i.e. $\Delta_1 + \Delta_2 = -2\kappa$. We find the minimal variance with respect to Δ_+

$$\sigma^2 = \frac{\kappa}{8(\Delta_1 - \omega_m + \kappa + K)}. \tag{5.1.16}$$

The minimal achievable Fano factor is then given by

$$F = 4\sigma^2 = \frac{\kappa}{2(\Delta_1 - \omega_m + \kappa + K)}. \tag{5.1.17}$$

We find squeezed number states for $F < 1$. This is achieved for a wide set of parameters. For $\Delta_1 \geq \omega_m$ we find non-classical states for any values of κ and K as long as the cooperativity is large enough. In the case of small nonlinearities $K \ll \kappa$ the Fano factor is again approximately independent of K.

In Section 3.5 we derived the Fano factor of the system with one cavitiy and one laser in Eq. (3.5.6). We found $F = \frac{1}{2}$ for zero temperature and large cooperativity. Here we can achieve a Fano factor close to zero by increasing the detuning. Note that again our limit cycle will not start if Δ_1 is too large. Another advantage of this system is that the approximation of the Duffing-nonlinearity as a Kerr-nonlinearity is satisfied independent of the cooperativity. We find the condition

$$2K \langle b^\dagger b \rangle \approx 2K \langle B^2 \rangle_W = \Delta_1 - \omega_m + \kappa + K \ll \omega_m. \tag{5.1.18}$$

For small nonlinearity $K \ll \omega_m$ the rotating wave approximation of the Duffing oscillator is valid for $\Delta_1 - \omega_m + \kappa \ll \omega_m$. Compared to the system with one cavity we have no dependence on the cooperativity. Our analytical description is therefore valid for a larger set of parameters than in the system with one cavity.

Let us now compare our analytical solution of the steady-state to numerical results (for the oscillator with Kerr-nonlinearity). In Fig. 5.1.3 we plot the mean and variance of B^2 as a function of the decay rate κ/ω_m and detuning Δ_1/ω_m. We used three states for each cavity and 40 states for the mechanical oscillator, truncating the Fock space around the expected mean value. The second laser is detuned by $\Delta_2 = -\Delta_1 - 2\kappa$. We used the effective coupling constant $g/\omega_m = 0.01$ and Kerr-nonlinearity $K/\omega_m = 0.01$. The mechanical damping is assumed to be weak with $\Gamma_m/\omega_m = 10^{-5}$ which leads to a cooperativity of $C = 100$. We find excellent agreement for the mean value $\langle B^2 \rangle_W$. The analytical solution of the variance $\mathrm{Var}(B^2)$ is generally too low with an error of around 10-15 percent.

We plot the relative error in Fig. 5.1.4. The highest deviations compared to the numerical solution are found for small κ/ω_m and large Δ_1/ω_m. A small contribution of around one to two percent is explained by the fact that we neglected the mechanical damping. We also assumed $\kappa \gg g$ but used $g/\kappa \sim 0.1$. The largest contribution originates from the assumption that the diffusion is constant at B_0. The diffusion in Eq. (5.1.12) is a sum of two Lorentzian-like peaks as is the optical damping in Eq. (5.1.10), the only difference is the sign of the peak at $\omega_m(B) = \Delta_1$. For $\Gamma_{\mathrm{opt}}(B_0) = 0$ we are in-between the two positive peaks of the diffusion D_B. In fact D_B takes a minimal value at B_0. This can be seen in Fig. 5.1.2(b).

The analytical Fano factor is compared with the numerical solution to the master equation in Fig. 5.1.5. We note again that the Fano factor is basically the variance of B^2 divided by its

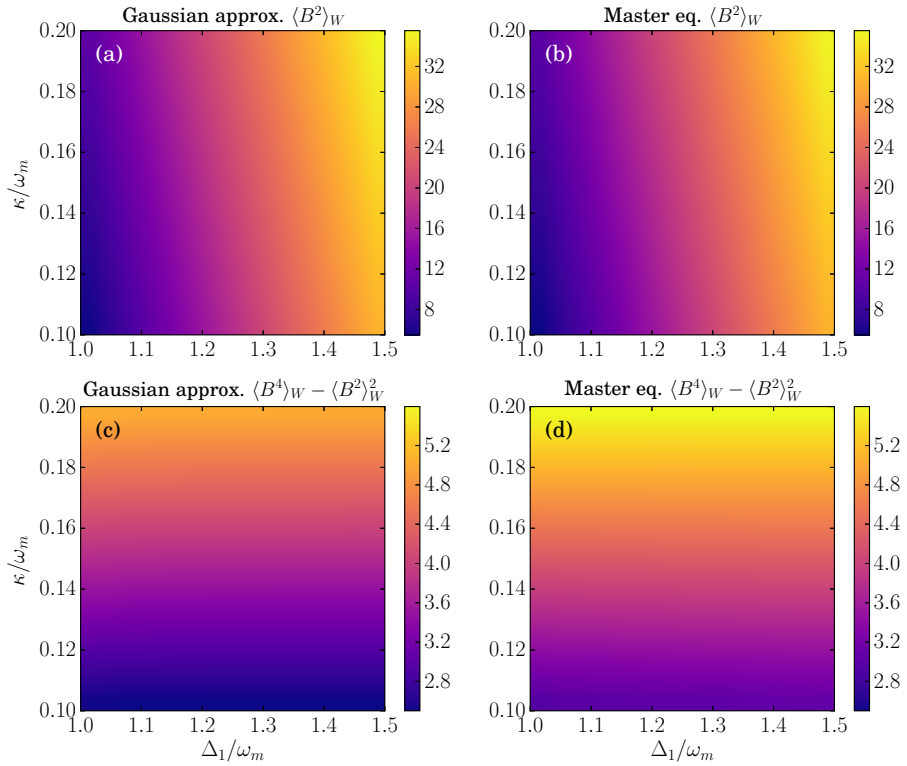

Figure 5.1.3: Mean $\langle B^2\rangle_W$ and variance $\langle B^4\rangle_W - \langle B^2\rangle_W^2$ as a function of the detuning Δ_1/ω_m and decay rate κ/ω_m. We used the parameters $g/\omega_m = 0.01$, $K/\omega_m = 0.01$, $\Gamma_m/\omega_m = 10^{-5}$, $\bar{n} = 0$. (a) and (c) show the Gaussian approximation, while (b) and (d) show the numerical solution of the master equation.

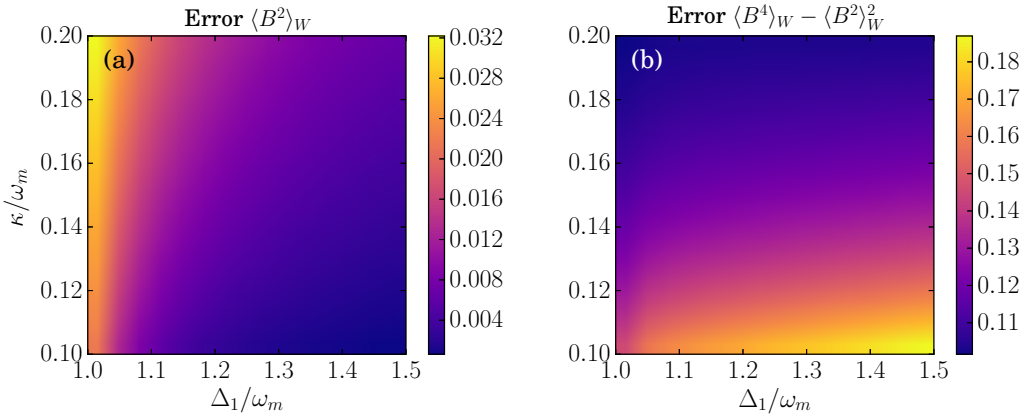

Figure 5.1.4: Relative error of the Gaussian approximated mean $\langle B^2\rangle_W$ (a) and variance $\langle B^4\rangle_W - \langle B^2\rangle_W^2$ (b) as a function of the detuning Δ_1/ω_m and decay rate κ/ω_m. We used the parameters $g/\omega_m = 0.01$, $K/\omega_m = 0.01$, $\Gamma_m/\omega_m = 10^{-5}$, $\bar{n} = 0$.

mean. We therefore find similar errors as in Fig. 5.1.4. F is smaller than 1 for all values of Δ_1 and κ. Highly non-classical states with a Fano factor of around 0.1 are achieved for large detunings.

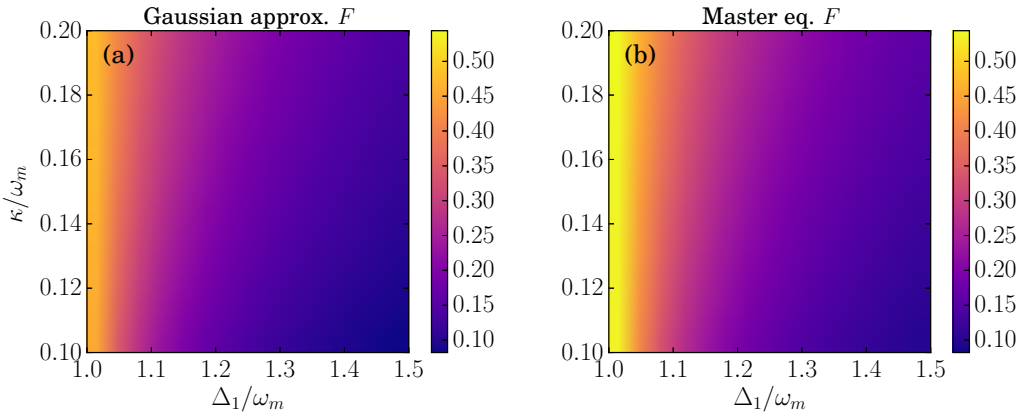

Figure 5.1.5: Fano factor F as a function of the detuning Δ_1/ω_m and decay rate κ/ω_m. We used the parameters $g/\omega_m = 0.01$, $K/\omega_m = 0.01$, $\Gamma_m/\omega_m = 10^{-5}$, $\bar{n} = 0$. (a) shows the Gaussian approximation and (b) the numerical solution of the master equation.

5.2 One Cavity

We derived the Fano factor for a system with two cavities and two lasers. In our calculations we assumed the two cavities to be independent. In practice it might be easier to implement a similar system where we use only one cavity driven by two lasers L_1, L_2. We will derive an expression for the amplitude diffusion of this system and discuss the new terms.

In Fig. 5.2.1 we show a schematic illustration of this system which is described by the master equation

$$\dot{\rho} = -i[H, \rho] + \mathcal{L}_m\rho + \mathcal{L}_c\rho, \tag{5.2.1}$$

where the dissipators are defined in Eq. (3.1.4). The (non-linearized) Hamiltonian is given by

$$\begin{aligned} H =& H_c + H_m + H_{int} + H_K + H'_D = \omega_c a^\dagger a + \omega_m b^\dagger b - g_0 a^\dagger a(b + b^\dagger) + K(b^\dagger b)^2 \\ &+ E_1(ae^{i\omega_{L_1}t} + a^\dagger e^{-i\omega_{L_1}t}) + E_2(ae^{i\omega_{L_2}t} + a^\dagger e^{-i\omega_{L_2}t}), \end{aligned} \tag{5.2.2}$$

where H'_D denotes the driving Hamiltonian with amplitudes E_1, E_2 and laser frequencies $\omega_{L_1}, \omega_{L_2}$. The Hamiltonian cannot be linearized in the same fashion as in the case with one laser, since the second laser has a different frequency than the first one. This leads to a time dependence that we cannot get rid of. Instead we change into the rotating frame of the cavity with $U = e^{i\omega_c a^\dagger a t}$. According to the transformation rule in Eq. (2.1.5) this will cancel out H_c and change the driving Hamiltonian to

$$H_D = E_1(ae^{i\Delta_1 t} + a^\dagger e^{-i\Delta_1 t}) + E_2(ae^{i\Delta_2 t} + a^\dagger e^{-i\Delta_2 t}), \tag{5.2.3}$$

with laser detunings $\Delta_i = \omega_{L_i} - \omega_c$ $(i = 1, 2)$.

To calculate the amplitude diffusion we follow the same approach as in the earlier sections. We rewrite the master equation as a partial differential equation for the Wigner function. Neglecting

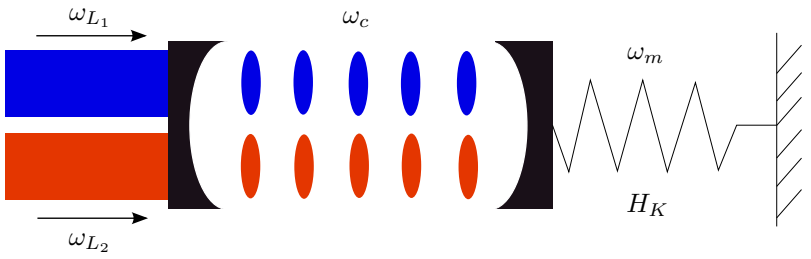

Figure 5.2.1: Schematic illustration of the optomechanical setup with Kerr Hamiltonian H_K. ω_{L_1}, ω_{L_2} are the driving frequencies, ω_c is the cavity frequency and ω_m is the mechanical frequency.

third-order derivatives in a system size expansion, we find the corresponding Langevin equations

$$\begin{aligned}\dot{\alpha} &= -\kappa\alpha + ig_0(\beta+\beta^*)\alpha - i(E_1 e^{-i\Delta_1 t} + E_2 e^{-i\Delta_2 t}) + \sqrt{\kappa}\eta_\alpha, \\ \dot{\beta} &= (-i\omega_m - iK[2|\beta|^2 - 1] - \Gamma_m)\beta + ig_0\left(|\alpha|^2 - \frac{1}{2}\right) + \sqrt{\Gamma_m(2\bar{n}+1)}\eta_\beta,\end{aligned} \tag{5.2.4}$$

where η_α, η_β are complex white-noise processes and g_0 is the single-photon coupling constant. Note that for the linearization of the optomechanical system in Sec 2.1 we introduced a displacement of the oscillator position x. This shift is not yet taken care of in our Hamiltonian (5.2.2) and Langevin equations (5.2.4). We include this displacement β_c in the ansatz for the oscillator variable β

$$\beta = \beta_c + Be^{-i\omega_m(B)t}e^{-i\phi}, \quad \text{with} \quad \omega_m(B) = \omega_m + 2KB^2 - K, \tag{5.2.5}$$

where $\phi(t)$ and $B(t)$ are assumed to be slowly varying functions in time compared to α. We will again solve for α by adiabatic elimination. Note that the equation for $\dot{\alpha}$ has the form

$$\dot{\alpha}(t) = \lambda(t)\alpha(t) + F(t), \tag{5.2.6}$$

with

$$\begin{aligned}\lambda(t) &= -\kappa + ig_0(\beta+\beta^*), \\ F(t) &= -i(E_1 e^{-i\Delta_1 t} + E_2 e^{-i\Delta_2 t}) + \sqrt{\kappa}\eta_\alpha.\end{aligned}$$

Equation (5.2.6) has the long-time solution (for $\kappa > 0$)

$$\alpha(t) = \int_{-\infty}^{t} \mathrm{d}t' \exp\left(\int_{t'}^{t} \mathrm{d}\tilde{t}\lambda(\tilde{t})\right) F(t'). \tag{5.2.7}$$

We can calculate this integral explicitly by using the identity

$$e^{ix\sin(y)} = \sum_{n=-\infty}^{\infty} e^{iny} J_n(x), \tag{5.2.8}$$

where J_n denotes the n-th Bessel function. We split $\alpha(t) = \langle\alpha(t)\rangle + \delta\alpha(t)$ into a deterministic and a stochastic part with zero mean. The solution to the deterministic part is given by

$$\langle\alpha(t)\rangle = e^{i\varphi(t)} \sum_{n=-\infty}^{\infty} \alpha_n e^{in(\omega_m(B)t+\phi)}, \tag{5.2.9}$$

where we introduced the global phase

$$\varphi(t) = z\sin(\omega_m(B)t + \phi), \tag{5.2.10}$$

with the small parameter

$$z = \frac{2Bg_0}{\omega_m(B)}. \tag{5.2.11}$$

The sum coefficients are given by

$$\alpha_n = -iJ_n(-z)\left(\frac{E_1 e^{-i\Delta_1 t}}{in\omega_m(B) - i\tilde{\Delta}_1 + \kappa} + \frac{E_2 e^{-i\Delta_2 t}}{in\omega_m(B) - i\tilde{\Delta}_2 + \kappa}\right), \tag{5.2.12}$$

furthermore we defined the shifted detuning

$$\tilde{\Delta}_i = \Delta_i + 2g_0\mathrm{Re}[\beta_c]. \tag{5.2.13}$$

Note that in the following part we will write Δ instead of $\tilde{\Delta}$. Since z is assumed to be small we will approximate $\langle\alpha\rangle$ with its first-order Taylor expansion in z. We find

$$\langle\alpha(t)\rangle = -ie^{i\varphi(t)}\sum_{j=1,2} E_j e^{-i\Delta_j t}\left(\frac{1}{h_{j,0}} - \frac{z}{2}\frac{e^{i(\omega_m(B)t+\phi)}}{h_{j,1}} + \frac{z}{2}\frac{e^{-i(\omega_m(B)t+\phi)}}{h_{j,-1}}\right), \tag{5.2.14}$$

where we defined for simplification

$$h_{j,n} = in\omega_m(B) - i\Delta_j + \kappa. \tag{5.2.15}$$

Note that we did not approximate the phase factor $e^{i\varphi(t)}$ even though it depends on z since it will cancel out in the equation of motion for β. The stochastic part of α is given by

$$\delta\alpha(t) = e^{i\varphi(t)}\mathcal{F}^{-1}\left[\frac{e^{-iz\sin(\omega_m(B)t+\phi)}\eta_\alpha(\omega)}{i\omega + \kappa - 2ig_0\mathrm{Re}[\beta_c]}\right]. \tag{5.2.16}$$

Let us now solve for the mechanical oscillator variable β. In its equation of motion the interaction term is given by $ig_0\left(|\alpha|^2 - \frac{1}{2}\right)$. Since we split α into a deterministic and a stochastic part we find

$$|\alpha|^2 = \langle\alpha\rangle\langle\alpha^*\rangle + \langle\alpha\rangle\delta\alpha^* + \langle\alpha^*\rangle\delta\alpha + \delta\alpha\delta\alpha^*. \tag{5.2.17}$$

We assume $\delta\alpha$ to be small but do not neglect the term $\sim\delta\alpha\delta\alpha^*$ since this would lead to a term $-\frac{1}{2}ig_0$ in the equation of motion. Instead we approximate it by its average $\langle\delta\alpha(t)\delta\alpha^*(t)\rangle = \frac{1}{2}$ which cancels out the other term. Using this and Eq. (5.2.4) we obtain the equation of motion of the oscillating part $\tilde{\beta} = \beta - \beta_c$

$$\dot{\tilde{\beta}} = (-i\omega_m(B) - \Gamma_m)(\tilde{\beta} + \beta_c) + ig_0\big(\langle\alpha\rangle\langle\alpha^*\rangle + \langle\alpha\rangle\delta\alpha^* + \langle\alpha^*\rangle\delta\alpha\big) + \sqrt{\Gamma_m(2\bar{n}+1)}\eta_\beta. \tag{5.2.18}$$

Note that we neglected the small shift β_c in the Kerr term assuming that we have large steady-state amplitudes. For the further calculations we have to make assumptions about the detunings since otherwise we cannot perform a rotating wave approximation. Motivated by Section (5.1), where for the system with two cavities we found $\Delta_1 - \Delta_2 = 2\omega_m(B_0)$, we will now assume that $\Delta_1 - \Delta_2 = 2\omega_m(B) + \delta$, where $|\delta| \ll \omega_m$ is a small deviation from the effective frequency. Let us now look at the term $\langle\alpha\rangle\langle\alpha^*\rangle$. We neglect the terms of second and higher order in z since it is a small parameter. Since $\tilde{\beta}$ approximately rotates with $\omega_m(B)$ we neglect the terms

$\sim ze^{-i(\omega_m(B)-\Delta\omega)t}$ and $\sim ze^{i\Delta\omega t}$ with $\Delta\omega \gtrsim \omega_m(B)$ in a rotating wave approximation. We are left with

$$\begin{aligned}\langle\alpha\rangle\langle\alpha^*\rangle = &\sum_{j=1,2}\frac{E_j^2}{|h_{j,0}|^2} + \sum_{j=1,2}E_j^2 e^{-i(\omega_m(B)t+\phi)}\frac{z}{2}\left(\frac{1}{h_{j,-1}h_{j,0}^*} - \frac{1}{h_{j,0}h_{j,1}^*}\right)\\ &+ E_1E_2e^{-i(\Delta_1-\Delta_2)}e^{i(\omega_m(B)t+\phi)}\frac{z}{2}\left(\frac{1}{h_{1,0}h_{2,-1}^*} - \frac{1}{h_{1,1}h_{2,0}^*}\right)\\ &+ \frac{E_1E_2}{h_{1,0}h_{2,0}^*}e^{-i(\Delta_1-\Delta_2)t} + \frac{E_2E_1}{h_{2,0}h_{1,0}^*}e^{-i(\Delta_2-\Delta_1)t}.\end{aligned} \tag{5.2.19}$$

The first term in this expression does not rotate. It is therefore responsible for the shift β_c since this is the only other constant term in Eq. (5.2.18). We find

$$\beta_c = \frac{g_0}{\omega_m - i\Gamma_m}\sum_{j=1,2}\frac{E_j^2}{|h_{j,0}|^2} = \frac{g_0}{\omega_m - i\Gamma_m}\sum_{j=1,2}\frac{E_j^2}{\Delta_j^2+\kappa^2}. \tag{5.2.20}$$

The second and third term in Eq. (5.2.19) rotate with $\sim\omega_m(B)$ and are proportional to B (note that $z\sim B$). They give rise to the optically induced damping and frequency shift

$$-i\delta\omega - \Gamma_{\text{opt}} = F_{\text{same}} + F_{\text{mix}}, \tag{5.2.21}$$

where we defined a contribution from the same lasers

$$F_{\text{same}} = i\sum_{j=1,2}E_j^2\frac{g_0^2}{\omega_m(B)}\left(\frac{1}{h_{j,-1}h_{j,0}^*} - \frac{1}{h_{j,0}h_{j,1}^*}\right) \tag{5.2.22}$$

and a mixed contribution

$$F_{\text{mix}} = iE_1E_2e^{-i\delta t}e^{2i\phi}\frac{g_0^2}{\omega_m(B)}\left(\frac{1}{h_{1,0}h_{2,-1}^*} - \frac{1}{h_{1,1}h_{2,0}^*}\right). \tag{5.2.23}$$

Note that the h-terms were defined in Eq. (5.2.15). The term F_{same} leads to the same optically induced frequency shift and damping as for the system with two independent cavities if we write $g = g_0\sqrt{n_{\text{cav}}}$ with the assumption

$$n_{\text{cav}} = \frac{E_1^2}{\Delta_1^2+\kappa^2} = \frac{E_2^2}{\Delta_2^2+\kappa^2}. \tag{5.2.24}$$

Having two lasers in one cavity leads to a new term F_{mix} that is dependent on the phase ϕ of the oscillator. We discuss this later when we compare with the numerical solution. The last two terms in Eq. (5.2.19) give rise to a time dependent force term $f(t)$

$$f(t) = \frac{E_1E_2}{h_{1,0}h_{2,0}^*}e^{-i(\Delta_1-\Delta_2)t} + \frac{E_1E_2}{h_{2,0}h_{1,0}^*}e^{-i(\Delta_2-\Delta_1)t}. \tag{5.2.25}$$

Even though this term rotates with $\sim 2\omega_m(B)$ we cannot necessarily neglect it as its amplitude can be large. We insert the solution α into the equation of motion (5.2.18). With the introduced definitions of optical damping, frequency shift and force term f the equation reads

$$\dot{\tilde{\beta}} = -i(\omega_m(B)+\delta\omega)\tilde{\beta} - (\Gamma_m+\Gamma_{\text{opt}})\tilde{\beta} + ig_0(\langle\alpha\rangle\,\delta\alpha^* + \langle\alpha^*\rangle\,\delta\alpha) + ig_0f(t) + \sqrt{\Gamma_m(2\bar{n}+1)}\eta_\beta. \tag{5.2.26}$$

Similarly to the last sections we can derive an equation of motion for the amplitude by writing $\tilde{\beta} = Be^{-i\omega_m(B)t}e^{-i\phi}$ and taking the radial part of Eq. (5.2.26). We find

$$\dot{B} = -(\Gamma_m + \Gamma_{\text{opt}})B - g_0 f(t)\sin(\omega_m(B)t + \phi) + \eta_T^-, \tag{5.2.27}$$

where we defined the noise term

$$\begin{aligned}\eta_T^- =& \frac{\sqrt{\Gamma(2\bar{n}+1)}}{2}\left(\eta_\beta e^{i(\omega_m(B)t+\phi)} + \eta_\beta^* e^{-i(\omega_m(B)t+\phi)}\right) \\ &+ \frac{ig_0}{2}\left(\langle\alpha\rangle\,\delta\alpha^* + \langle\alpha^*\rangle\,\delta\alpha\right)\left(e^{i(\omega_m(B)t+\phi)} - e^{-i(\omega_m(B)t+\phi)}\right).\end{aligned} \tag{5.2.28}$$

The amplitude diffusion D_B is found the same way as in the previous sections with Eq. (3.3.6). We neglect the rotating terms $\sim ze^{\pm i\Delta\omega t}$ with $\Delta\omega \gtrsim \omega_m(B)$ in a rotating wave approximation. Furthermore we neglect terms of second order in z. We find the amplitude diffusion

$$D_B = \frac{1}{2}(D_m + D_{\text{opt-same}} + D_{\text{opt-mix}}), \tag{5.2.29}$$

where we defined the same laser contribution to the diffusion

$$D_{\text{opt-same}} = g_0^2\kappa\left(\frac{E_1^2}{\Delta_1^2+\kappa^2}\frac{1}{(\omega_m(B)-\Delta_1)^2+\kappa^2} + \frac{E_2^2}{\Delta_2^2+\kappa^2}\frac{1}{(\omega_m(B)+\Delta_2)^2+\kappa^2}\right) \tag{5.2.30}$$

and the mixed laser contribution

$$\begin{aligned}D_{\text{opt-mix}} =& -\frac{g_0^2\kappa}{2}\left(\frac{E_1E_2}{h_{1,0}h_{2,0}^*}\frac{e^{-i(\Delta_1-\Delta_2)t}e^{2i(\omega_m(B)t+\phi)}}{(\omega_m(B)+\Delta_2)^2+\kappa^2}\right. \\ &\left. + \frac{E_1E_2}{h_{2,0}h_{1,0}^*}\frac{e^{-i(\Delta_2-\Delta_1)t}e^{-2i(\omega_m(B)t+\phi)}}{(\omega_m(B)-\Delta_1)^2+\kappa^2} + \text{h.c.}\right).\end{aligned} \tag{5.2.31}$$

Note that we dropped the non-resonant terms. With the condition in Eq. (5.2.24), $D_{\text{opt-same}}$ is equal to the amplitude diffusion in the case of two independent cavities. Having both lasers in one cavity gives rise to the new term $D_{\text{opt-mix}}$. This term is dependent on the phase of the oscillator which is why we cannot proceed as in the earlier sections.

This system needs further studying. Nevertheless we now want to look at numerical results and try to interpret them. We simulated 2000 trajectories of the Langevin equations (5.2.4) with a fourth-order Runge-Kutta method [37] using MATLAB. Figure 5.2.2(a) shows the mean value $\langle B^2\rangle_W$ as a function of time. We used the parameters $g_0/\omega_m = 3\cdot 10^{-3}$, $\Delta_1/\omega_m = 1$, $\kappa/\omega_m = 0.3$, $\Gamma_m = 0$, $K/\omega_m = 0.01$, $\Delta_2 = \Delta_1 - 2\kappa$. E_1 and E_2 are chosen such that $n_{\text{cav}} = 100$ (see Eq. (5.2.24)). All trajectories start with $|\beta| = B_0$, where B_0 is the expected steady-state amplitude of the system with two cavities. The starting phase is a uniformly distributed random number on $[-\pi, \pi]$. For large times the mean value $\langle B^2\rangle_W$ periodically fluctuates around ~ 15.4 with an amplitude of around ~ 0.40. Since the mean value is averaged over all phases we expect it to be the same as in the case for two cavities, i.e. $\langle B^2\rangle_W = 15.62$. The fluctuations around this value might be explained by the additional force term $g_0 f(t)\sin(\omega_m(B)t+\phi)$ in the equation of motion (5.2.27) which has an amplitude of $0.53\omega_m$ with these parameters. In Fig. 5.2.2(b) we plot the variance of B^2 for the same parameters. It oscillates strongly and periodically around a value of ~ 12.6 with an amplitude of ~ 5.5. This behaviour cannot be explained by the model with two independent cavities where we would expect $\text{Var}(B) = 7.75$. This might be induced by the additional force term.

In our calculations we found that both the optical damping and diffusion were phase dependent. In Fig. 5.2.3 we plot the mean value and variance of B^2 as a function of the phase of β

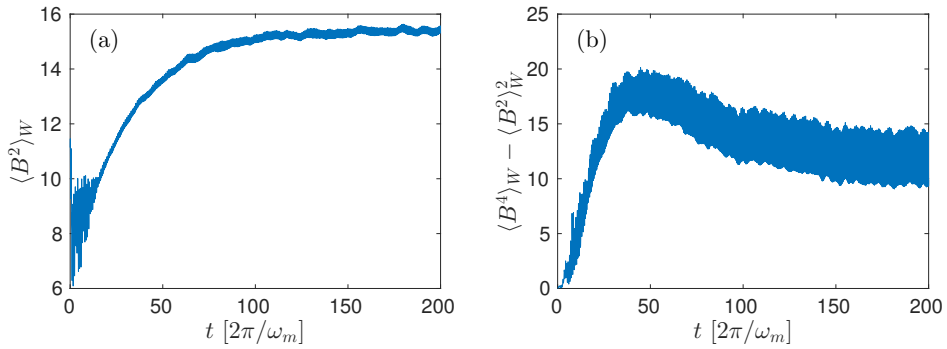

Figure 5.2.2: Simulation of the Langevin equations (5.2.4). We plot the mean value $\langle B^2\rangle_W$(a) and variance $\langle B^4\rangle_W - \langle B^2\rangle_W^2$(b) as a function of time. The used parameters are $g_0/\omega_m = 3{\cdot}10^{-3}$, $\Delta_1/\omega_m = 1$, $\kappa/\omega_m = 0.3$, $\Delta_2 = \Delta_1 - 2\kappa$, $\Gamma_m/\omega_m = 0$, $K/\omega_m = 0.01$, $n_{\text{cav}} = 100$.

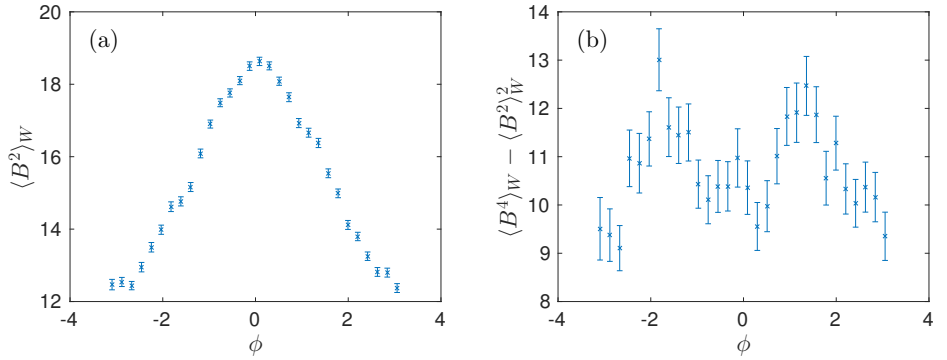

Figure 5.2.3: Simulation of the Langevin equations (5.2.4). We plot the mean value $\langle B^2\rangle_W$(a) and variance $\langle B^4\rangle_W - \langle B^2\rangle_W^2$(b) as a function of the phase of β. The results are averaged over 10 different points in time in the steady state. The error bars represent one standard deviation. We used the parameters $g_0/\omega_m = 3 \cdot 10^{-3}$, $\Delta_1/\omega_m = 1$, $\kappa/\omega_m = 0.3$, $\Delta_2 = \Delta_1 - 2\kappa$, $\Gamma_m/\omega_m = 0$, $K/\omega_m = 0.01$, $n_{\text{cav}} = 100$.

on the interval $[-\pi, \pi]$, which we divided into 30 bins. We averaged the results of 10 different points in time in the steady state. The error bars represent one standard deviation. We see that the mean $\langle B^2\rangle_W$ depends strongly on the phase while the variance of B^2 shows two peaks at approximately $-\frac{\pi}{2}$ and $\frac{\pi}{2}$.

It is known that applying a periodic force on a self-oscillator can cause synchronization. This is why in Fig 5.2.4 we plot the phase histogram of β at four different points in time in the steady state. We use the same parameters as before. The y-axis indicates the number of trajectories that are found in each bin. It seems like the oscillator prefers to be in one of two phases with equal probability. This indicates some form of synchronization and might be interesting to study. Note that in Fig 5.2.4(b) one peak is at approximately $\pm\pi$. Since we plot the histogram on the interval $[-\pi, \pi]$ it appears to have three peaks ieq: Langevin two lasersnstead of two on the first view.

Since both the optical damping and diffusion are phase dependent, let us choose a different set of parameters to illustrate that these effects are caused by the force term. In Fig. 5.2.5(a) we plot the mean value $\langle B^2\rangle_W$ as a function of time. We used the same parameters as before

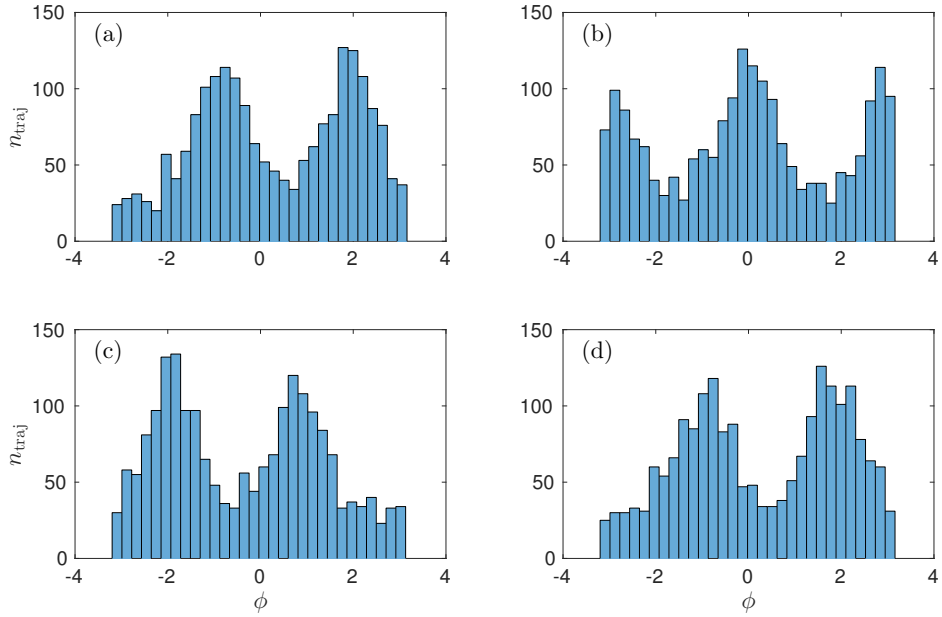

Figure 5.2.4: Simulation of the Langevin equations (5.2.4). We plot the phase histogram of β at four different points in time in the steady state. We used the parameters $g_0/\omega_m = 3 \cdot 10^{-3}$, $\Delta_1/\omega_m = 1$, $\kappa/\omega_m = 0.3$, $\Delta_2 = \Delta_1 - 2\kappa$, $\Gamma_m/\omega_m = 0$, $K/\omega_m = 0.01$, $n_{\text{cav}} = 100$.

with the exception of $g_0/\omega_m = 3 \cdot 10^{-4}$. The amplitude of the force term is $0.053\omega_m$. Here we can neglect this term in a rotating wave approximation. The mean value $\langle B^2 \rangle_W$ converges to ~ 17.15. From the system with two cavities we would expect $\langle B^2 \rangle_W = 15.62$ which is a deviation of around 9 percent. Fig. 5.2.5(b) shows the variance of B^2. It converges to ~ 8.6 whereas we would expect $\text{Var}(B^2) = 7.75$ with two cavities. This leads to a numerical Fano factor of $F = 0.50$ for both systems.

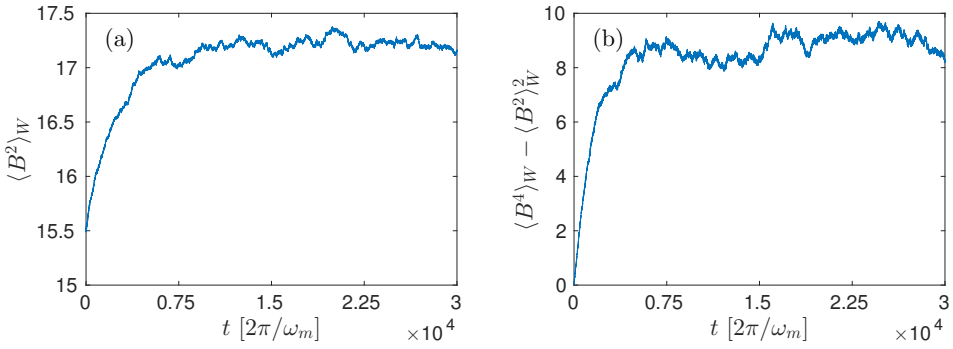

Figure 5.2.5: Simulation of the Langevin equations (5.2.4). We plot the mean value $\langle B^2 \rangle_W$(a) and variance $\langle B^4 \rangle_W - \langle B^2 \rangle_W^2$(b) as a function of time. The used parameters are $g_0/\omega_m = 3 \cdot 10^{-4}$, $\Delta_1/\omega_m = 1$, $\kappa/\omega_m = 0.3$, $\Delta_2 = \Delta_1 - 2\kappa$, $\Gamma_m/\omega_m = 0$, $K/\omega_m = 0.01$, $n_{\text{cav}} = 100$.

In Fig. 5.2.6 we plot the mean value and variance of B^2 as a function of the phase of β on the interval $[-\pi, \pi]$. Here the mean value $\langle B^2 \rangle_W$ is still phase dependent but not to such a large

extent as in Fig. 5.2.3. Furthermore the phase dependence of the variance $\langle B^4\rangle_W - \langle B^2\rangle_W^2$ seems to be small or even non-existent.

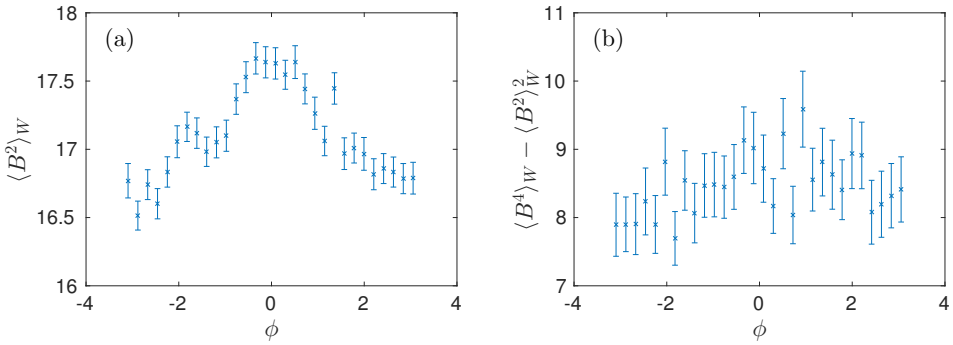

Figure 5.2.6: Simulation of the Langevin equations (5.2.4). We plot the mean value $\langle B^2\rangle_W$(a) and variance $\langle B^4\rangle_W - \langle B^2\rangle_W^2$(b) as a function of the phase of β. The results are averaged over 10 different points in time in the steady state. The error bars represent one standard deviation. We used the parameters $g_0/\omega_m = 3 \cdot 10^{-4}$, $\Delta_1/\omega_m = 1$, $\kappa/\omega_m = 0.3$, $\Delta_2 = \Delta_1 - 2\kappa$, $\Gamma_m/\omega_m = 0$, $K/\omega_m = 0.01$, $n_{\text{cav}} = 100$.

Lastly in Fig. 5.2.7 we plot the phase histogram of β at four different points in time in the steady state. We see that the phase is approximately uniformly distributed which suggests that the force term $g_0 f \sin(\omega_m(B)t + \phi)$ causes the aforementioned phase synchronization.

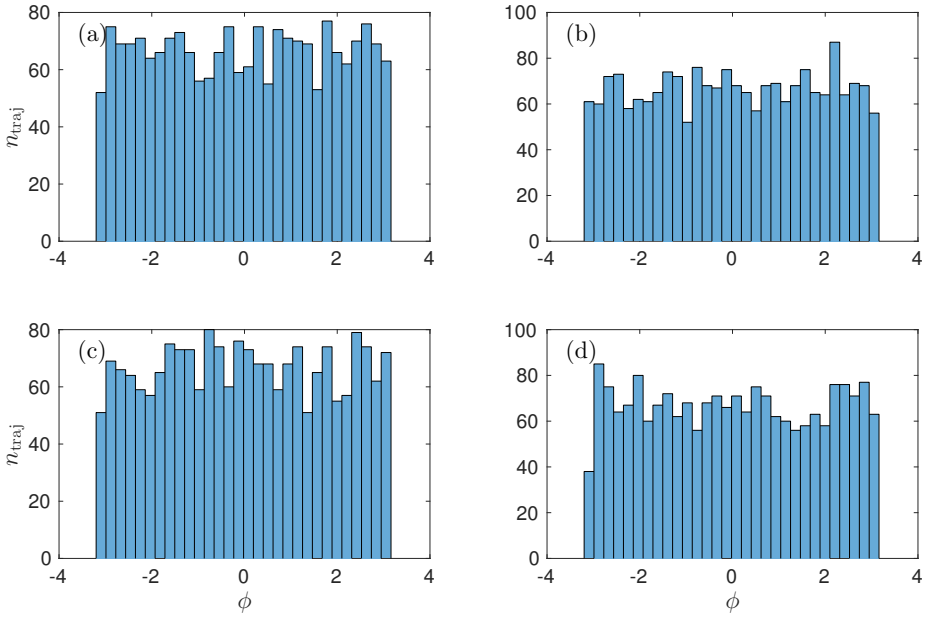

Figure 5.2.7: Simulation of the Langevin equations (5.2.4). We plot the phase histogram of β at four different points in time in the steady state. We used the parameters $g_0/\omega_m = 3 \cdot 10^{-4}$, $\Delta_1/\omega_m = 1$, $\kappa/\omega_m = 0.3$, $\Delta_2 = \Delta_1 - 2\kappa$, $\Gamma_m/\omega_m = 0$, $K/\omega_m = 0.01$, $n_{\text{cav}} = 100$.

6 Conclusion and outlook

In the first part of this thesis we have studied three optomechanical systems, in particular their steady-state amplitude distribution and the Fano factor. First we considered a mechanical oscillator with intrinsic Kerr-nonlinearity coupled to a driven cavity. We used a Kramers-Moyal expansion to derive equations of motion for the Wigner function of this system valid for large amplitudes. Driving on the blue sideband leads to self-oscillations of the mechanical oscillator. We described the steady-state amplitude distribution with a Gaussian approximation and derived an expression for the Fano factor. We compared with numerical results and found excellent agreement. We showed that the Kerr-nonlinearity can be derived as a rotating wave approximation of the Duffing-nonlinearity.

We studied the system where such a resonator is coupled to two independent cavities. One cavity is driven with a red-detuned laser and one cavity with a blue-detuned laser. We derived a Gaussian approximation for the steady-state amplitude distribution in the Wigner representation. The comparison to the numerical results showed a deviation of around 10 percent. We explained this with the assumption of a constant diffusion which is not valid. For a wide range of detunings and cavity decay rates we found a Fano factor close to zero which implies highly non-classical states.

The last system we considered was a mechanical oscillator with intrinsic nonlinearity coupled to one cavity. This cavity is driven by both a red- and a blue-detuned laser. New terms appeared in the optical damping and diffusion with contributions from both lasers. We were not able to analyze this system in detail but presented Langevin simulations for two sets of parameters. First we chose the parameters such that the force term was not negligible. We saw some kind of synchronization which might be interesting to study. Furthermore the mean value and variance of B^2 showed a strong phase dependence. For the second set of parameters the force term could be neglected in a rotating wave approximation. We saw similar steady-state expectation values for the mean and variance of B^2 as in the case with two independent cavities. This system showed interesting effects but needs further studying for which our calculations can be used as a starting point.

Part II
Numerical implementation of homodyne detection

7 Introduction to homodyne detection

Direct photo detection of a laser beam allows the measurement of its mean photon number which is proportional to the light's intensity. Not all characteristics can be found like this, but important properties lie in the quadratures of the light. These can be measured via homodyne detection which is illustrated in Fig. 7.0.8. The output field of the system is interfered with a strong coherent light field of the same frequency at a beam splitter with large transmittance. This light field is also referred to as the local oscillator. Most of the system's output goes through the beam-splitter and is mixed with a small amount of the coherent light. Since the latter is so strong, it still dominates the intensity. The measured photocurrent consists of a constant term from the local oscillator plus a term proportional to the output field's quadrature. One can measure any quadrature by tuning the phase of the local oscillator.

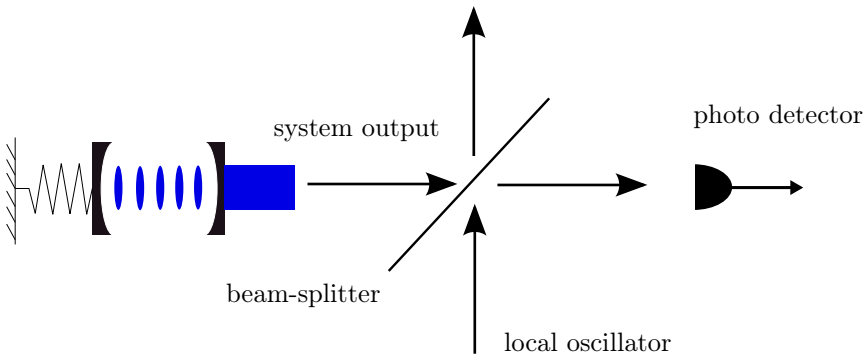

Figure 7.0.8: Schematic illustration of homodyne detection. The system output is interfered with the local oscillator at a beam-splitter. The photo detector indirectly measures the output field's quadrature.

Another possible measurement setup is the balanced homodyne detection illustrated in Fig. 7.0.9. This method uses a beam-splitter with transmittance of one half. Each beam is measured. The difference of the photocurrent is then again proportional to the quadrature of the system's output. The advantage of this setup is that intensity fluctuations of the local oscillator cancel out. These are indistinguishable from the signal in the simple homodyne detection. Furthermore this setup works with smaller intensities of the local oscillator light as all of its light is measured.

Homodyne detection finds many applications, in particular in the measurement of quadrature squeezed light [38]. It was used in the gravitational wave detectors at the LIGO project to detect gravitational waves [2]. It allows the experimental measurement of the Wigner function via quantum state tomography [39]. Homodyne detection can be used to demonstrate the violation of Bell's inequality [40]. It also finds applications in quantum cryptography [41]. One can indirectly measure observables that couple to the light's quadrature like the atomic motion in a standing light field [42]. In optomechanical setups the measurement of the output phase allows the indirect measurement of the mechanical oscillator's position without adding further noise to

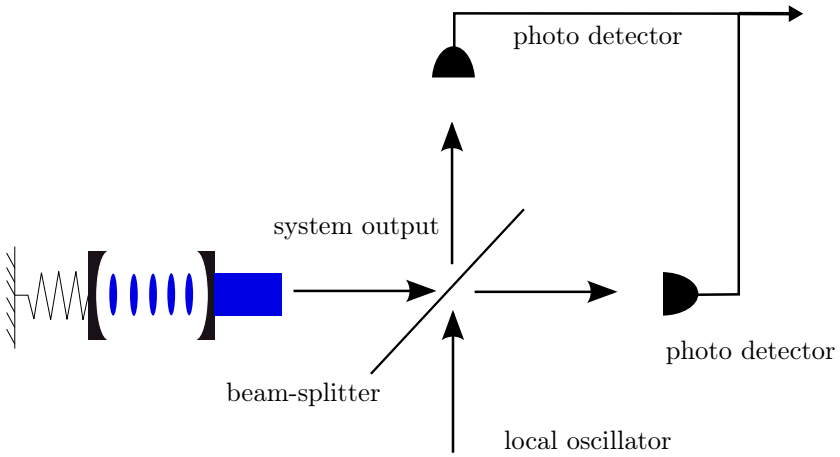

Figure 7.0.9: Schematic illustration of balanced homodyne detection. The system output is interfered with the local oscillator at a beam-splitter. Both output beams are measured. This setup is advantageous as on can use smaller intensities for the local oscillator and its fluctuations cancel out.

the system. Homodyne detection can also be used in measurement based feedback control. This allows ground state cooling of the mechanical oscillator in optomechanics [11].

In this second part of the master thesis we numerically implement the stochastic master equation generated by homodyne detection in Python using the framework of QuTiP [32]. In Section 8 we introduce the Itô and Stratonovich calculus and review the derivation of the stochastic master equation. We present numerical methods to solve this master equation in Section 9. In Section 10 we compare our implementations, namely the strong order Taylor 1.5 and Taylor 2.0 scheme, with other numerical methods. These two schemes show improved stability and convergence compared to the schemes in QuTiP. Finally we conclude in Section 11 with a brief summary of the results.

8 Theory of homodyne detection

In this section we introduce the theoretical basics to describe homodyne detection and its numerical implementation. First we briefly summarize the Itô and Stratonovich calculus closely following the book "Handbook of Stochastic Methods" by C. Gardiner [43]. Then we review the derivation of the quantum trajectory generated by homodyne detection following "Quantum Measurement and Control" by M. Wiseman and G. Milburn [44] as well as "Quantum Measurement Theory and its Applications" by K. Jacobs [45].

8.1 Itô and Stratonovich calculus

In the first part of this master thesis we used Langevin equations to describe equations of motion for the phase space distribution of cavity and oscillator. In the one-dimensional case such a simple Langevin equation for the variable x is given by

$$\partial_t x = a(x,t) + b(x,t)\xi(t), \tag{8.1.1}$$

where $\xi(t)$ is a Gaussian white-noise process. This kind of equation was used to describe Brownian motion in terms of a differential equation. The physical interpretation would be a motion given by the deterministic drift $a(x,t)$ and some fluctuating noise or force $b(x,t)\xi(t)$. The white noise $\xi(t)$ is an idealization of physical processes with very short correlation times.

First we consider the case where the drift term is zero, i.e. $a(x,t) \equiv 0$, and the diffusive term is constant, i.e. $b(x,t) \equiv 1$. This is described by the Langevin equation

$$\partial_t x = \xi(t). \tag{8.1.2}$$

The solution to this differential equation is found by integration. For the initial condition $x(t=0) = 0$ we find

$$W(t) \equiv x(t) = \int_0^t \mathrm{d}s \xi(s). \tag{8.1.3}$$

We write $W(t)$ since this is the definition of a Wiener process. As we showed in the first part of this master thesis, a Langevin equation can equivalently be written as a Fokker-Planck equation for the (conditional) probability distribution $P(x,t|x_0,t_0)$. This leads to

$$\partial_t P(x,t|x_0,t_0) = \frac{1}{2}\partial_x^2 P(x,t|x_0,t_0). \tag{8.1.4}$$

With the initial condition $P(x,t_0|x_0,t_0) = \delta(x-x_0)$ we find the solution

$$P(x,t|x_0,t_0) = \frac{1}{\sqrt{2\pi(t-t_0)}} e^{-\frac{(x-x_0)^2}{2(t-t_0)}}. \tag{8.1.5}$$

This is a Gaussian distribution with mean x_0 and variance $t-t_0$. Unfortunately the sample paths of this distribution are not differentiable, since

$$\lim_{\Delta t\to 0} \mathrm{Prob}\left[\left|\frac{W(t+\Delta t)-W(t)}{\Delta t}\right| > \epsilon\right] = \lim_{\Delta t\to 0} 2\int_{\epsilon\Delta t}^{\infty} \mathrm{d}x \frac{1}{\sqrt{2\pi\Delta t}} e^{-\frac{x^2}{2\Delta t}} = 1. \tag{8.1.6}$$

No matter what value we choose for ϵ, the time derivative of $|W(t)|$ is always larger and therefore infinite. Since $W(t)$ is not differentiable, the differential equations (8.1.1), (8.1.2) do not exist

within standard analysis. Nevertheless we interpret the general Langevin equation (8.1.2) as an integral equation

$$x(t) - x(0) = \int_0^t \mathrm{d}s a(x(s), s) + \int_0^t \mathrm{d}W(s) b(x(s), s), \tag{8.1.7}$$

where $\mathrm{d}W(t) \equiv W(t + \mathrm{d}t) - W(t) = \xi(t)\mathrm{d}t$ is the infinitesimal Wiener increment given by the Wiener process $W(t)$. From Eq. (8.1.5) we know that $\mathrm{d}W(t)$ is a Gaussian random variable with zero mean and variance Δt. The question remains how the integral with respect to $\mathrm{d}W(t)$ should be interpreted. In analogy to Riemann integrals we divide the integration interval $[t_0, t]$ into N intervals

$$t_0 < t_1 < t_2 < ... < \ t_{N-1} < t. \tag{8.1.8}$$

The stochastic integral for a function $f(t)$ is then defined as the mean square limit of the partial sums for N going to infinity

$$\int_{t_0}^t \mathrm{d}W(s) f(s) = \lim_{N\to\infty} \sum_{n=1}^N f(\tau_n) \Delta W(t_n), \tag{8.1.9}$$

where the intermediate points τ_n are chosen such that $t_{n-1} \leq \tau_n \leq t_n$. Here we defined the (finite) Wiener increment $\Delta W(t_n) = W(t_n) - W(t_{n-1})$ with zero mean and variance $t_n - t_{n-1}$. The value of the stochastic integral depends now on which intermediate points we choose. In the Itô interpretation we choose the points $\tau_n = t_{n-1}$. The Itô integral is then defined as

$$\int_{t_0}^t \mathrm{d}W(s) f(s) = \lim_{N\to\infty} \sum_{n=1}^N f(t_{n-1}) \Delta W(t_n), \tag{8.1.10}$$

where the limit is in the mean square sense. It should be noted that the Itô integration rules differ from those for normal integrals. We find for example

$$\int_{t_0}^t \mathrm{d}W(s) W(s) = \frac{1}{2} \left(W(t)^2 - W(t_0)^2 - (t - t_0) \right). \tag{8.1.11}$$

In contrast to non-stochastic Riemann integrals we have an additional term $(t - t_0)$. The Itô integration rule also leads to differentiation rules that differ from the rules in standard analysis. For a variable $x(t)$ satisfying the Langevin equation (8.1.1) we find with the relation $\langle \mathrm{d}W^2 \rangle = \mathrm{d}t$

$$\mathrm{d}f(x) = \left(a(x,t) f'(x) + \frac{1}{2} b(x,t)^2 f''(x) \right) \mathrm{d}t + b(x,t) f'(x) \mathrm{d}W. \tag{8.1.12}$$

Another possible interpretation of the stochastic integral due to Stratonovich follows from the choice of intermediate points $\tau_n = \frac{1}{2}(t_n + t_{n-1})$. The Stratonovich integral is defined as

$$\int_{t_0}^t \circ \mathrm{d}W(s) f(s) = \lim_{N\to\infty} \sum_{n=1}^N f\left(\frac{1}{2}(t_n + t_{n-1}) \right) \Delta W(t_n), \tag{8.1.13}$$

where the limit is again in the mean square sense. We denote the Stratonovich integral with $\circ \mathrm{d}W$ to clarify the difference to the Itô integral. We find different integration rules compared to the Itô interpretation. Compared to Eq. (8.1.11) the Stratonovich integral yields

$$\int_{t_0}^t \circ \mathrm{d}W(s) W(s) = \frac{1}{2} \left(W(t)^2 - W(t_0)^2 \right). \tag{8.1.14}$$

This is the same expression that we would expect from a (deterministic) Riemann integral. We also find the usual differentiation rules

$$\mathrm{d}f(x) = f'(x)\left(a(x,t)\mathrm{d}t + b(x,t)\mathrm{d}W\right). \tag{8.1.15}$$

As it will turn out the stochastic differential equation generated by homodyne detection is in Itô form. For the numerical implementation of the Taylor 2.0 method we will use the Stratonovich form in Section 9.6. Using the differentiation rules in Eqs. (8.1.12), (8.1.15) we find the equivalent stochastic differential equations in Itô and Stratonovich form

$$\begin{aligned} \mathrm{d}x &= a\mathrm{d}t + b\mathrm{d}W(t), \\ \mathrm{d}x &= \left(a - \frac{1}{2}b\partial_x b\right)\mathrm{d}t + b \circ \mathrm{d}W. \end{aligned} \tag{8.1.16}$$

8.2 Homodyne detection

In this subsection we review the derivation of the stochastic differential equation generated by homodyne detection. We follow the book of H.M. Wiseman and G.J. Milburn [44] and the book of K. Jacobs [45].

First we consider the detection of discrete events such as single photons. We assume that an event takes place with probability rate λ, i.e. $P(\text{event}) = \lambda\mathrm{d}t$. The detection is done with measurement operators M_0 and M_1, where we define the outcome associated with M_0 to be no detection and the outcome with M_1 to be a detection. We assume the photo detectors to be perfect, i.e. every event is measured with certainty. The probability of such an event is then given by

$$P(\text{event}) = \langle M_1^\dagger M_1\rangle = \lambda\mathrm{d}t. \tag{8.2.1}$$

With this in mind we define

$$M_1 = c\sqrt{\mathrm{d}t}, \tag{8.2.2}$$

where c is an arbitrary operator that is constant in time. Note that c is in units of $\sqrt{\mathrm{Hz}}$. The probability rate λ is then equal to the average count rate, i.e. $\lambda = \langle c^\dagger c\rangle$. In the case of photon detection leaking out of a cavity the operator c is given by $c = \sqrt{2\kappa}a$, where κ is the amplitude decay rate of the photons and a the annihilation operator.

The measurement operators must satisfy the completeness relation $\sum M_n^\dagger M_n = 1$. If we consider only terms up to order $\mathrm{d}t$ we find

$$M_0 = 1 - \mathrm{d}t\frac{1}{2}c^\dagger c. \tag{8.2.3}$$

We write the total number of photon detections as $N(t)$. Since only single photons are detected, the stochastic increment $\mathrm{d}N$ is either one or zero, i.e. $\mathrm{d}N^2 = \mathrm{d}N$. Its expectation value must be equal to the probability of the event, i.e.

$$\mathrm{E}[\mathrm{d}N] = \langle c^\dagger c\rangle\,\mathrm{d}t. \tag{8.2.4}$$

We assume that the system is in a (pure) state $|\psi\rangle$. The detection of a photon at time t changes the state to

$$|\psi_1(t+\mathrm{d}t)\rangle = \frac{M_1|\psi(t)\rangle}{\sqrt{\langle M_1^\dagger M_1\rangle}} = \frac{c|\psi(t)\rangle}{\sqrt{c^\dagger c}}. \tag{8.2.5}$$

This corresponds to $\mathrm{d}N(t) = 1$. No detection, i.e. $\mathrm{d}N(t) = 0$, leads to

$$|\psi_0(t+\mathrm{d}t)\rangle = \frac{M_0|\psi(t)\rangle}{\sqrt{\langle M_0^\dagger M_0\rangle}} = \left[1 - \frac{1}{2}\mathrm{d}t\big((c^\dagger c - \langle c^\dagger c\rangle\big)\right]|\psi(t)\rangle, \tag{8.2.6}$$

where we only considered terms up to order $\mathrm{d}t$. We can then write the (non-unitary) evolution of the system as

$$|\psi(t+\mathrm{d}t)\rangle = \mathrm{d}N(t)\,|\psi_1(t+\mathrm{d}t)\rangle + (1-\mathrm{d}N(t))\,|\psi_0(t+\mathrm{d}t)\rangle\,. \tag{8.2.7}$$

This is allowed as $\mathrm{d}N(t)$ is either one or zero, i.e. the system stays in a pure state after the measurement. We now include the unitary evolution of the system determined by its Hamiltonian H. Since the photon jumps happen in an infinitesimal time we only have to include the unitary for $\mathrm{d}N(t) = 0$. Equivalently we could include the unitary evolution in the measurement operators with $M_0 = 1 - \mathrm{d}t(\frac{1}{2}c^\dagger c + iH)$. We can find a stochastic Schrödinger equation by defining $\mathrm{d}\,|\psi\rangle = |\psi(t+\mathrm{d}t)\rangle - |\psi(t)\rangle$. Taking terms up to order $\mathrm{d}t$ into account in Eq. (8.2.7), we arrive at

$$\mathrm{d}\,|\psi\rangle = \left[\mathrm{d}t\left(\frac{\langle c^\dagger c\rangle - c^\dagger c}{2} - iH\right) + \mathrm{d}N\left(\frac{c}{\sqrt{\langle c^\dagger c\rangle}} - 1\right)\right]|\psi(t)\rangle\,. \tag{8.2.8}$$

This is called a stochastic Schrödinger equation as it preserves the purity of the initial state $|\psi\rangle$ like a Schrödinger equation (in the usual sense). Further it involves stochastic jumps generated by the measurement which manifests itself in the term $\mathrm{d}N$.

Equivalently to the stochastic Schrödinger equation we can write the evolution of the density matrix ρ_I as a stochastic master equation. This is more general as it allows the creation of mixed states in the measurement. The stochastic master equation can be derived from Eq. (8.2.8) with $\rho_I(t) = |\psi(t)\rangle\langle\psi(t)|$. The result is

$$\mathrm{d}\rho_I = \left(-\mathrm{d}t\mathcal{H}[iH + \frac{1}{2}c^\dagger c] + \mathrm{d}N\mathcal{G}[c]\right)\rho_I, \tag{8.2.9}$$

where we defined the superoperators

$$\begin{aligned}\mathcal{G}[c]\rho &= \frac{c\rho c^\dagger}{\langle c^\dagger c\rangle} - \rho,\\ \mathcal{H}[c]\rho &= c\rho + \rho c^\dagger - \langle c + c^\dagger\rangle\,\rho.\end{aligned} \tag{8.2.10}$$

Note that we write ρ_I since the density matrix is conditioned on the measurement result $N(t)$. In experiments it is usual to measure a photocurrent rather than the photon count, i.e. $I(t) = \frac{\mathrm{d}N(t)}{\mathrm{d}t}$. The density matrix is then conditioned on the measured photocurrent.

We have to average over all possible outcomes if we make the measurement but ignore the result. Taking the average of all stochastic trajectories of the stochastic master equation (8.2.9) and writing $\langle\rho_I\rangle = \rho$, we arrive at the master equation in Lindblad form

$$\mathrm{d}\rho = -i[H,\rho]\mathrm{d}t + \mathcal{D}[c]\rho\mathrm{d}t. \tag{8.2.11}$$

This equation is invariant under the transformation

$$c \to c + \gamma, \quad H \to H - i\frac{1}{2}(\gamma^* c - \gamma c^\dagger), \tag{8.2.12}$$

where γ is a complex number. The master equation (8.2.9) after this transformation describes homodyne detection. The photons are not measured directly, but instead we interfere them with a strong coherent light field of the same frequency. This light field is referred to as the local oscillator. The interference is achieved with a beam-splitter as illustrated in Fig. 7.0.8. The incoming field operators are then transformed according to

$$c \to \sqrt{\eta}b + \sqrt{1-\eta}o, \quad o \to \sqrt{\eta}o - \sqrt{1-\eta}o, \tag{8.2.13}$$

where η is the transmittance and o is the field operator of the coherent light. Since the local oscillator is in a coherent state $|\alpha\rangle$ with complex amplitude α, i.e. the field operator satisfies $o|\alpha\rangle = \alpha|\alpha\rangle$, we can replace o with the complex number α. If the transmittance η is close to one and the amplitude α is large, the operator b transforms according to

$$b \to b + \gamma, \tag{8.2.14}$$

where we defined $\gamma \equiv \sqrt{1-\eta}\alpha$. Inserting this into the stochastic master equation (8.2.9) we find

$$\mathrm{d}\rho_I = \left(\mathrm{d}t\mathcal{H}[-iH - \gamma c - \frac{1}{2}c^\dagger c] + \mathrm{d}N\mathcal{G}[c+\gamma]\right)\rho_I. \tag{8.2.15}$$

For real-valued and large γ with $\gamma\langle c + c^\dagger\rangle \gg \langle c^\dagger c\rangle$, we find the expected measured photocurrent according to Eq. (8.2.4)

$$\mathrm{E}[I] = \mathrm{E}\left[\frac{\mathrm{d}N}{\mathrm{d}t}\right] = \langle \gamma^2 + \gamma(c + c^\dagger)\rangle\,. \tag{8.2.16}$$

The measured current is proportional to the amplitude quadrature $X = \frac{c+c^\dagger}{2}$. Depending on the complex phase of γ we can measure different quadratures. Alternatively we could choose γ to be purely imaginary which would lead to a phase quadrature measurement $Y = \frac{-i(c-c^\dagger)}{2}$.

We now consider the limit of infinite amplitude γ. We choose a finite time $\delta t = O(\gamma^{-\frac{3}{2}})$ such that it is small but the average number of photon detections $\delta N = O(\gamma^{\frac{1}{2}})$ is still large. We find the mean number of detections μ

$$\begin{aligned}\mu \equiv \mathrm{E}[\delta N] &= \delta t \mathrm{Tr}\left[\left(\gamma^2 + \gamma(c+c^\dagger) + c^\dagger c\right)\left(\rho_I(t) + O(\gamma^{-\frac{3}{2}})\right)\right] \\ &= \delta t\left(\gamma^2 + \gamma\langle c + c^\dagger\rangle + O(\gamma^{\frac{1}{2}})\right).\end{aligned} \tag{8.2.17}$$

The change of the system during time δt can be neglected as it is of order $\gamma^{-\frac{3}{2}}$. In this case the probability rate of counting a photon is constant (for this time interval). The number of events δN is then given by a Poisson distribution, i.e. the variance of δN is equal to its mean. Since the local oscillator is assumed to have a large amplitude, we will count many photons. In this limit we can approximate the Poisson distribution with a Gaussian distribution. Up to leading order in γ it has the variance $\sigma^2 = \gamma^2\delta t$. Since we know the mean $\mu = \delta t\left(\gamma^2 + \gamma\langle c + c^\dagger\rangle)\right)$ and variance σ^2 of the Gaussian distributed δN, we can equivalently write

$$\delta N = (\gamma^2 + \gamma\langle c + c^\dagger\rangle)\delta t + \gamma\delta W, \tag{8.2.18}$$

where $\delta W = W(t+\delta t) - W(t)$ is a Wiener increment with expectation value zero and variance δt as defined in Section 8.1. We insert this into the master equation (8.2.15) and go to the limit of infinitesimal time steps $\delta t \to \mathrm{d}t$. We find the stochastic master equation generated by homodyne detection by taking the leading terms in γ. We arrive at

$$\mathrm{d}\rho_I = -i[H, \rho_I]\mathrm{d}t + \mathcal{D}[c]\rho_I\mathrm{d}t + \mathcal{H}[c]\rho_I\mathrm{d}W, \tag{8.2.19}$$

where $\mathrm{d}W$ is an infinitesimal Wiener increment as defined in Section 8.1. This is a stochastic master equation in Itô form. We note that the balanced homodyne detection mentioned in Section 7 (see Fig. 7.0.9) leads to the same equation.

9 Numerical methods

We reviewed the derivation of the master equation generated by homodyne detection. It is an Itô stochastic differential equation for the density matrix of the system. In this section we introduce different time-discrete schemes to solve stochastic differential equations. We consider the general Itô stochastic equation for the vector $\vec{Y}$

$$\mathrm{d}\vec{Y} = \vec{a}(\vec{Y}, t)\mathrm{d}t + b(\vec{Y}, t)\mathrm{d}\vec{W}, \tag{9.0.20}$$

where $\vec{a}$ is the drift vector, b is the diffusive matrix and $\mathrm{d}\vec{W}$ is a vector of independent Wiener processes. This is a generalization of the one-dimensional Itô process introduced in Section 8.1 (see Eq. (8.1.16)). The k-th element of $\vec{Y}$ satisfies

$$\mathrm{d}Y^k = a^k\mathrm{d}t + \sum_{j=1}^{m} b^{k,j}\mathrm{d}W^j. \tag{9.0.21}$$

Our goal is to solve the stochastic master equation

$$\mathrm{d}\rho = -i[H,\rho]\mathrm{d}t + \sum_i \mathcal{D}[d_i]\rho\mathrm{d}t + \sum_j \mathcal{D}[c_j]\rho\mathrm{d}t + \sum_j \mathcal{H}[c_j]\rho\mathrm{d}W^j. \tag{9.0.22}$$

This is a generalization of the master equation (8.2.19) generated by homodyne detection, the derivation of which we reviewed in Section 8.2. Here we added an additional deterministic part via the operators d_i. This can be induced by coupling to the environment or by measuring the d_i operators and neglecting the results (see Eq. (8.2.11)). Furthermore we record the homodyne measurement results of several stochastic operators c_j.

This equation describes the evolution of a density matrix as opposed to Eq. (9.0.20), which describes the evolution of a vector. A straightforward method to implement schemes for the density operator is to vectorize the matrix ρ, i.e. rearrange its entries in form of a vector $\vec{\rho}$. By doing this we also have to transform all operators. We differentiate between an operator c acting on the density matrix from the left or from the right. We write this as $\mathrm{pre}(c)\vec{\rho}$ and $\mathrm{post}(c)\vec{\rho}$, respectively.

In the case of homodyne detection we identify $\vec{Y}$ in the general Itô equation (9.0.20) with the rearranged density matrix, i.e. $\vec{Y} = \vec{\rho}$. The drift vector $\vec{a}$ is given by the vectorization of the matrix

$$a = -i[H,\rho] + \sum_i \mathcal{D}[d_i]\rho \sum_j \mathcal{D}[c_j]\rho. \tag{9.0.23}$$

This is just the deterministic part of the stochastic master equation (9.0.22). We abbreviate $\vec{a} = \mathcal{L}\vec{\rho}$ and assume that the Hamiltonian H does not depend on ρ and t. $\mathcal{L}$ is then a matrix that does not depend on ρ and t. We define $\vec{b_j}$ as the vectorization of the matrix

$$b_j = \mathcal{H}[c_j]\rho = c_j\rho + \rho c_j^\dagger - \mathrm{Tr}[c_j\rho + \rho c_j^\dagger]\rho. \tag{9.0.24}$$

The diffusive term $b^{k,j} \equiv b_j^k$ can be interpreted as the k-th element of the vector $\vec{b}_j$.

In this section we introduce different numerical schemes as presented in "Numerical Solution of Stochastic Differential Equations" by P. Kloeden and E. Platen [46]. We follow their notation and introduce the operators

$$L^0 = \frac{\partial}{\partial t} + \sum_{k=1}^{d} a^k \frac{\partial}{\partial x^k} + \frac{1}{2}\sum_{k,l=1}^{d}\sum_{j=1}^{m} b^{k,j}b^{l,j}\frac{\partial^2}{\partial x^k \partial x^l}, \tag{9.0.25}$$

$$\underline{L}^0 = \frac{\partial}{\partial t} + \sum_{k=1}^{d} \underline{a}^k \frac{\partial}{\partial x^k}, \tag{9.0.26}$$

$$L^j = \underline{L}^j = \sum_{k=1}^{d} b^{k,j} \frac{\partial}{\partial x^k}, \quad j = 1, 2, ..., m, \tag{9.0.27}$$

where the drift term in Stratonovich form is defined as

$$\underline{a}^k = a^k - \frac{1}{2} \sum_{j=1}^{m} \underline{L}^j b^{k,j}, \quad j = 1, 2, ..., d. \tag{9.0.28}$$

d and m are the dimensions of the vectors $\vec{Y}$ and $\mathrm{d}\vec{W}$, respectively. Multiple stochastic Itô and Stratonovich integrals are abbreviated as

$$\begin{aligned} I_{(j_1,...,j_l)} &= \int_{\tau_n}^{\tau_{n+1}} \mathrm{d}W_{s_1}^{j_1} ... \int_{\tau_n}^{s_2} \mathrm{d}W_{s_l}^{j_l}, \\ J_{(j_1,...,j_l)} &= \int_{\tau_n}^{\tau_{n+1}} \circ \mathrm{d}W_{s_1}^{j_1} ... \int_{\tau_n}^{s_2} \circ \mathrm{d}W_{s_l}^{j_l}, \end{aligned} \tag{9.0.29}$$

where $\int \mathrm{d}W_{s_i}^0 \equiv \int \mathrm{d}s_i$ is an integration over time.

9.1 Strong and weak convergence

Before we present the numerical schemes let us introduce the strong and weak convergence as defined by Kloeden/Platen [46]. The numerical implementation of a stochastic differential equation requires finite time steps. This discretization can lead to deviations from the real solution. Depending on the method and the size of the time steps we find different errors. To compare them we have to define a measure of convergence.

Suppose $X(t)$ is an Itô process and $Y_{\Delta t}(t)$ is its time-discrete numerical approximation with maximum step size Δt. We say that $Y_{\Delta t}$ converges strongly with order $\gamma > 0$ if there exists a $\delta > 0$ such that the absolute error ϵ satisfies

$$\epsilon \equiv \langle |X(t) - Y_{\Delta t}(t)| \rangle \leq C \Delta t^{\gamma} \tag{9.1.1}$$

for any time discretization $\Delta t \in (0, \delta)$, where C is a positive constant. This corresponds to convergence in the mean square limit since

$$\langle |X(t) - Y_{\Delta t}(t)| \rangle \leq \sqrt{\langle |X(t) - Y_{\Delta t}(t)|^2 \rangle}. \tag{9.1.2}$$

The absolute error goes to zero if we decrease the maximum time step. Therefore the trajectory of the numerical solution converges to the real solution.

We can also define a weak order convergence. $Y_{\Delta t}$ converges with weak order $\gamma > 0$ if there exists a $\delta > 0$ such that

$$| \langle g(X(t)) \rangle - \langle g(Y_{\Delta t}(t)) \rangle | \leq K \Delta t^{\gamma} \tag{9.1.3}$$

for any polynomial function g, a positive constant K and any time-discretization $\Delta t \in (0, \delta)$. The weak convergence corresponds to convergence of the distribution. This means that the expectation values of the numerical solution converge to the expectation values of the real solution.

Numerical schemes are usually only efficient with respect to one kind of convergence. If one is interested in expectation values of some Itô process X, a method with preferably large weak convergence should be used. If the simulation of single trajectories is needed, a numerical method with strong convergence is advantageous. For the implementation of homodyne detection we will use schemes with strong convergence.

9.2 Derivatives of the drift vector and diffusive matrix

In the following subsections we introduce numerical schemes to solve stochastic equations. In particular we want to solve the stochastic master equation (9.0.22). These schemes include derivatives of the drift vector $\vec{a}$ and the diffusive matrix b. Here we derive general differentiation rules for our problem.

Let A be a constant $d \times d$ - matrix acting on the vector $\vec{\rho}$ with dimension d. We find the derivative with respect to the l-th element of $\vec{\rho}$

$$\frac{\partial}{\partial x^l}(A\vec{\rho})^k = \frac{\partial}{\partial x^l}\left(\sum_{i=1}^{d} A^{k,i}x^i\right) = A^{k,l}. \tag{9.2.1}$$

With this equation we can find for a second vector $\vec{v}$ of dimension d

$$\sum_{l=1}^{d} v^l \frac{\partial}{\partial x^l}(A\vec{\rho})^k = \sum_{l=1}^{d} A^{k,l}v^l = (A\vec{v})^k. \tag{9.2.2}$$

We can equivalently write this in vector form

$$\sum_{l=1}^{d} v^l \frac{\partial}{\partial x^l}(A\vec{\rho}) = A\vec{v}. \tag{9.2.3}$$

These differentiation rules can be used for derivatives of the drift vector $\vec{a} = \mathcal{L}\rho$ since we assumed that $\mathcal{L}$ is a linear operator. For the derivatives of the stochastic parts $\vec{b_i}$ (see Eq. (9.0.24)) we have to introduce further differentiation rules, as they do not only have a linear dependence on $\vec{\rho}$ but also a quadratic dependence. Let $\bar{A}$ be the operator acting on ρ corresponding to A acting on $\vec{\rho}$. Then

$$\frac{\partial}{\partial x^l}(\mathrm{Tr}[\bar{A}\rho]\vec{\rho})^k = \delta_{l,k}\mathrm{Tr}[\bar{A}\rho] + x^k \frac{\partial}{\partial x^l}(\mathrm{Tr}[\bar{A}\rho]). \tag{9.2.4}$$

The second expression on the right-hand side can be rewritten by writing the trace of the matrix as a sum over the entries of its vectorized form

$$\mathrm{Tr}[\bar{A}\rho] = \sum_{n=0}^{d-1}(A\vec{\rho})^{1+n(d+1)}. \tag{9.2.5}$$

With Eq. (9.2.2) we find

$$\sum_{l=1}^{d} v^l \frac{\partial}{\partial x^l}(\mathrm{Tr}[\bar{A}\rho]\vec{\rho})^k = \mathrm{Tr}[\bar{A}\rho]v^k + \mathrm{Tr}[\bar{A}\bar{v}]x^k, \tag{9.2.6}$$

where we defined v as the matrix corresponding to the vector $\vec{v}$. We can write this in vector form

$$\sum_{l=1}^{d} v^l \frac{\partial}{\partial x^l}(\mathrm{Tr}[A\rho]\vec{\rho}) = \mathrm{Tr}[\bar{A}\rho]\vec{v} + \mathrm{Tr}[\bar{A}\bar{v}]\vec{\rho}. \tag{9.2.7}$$

9.3 Euler-Maruyama method

After introducing the weak and strong convergence as well as deriving differentiation rules, we now want to present numerical schemes to solve the Itô equation

$$\mathrm{d}\vec{Y} = \vec{a}(\vec{Y}, t)\mathrm{d}t + b(\vec{Y}, t)\mathrm{d}\vec{W} \tag{9.3.1}$$

on a time interval $[t_0, T]$. The solution of this equation is given by

$$\vec{Y}(t) = \vec{Y}(t_0) + \int_{t_0}^{t} \vec{a}(\vec{Y}(s), s)\mathrm{d}s + \int_{t_0}^{t} b(\vec{Y}(s), s)\mathrm{d}\vec{W}(s). \tag{9.3.2}$$

Applying the Itô differentiation rules in Eq. (8.1.12) to the drift vector and diffusive matrix we can write this as a Taylor expansion. In the case where both Y and W are one-dimensional we find

$$\begin{aligned} Y(t) =& Y(t_0) + \int_{t_0}^{t} \left(a(Y(t_0), t_0) + \int_{t_0}^{s} L^0 a(Y(z), z)\mathrm{d}z + \int_{t_0}^{s} L^1 a(Y(z), z)\mathrm{d}W(z) \right) \mathrm{d}s \\ &+ \int_{t_0}^{t} \left(b(Y(t_0), t_0) + \int_{t_0}^{s} L^0 b(Y(z), z)\mathrm{d}z + \int_{t_0}^{s} L^1 b(Y(z), z)\mathrm{d}W(z) \right) \mathrm{d}W(s), \end{aligned} \tag{9.3.3}$$

which includes multiple stochastic and deterministic integrals. The operators L^0 and L^1 are defined in Eqs. (9.0.25), (9.0.27). The Itô equation can then be solved by introducing discrete times and calculating these integrals with the Itô interpretation as sums. We evaluate $\vec{Y}$ at the times $t_0 < t_1 < ... < t_N = T$ with constant time steps $\Delta t = \frac{T - t_0}{N}$, where N is the number of intervals.

The simplest numerical scheme is obtained by taking the Taylor expansion up to order zero, i.e. neglecting the multiple integrals. This scheme is known as the Euler-Maruyama method. If we write $\vec{Y}(t_n) = \vec{Y}_n$ we arrive at

$$Y^k_{n+1} = Y^k_n + a^k \Delta t + \sum_{j=1}^{m} b^{k,j} \Delta W^j, \tag{9.3.4}$$

where the single integrals were evaluated as

$$\int_{t_n}^{t_{n+1}} \mathrm{d}s = \Delta t, \qquad \int_{t_n}^{t_{n+1}} \mathrm{d}W = \Delta W(t_{n+1}). \tag{9.3.5}$$

Here $\Delta W = W(t_n + \Delta t) - W(t_n)$ is a finite Wiener increment. As mentioned in Section 8.1, it can be simulated by a Gaussian random variable with zero mean and variance Δt.

In the case of homodyne detection we defined the drift vector and diffusive matrix with Eqs. (9.0.23), (9.0.24). With these relations we find the Euler-Maruyama scheme for the vectorized density matrix

$$\vec{\rho}_{n+1} = \vec{\rho}_n + \vec{a}\Delta t + \sum_j \vec{b}_j \Delta W^j. \tag{9.3.6}$$

9.4 Milstein method

The Euler-Maruyama method is a generalization of the Euler scheme for ordinary partial differential equations. For the stochastic case we find order of strong convergence 0.5 while the deterministic scheme has order of strong convergence 1.0. This can be explained by the fact that $\mathrm{d}W$ is of order $\sqrt{\mathrm{d}t}$ (since $\langle \mathrm{d}W^2 \rangle = \mathrm{d}t$). To achieve the same strong convergence as in the deterministic case we have to include $\mathrm{d}W$ up to second order.

We can again apply the Itô differentiation rules to the term $L^1 b(Y(z), z)$ in Eq. (9.3.3). We then include $\mathrm{d}W$ up to second order in our Taylor expansion, i.e. the term

$$b(Y(t_n), t_n) \int_{t_n}^{t_{n+1}} \int_{t_0}^{s} \mathrm{d}W(z)\mathrm{d}W(s) = b(Y(t_n), t_n)\frac{1}{2}\left((\Delta W)^2 - \Delta t\right). \tag{9.4.1}$$

For the general multidimensional case the resulting scheme is

$$Y_{n+1}^k = Y_n^k + a^k \Delta t + \sum_{j=1}^{m} b^{k,j}\Delta W^j + \sum_{j_1,j_2=1}^{m} L^{j_1} b^{k,j_2} I_{(j_1,j_2)}, \tag{9.4.2}$$

where L^j are the differential operators in Eq. (9.0.25), (9.0.27) and $I_{(j_1,j_2)}$ are double Itô integrals defined in Eq. (9.0.29). Depending on the form of the diffusive matrix b the Milstein method can be simplified considerably. For commutative noise satisfying

$$L^{j_1} b^{k,j_2} = L^{j_2} b^{k,j_1} \tag{9.4.3}$$

we can use the relation between multiple Itô integrals

$$I_{(j_1,j_2)} + I_{(j_2,j_1)} = \Delta W^{j_1}\Delta W^{j_2}. \tag{9.4.4}$$

The Milstein method is then given by

$$\begin{aligned} Y_{n+1}^k =& Y_n^k + a^k\Delta t + \sum_{j=1}^{m} b^{k,j}\Delta W^j + \sum_{j=1}^{m} L^j b^{k,j}\left((\Delta W^j)^2 - \Delta t\right) \\ &+ \sum_{j_1=1}^{m}\sum_{j_2=1}^{j_1-1} L^{j_1} b^{k,j_2}\Delta W^{j_1}\Delta W^{j_2}. \end{aligned} \tag{9.4.5}$$

In the case of homodyne detection, commutative noise corresponds to commuting stochastic operators. A proof of this is given in Appendix B.1. Note that the last term on the right-hand side is only non-zero if we have several stochastic operators. The first three terms are known from the Euler-Maruyama method. We only need to find an expression for the term $L^{j_1} b^{k,j_2} \equiv L^{j_1} b^k_{j_2}$.

We derive an expression for $L^{j_1}\vec{b}_{j_2}$ by using the differentiation rules in Eqs. (9.2.3), (9.2.7). We find

$$L^{j_1}\vec{b}_{j_2} = \left(\mathrm{pre}(c_{j_2}) + \mathrm{post}(c_{j_2}^\dagger) - \mathrm{Tr}[c_{j_2}\rho + \rho c_{j_2}^\dagger]\right)\vec{b}_{j_1} - \mathrm{Tr}[c_{j_2} b_{j_1} + b_{j_1} c_{j_2}^\dagger]\vec{\rho}. \tag{9.4.6}$$

In the following we will leave out pre(.) and post(.) as it should be clear from the context. We arrive at the Milstein scheme for homodyne detection with commuting stochastic operators

$$\begin{aligned} \vec{\rho}_{n+1} =& \vec{\rho}_n + \vec{a}\Delta t + \vec{b}\Delta W \\ &+ \frac{1}{2}\sum_{j=1}^{m}\left(\left(c_j + c_j^\dagger - \mathrm{Tr}[c_j\rho + \rho c_j^\dagger]\right)\vec{b}_j - \mathrm{Tr}[c_j b_j + b_j c_j^\dagger]\right)\vec{\rho}\left((\Delta W^j)^2 - \Delta t\right) \\ &+ \sum_{j_1=1}^{m}\sum_{j_2=1}^{j_1-1}\left(\left(c_{j_2} + c_{j_2}^\dagger - \mathrm{Tr}[c_{j_2}\rho + \rho c_{j_2}^\dagger]\right)\vec{b}_{j_1} - \mathrm{Tr}[c_{j_2} b_{j_1} + b_{j_1} c_{j_2}^\dagger]\right)\vec{\rho}\Delta W^{j_1}\Delta W^{j_2}. \end{aligned} \tag{9.4.7}$$

9.5 Strong order 1.5 Taylor method

We have presented the Euler-Maruyama and the Milstein method with order of strong convergence 0.5 and 1.0, respectively. These two methods are already implemented in QuTiP. We can achieve higher order of strong convergence by including more terms in the Taylor expansion of the stochastic differential equation. The strong order 1.5 Taylor scheme is given by [46]

$$\begin{aligned} Y_{n+1}^k =& Y_n^k + a^k\Delta + \frac{1}{2}L^0a^k\Delta^2 \\ &+ \sum_{j=1}^{m}\left(b^{k,j}\Delta W^j + L^0b^{k,j}I_{(0,j)} + L^ja^kI_{(j,0)}\right) \\ &+ \sum_{j_1,j_2=1}^{m} L^{j_1}b^{k,j_2}I_{(j_1,j_2)} + \sum_{j_1,j_2,j_3=1}^{m} L^{j_1}L^{j_2}b^{k,j_3}I_{(j_1,j_2,j_3)}. \end{aligned} \tag{9.5.1}$$

Similar as for the Milstein method we can use relations between multiple stochastic integrals to simplify the strong order 1.5 Taylor scheme. For commutative noise of the second kind the diffusive matrix b must satisfy the commutation relation in Eq. (9.4.3) as well as

$$L^{j_1}L^{j_2}b^{k,j_3} = L^{j_2}L^{j_1}b^{k,j_3}. \tag{9.5.2}$$

In the case of homodyne detection these conditions are satisfied if the stochastic operators commute. This is proven in Appendix B.2. We arrive at the scheme

$$\begin{aligned} Y_{n+1}^k =& Y_n^k + a^k\Delta t + \sum_{j=1}^{m} b^{k,j}\Delta W^j + \frac{1}{2}\sum_{j=1}^{m} L^jb^{k,j}\left((\Delta W^j)^2 - \Delta t\right) \\ &+ \sum_{j_1=1}^{m}\sum_{j_2=1}^{j_1-1} L^{j_1}b^{k,j_2}\Delta W^{j_1}\Delta W^{j_2} + \frac{1}{2}L^0a^k(\Delta t)^2 \\ &+ \sum_{j=1}^{m}\left(L^0b^{k,j}(\Delta W^j\Delta t - \Delta Z^j) + L^ja^k\Delta Z^j\right) \\ &+ \frac{1}{2}\sum_{j=1}^{m} L^jL^jb^{k,j}\Delta W^j \\ &+ \frac{1}{2}\sum_{\substack{j_1,j_2=1 \\ j_1\neq j_2}}^{m} L^{j_1}L^{j_2}b^{k,j_2}\Delta W^{j_1}\left((\Delta W^{j_2})^2 - \Delta t\right) \\ &+ \sum_{j_1=1}^{m}\sum_{j_2=1}^{j_1-1}\sum_{j_3=1}^{j_2-1} L^{j_1}L^{j_2}b^{k,j_3}\Delta W^{j_1}\Delta W^{j_2}\Delta W^{j_3}. \end{aligned} \tag{9.5.3}$$

Here we abbreviated the stochastic integral following the notation of Kloeden/Platen [46]

$$\Delta Z \equiv I_{(1,0)} = \int_{t_n}^{t_{n+1}} \mathrm{d}s \int_{t_n}^{s} \mathrm{d}W. \tag{9.5.4}$$

We could calculate ΔZ with the Itô sum rule, i.e. by dividing the time intervals $[t_n, t_{n+1}]$ into further subintervals and approximating the Itô integrals with their corresponding sums in Eq. (8.1.10). Instead we use that the random variable ΔZ satisfies $\langle\Delta Z\rangle = 0$, $\langle(\Delta Z)^2\rangle = \frac{1}{3}(\Delta t)^3$

and $\langle \Delta Z \Delta W \rangle = \frac{1}{2}(\Delta t)^2$. We can then determine ΔW and ΔZ with two independent, normally distributed variables U_1, U_2 satisfying

$$\Delta W = U_1 \sqrt{\Delta t}, \quad \Delta Z = \frac{1}{2}\Delta t^{3/2}\left(U_1 + \frac{1}{\sqrt{3}}U_2\right). \tag{9.5.5}$$

Note that the first five terms on the right-hand side of the Taylor 1.5 scheme in Eq. (9.5.3) are the same terms as for the Milstein method. The other terms can be derived with the differentiation rules in Eqs. (9.2.3), (9.2.7), see Appendix A.1. The last term in Eq. (9.5.3) is zero if we have one or two stochastic operators. We only implemented these cases as it is unusual to have more stochastic operators in physical experiments.

9.6 Strong order 2.0 Taylor method

We presented the Taylor 1.5 scheme with order of strong convergence 1.5. We can achieve even higher order of strong convergence if we include more terms in the Taylor expansion of the stochastic differential equation. Here we use the Taylor 2.0 scheme in Stratonovich form as presented by Kloeden/Platen [46] since it has a simpler form. We have to include triple stochastic integrals. These can only be approximated with normally distributed random numbers in the case of scalar noise, i.e. $\mathrm{d}\vec{W} \equiv \mathrm{d}W$ is a scalar. In the case of homodyne detection this corresponds to having only one stochastic operator. The strong order 2.0 Taylor scheme for scalar noise in Stratonovich form reads

$$\begin{aligned} Y_{n+1}^k =& Y_n^k + \underline{a}^k \Delta t + b^k \Delta W + \frac{1}{2!}\underline{L}^1 b^k (\Delta W)^2 + \underline{L}^1 \underline{a}^k \Delta Z \\ &+ \frac{1}{2}\underline{L}^0 \underline{a}^k (\Delta t)^2 + \underline{L}^0 b^k (\Delta W \Delta t - \Delta Z) \\ &+ \frac{1}{3!}\underline{L}^1 \underline{L}^1 b^k (\Delta W)^3 + \frac{1}{4!}\underline{L}^1 \underline{L}^1 \underline{L}^1 b^k (\Delta W)^4 \\ &+ \underline{L}^0 \underline{L}^1 b^k J_{(0,1,1)} + \underline{L}^1 \underline{L}^0 b^k J_{(1,0,1)} + \underline{L}^1 \underline{L}^1 \underline{a}^k J_{(1,1,0)}. \end{aligned} \tag{9.6.1}$$

The analytical expressions for these terms in the case of homodyne detection can be found in Appendix A.2.

The multiple Stratonovich integrals in Eq. (9.6.1) have to be approximated numerically. We could divide the time interval $[t_n, t_{n+1}]$ into subintervals and approximate the Stratonovich integrals with their respective sums in Eq. (8.1.13). It is easier to use Itô integrals as we only have to evaluate functions at one time step instead of two for each summand. The triple Stratonovich integrals are related to the Itô integrals by

$$\begin{aligned} J_{(0,1,1)} &= I_{(0,1,1)} + \frac{1}{4}(\Delta t)^2, \\ J_{(1,1,0)} &= I_{(1,1,0)} + \frac{1}{4}(\Delta t)^2, \\ J_{(1,0,1)} &= I_{(1,0,1)}. \end{aligned} \tag{9.6.2}$$

Unfortunately the approximation by sums is numerically inefficient. It is usually better to use the Taylor 1.5 scheme or to approximate the stochastic integrals in other ways. Here we use the method presented by Kloeden/Platen [46]. The multiple stochastic integrals are approximated

for a positive integer p with

$$\begin{aligned}
\Delta W &= J^p_{(1)} = \sqrt{\Delta t}\zeta_1, \\
\Delta Z &= J^p_{(1,0)} = \frac{1}{2}\Delta t\left(\sqrt{\Delta t}\zeta_1 + a_{1,0}\right), \\
J_{(1,0,1)} &= \frac{1}{3!}\Delta t^2\zeta_1^2 - \frac{1}{4}\Delta t a_{1,0}^2 + \frac{1}{\pi}\Delta t^{3/2}\zeta_1 b_1 - \Delta t^2 B^p_{1,1}, \\
J^p_{(0,1,1)} &= \frac{1}{3!}\Delta t^2\zeta_1^2 - \frac{1}{2\pi}\Delta t^{3/2}\zeta_1 b_1 + \Delta t^2 B^p_{1,1} - \frac{1}{4}\Delta t^{3/2} a_{1,0}\zeta_1 + \Delta t^2 C^p_{1,1}, \\
J^p_{(1,1,0)} &= \frac{1}{3!}\Delta t^2\zeta_1^2 + \frac{1}{4}\Delta t a_{1,0}^2 - \frac{1}{2\pi}\Delta t^{3/2}\zeta_1 b_1 + \frac{1}{4}\Delta t^{3/2} a_{1,0}\zeta_1 - \Delta t^2 C^p_{1,1},
\end{aligned} \tag{9.6.3}$$

with the variables defined as

$$\begin{aligned}
a_{1,0} &= -\frac{1}{\pi}\sqrt{2\Delta t}\sum_{r=1}^{p}\frac{1}{r}\xi_{1,r} - 2\sqrt{\Delta t\rho_p}\mu_{1,p}, \quad \rho_p = \frac{1}{12} - \frac{1}{2\pi^2}\sum_{r=1}^{p}\frac{1}{r^2}, \\
b_1 &= \sqrt{\frac{\Delta t}{2}}\sum_{r=1}^{p}\frac{1}{r^2}\eta_{1,r} + \sqrt{\Delta t\alpha_p}\phi_{1,p}, \quad \alpha_p = \frac{\pi^2}{180} - \frac{1}{2\pi^2}\sum_{r=1}^{p}\frac{1}{r^4}, \\
B^p_{1,1} &= \frac{1}{4\pi^2}\sum_{r=1}^{p}\frac{1}{r^2}(\xi_{1,r}^2 + \eta_{1,r}^2), \\
C^p_{1,1} &= -\frac{1}{2\pi^2}\sum_{\substack{r,l=1 \\ r\neq l}}^{p}\frac{r}{r^2-l^2}\left(\frac{1}{l}\xi_{1,r}\xi_{1,l} - \frac{l}{r}\eta_{1,r}\eta_{1,l}\right).
\end{aligned} \tag{9.6.4}$$

The variables ζ_1, $\xi_{1,r}$, $\eta_{1,r}$, $\mu_{1,p}$, $\phi_{1,p}$ are independent and normally distributed. We have to choose p appropriately. If for all time intervals $[t_n, t_{n+1}]$ the multiple approximated Stratonovich integrals J^p_α satisfy

$$\mathrm{E}\left[|J_\alpha - J^p_\alpha|^2\right] \leq C\Delta t^5, \tag{9.6.5}$$

where C is a constant, then the scheme in Eq. (9.6.1) converges with strong order 2.0 if we choose

$$p \geq \frac{1}{2\pi^2 C}\Delta t^{-3}. \tag{9.6.6}$$

9.7 Drift-implicit and predictor-corrector methods

We have introduced four explicit numerical methods to solve stochastic differential equations. These schemes calculate Y_{n+1} as a function of Y_n. Alternatively one can use implicit methods. Their advantage lies in better numerical stability. They solve implicit equations to calculate the numerical solution. A simple example would be the backward Euler method for ordinary differential equations. Assume we have an ordinary differential equation $\partial_t x = f(x)$. If we discretize the time this can be interpreted with forward differentiation as $\frac{x_{n+1}-x_n}{\Delta t} = f(x_n)$. This leads to the (forward) Euler scheme. With backward differentiation we interpret it as $\frac{x_{n+1}-x_n}{\Delta t} = f(x_{n+1})$. This leads to the (implicit) backward Euler scheme $x_{n+1} = x_n + f(x_{n+1})\Delta t$ where have to solve for x_{n+1}. More generally the derivative could be interpreted as a mixture of forward and backwards differentiation which would lead to the scheme $x_{n+1} = x_n + (\theta f(x_n) + (1-\theta)f(x_{n+1}))$, where $\theta \in [0,1]$.

In the case of stochastic differential equations this implicitness can similarly be introduced in the drift term which leads to the drift-implicit methods. The diffusive term is still described explicitly. In particular we find a drift-implicit Milstein method for scalar noise (i.e. one stochastic operator in the case of homodyne detection)

$$Y_{n+1}^k = Y_n^k + \left(\theta a^k(t_{n+1}, Y_{n+1}) + (1-\theta)a^k(t_n, Y_n)\right)\Delta t + \; b^k \Delta W + \frac{1}{2}L^1 b^k \left((\Delta W)^2 - \Delta t\right). \tag{9.7.1}$$

Similarly the drift-implicit Taylor 1.5 scheme for scalar noise reads

$$\begin{aligned} Y_{n+1}^k =& Y_n^k + \left(\theta a^k(t_{n+1}, Y_{n+1}) + (1-\theta)a^k(t_n, Y_n)\right)\Delta t + \; b^k \Delta W + \frac{1}{2}L^1 b^k \left((\Delta W)^2 - \Delta t\right) \\ &+ \left(\frac{1}{2} - \theta\right)\left(\eta L^0 a^k(t_{n+1}, Y_{n+1}) + (1-\eta)L^0 a^k(t_n, Y_n)\right)\Delta t^2 \\ &+ L^1 a^k \left(\Delta Z - \theta \Delta W \Delta t\right) + L^0 b^k \left(\Delta W \Delta - \Delta Z\right) \\ &+ L^1 L^1 b^k \left(\frac{1}{3}(\Delta W)^2 - \Delta t\right)\Delta W. \end{aligned} \tag{9.7.2}$$

Here θ and η are real numbers between zero and one. In the case of homodyne detection the drift term is linear in $\vec{\rho}$ and the implicit equation can be efficiently solved with a linear solver. These two schemes have strong order 1.0 and 1.5, respectively, just as in the case of their explicit counterpart.

Implicitness in the diffusion term is not as easy to achieve. One method is the balanced implicit method which has strong convergence 0.5. We will not consider this scheme here but it can be found in [47].

Other possible methods are the predictor-corrector schemes. They use a predictor to estimate the solution $\bar{Y}_{n+1}$ for one time step. This is done with an explicit method, e.g. the Euler scheme. The corrector then uses this value to calculate the solution Y_{n+1}. This introduces quasi-implicitness in the drift and diffusion term which can lead to better numerical stability compared to other schemes. The predictor-corrector Euler method for scalar noise is given by [47]

$$Y_{n+1}^k = Y_n^k + \left(\theta \bar{a}_\eta^k(t_{n+1}, \bar{Y}_{n+1}) + (1-\theta)\bar{a}_\eta^k\right)\Delta t + \left(\eta b^k(t_{n+1}, \bar{Y}_{n+1}) + (1-\eta)b^k\right)\Delta W, \tag{9.7.3}$$

where we defined a drift term $\bar{a}_\eta^k = a^k - \eta L^1 b^k$. The predictor is found with the Euler method, i.e. $\bar{Y}_{n+1}^k = Y_n^k + a^k \Delta t + b^k \Delta W$. The real numbers η and θ are between zero and one.

10 Benchmarks

We introduced different numerical schemes to solve the stochastic master equation generated by homodyne detection. The Euler-Maruyama and Milstein methods are already implemented in QuTiP. In this section we compare the strong order Taylor 1.5 and 2.0 scheme with these methods for different problems. Further we compare with the predictor-corrector Euler scheme as well as the drift-implicit Milstein and Taylor 1.5 methods which were implemented by Denis Vasilyev. We use $\theta = \eta = 0.5$ for the implicit and predictor-corrector schemes. The linear system is solved using the biconjugate gradient stabilized method (BiCGSTAB) as implemented in Python.

Depending on the specific physical system different schemes are more suitable to solve the stochastic master equation. We demonstrate this by comparing the methods on different test problems. First we consider oscillator squeezing. This system has an exact analytical solution which allows us to check the validity of the methods. Then we compare the stability of the schemes. We consider an optomechanical setup where the deterministic part of the stochastic master equation dominates and phonon jumps where the stochastic term dominates. The test problems for the oscillator squeezing and phonon jumps were written by Denis Vasilyev.

10.1 Oscillator squeezing

We consider an oscillator coupled to a one-dimensional light field. Homodyne detection leads to the effective stochastic master equation [48]

$$\mathrm{d}\rho = \gamma\mathcal{D}[a]\rho\mathrm{d}t + g\mathcal{D}[s]\rho\mathrm{d}t + \sqrt{g}\mathcal{H}[s]\rho\mathrm{d}W. \tag{10.1.1}$$

Here $\mathcal{D}[.]$ denotes the Lindblad superoperator and $\mathcal{H}[.]$ was defined in Eq. (8.2.10). The interaction strength g has dimension Hz. The jump operator s is given by $s = \frac{\alpha+\beta}{2}a + \frac{\alpha-\beta}{2}a^\dagger$, where α and β parametrize the interaction between light and oscillator with $\alpha^2 + \beta^2 = 1$. An ordinary differential equation for the variance V of $x = \frac{a+a^\dagger}{\sqrt{2}}$ can be derived from this. It reads

$$\partial_t V = -(\gamma - \alpha\beta)V - 2\alpha^2V^2 + 0.5\gamma. \tag{10.1.2}$$

Note that this equation is exact. We numerically solve the stochastic master equation with different schemes and test their absolute error compared to the solution of this equation. We used the parameters $g/\gamma = 1$, $\alpha = \cos(0.1)$, $\beta = \sin(0.1)$. The simulation was done with 20 Fock states starting in the vacuum state at $t = 0$.

Fig. 10.1.1 shows the error of all the presented schemes (excluding Taylor 2.0) for different time steps in a log-log plot. We simulated the noise terms by dividing each time step into subintervals and approximating the stochastic integrals with sums. With this method we can use the same Wiener paths for different time steps. We used 100 different trajectories with each a unique Wiener path and tested the methods for each path. The absolute error compared to the analytical solution was then averaged over the trajectories. We do not show an error bar in the plot as it is negligibly small. Note that in Section 9.1 we defined the absolute error at each time step. Here we calculated the absolute error compared to the analytical solution as an average over time. The black solid lines with slopes 0.5, 1.0 and 1.5 (from top to bottom) illustrate the convergence of the methods. Note that the absolute error of the implicit Taylor 1.5 scheme convergences against $\sim 10^{-7}$ since we chose this value as the tolerance for the numerical linear solver.

In Fig. 10.1.2 we plot the time averaged absolute error for all methods (including Taylor 2.0) as a function of the step size. This time we generated the noise with Gaussian random variables for all schemes except Taylor 2.0. For the latter we used the approximation by Kloeden/Platen (see Eq. (9.6.3)) with p-values of 10 and 50. We see the same convergence as for the first plot.

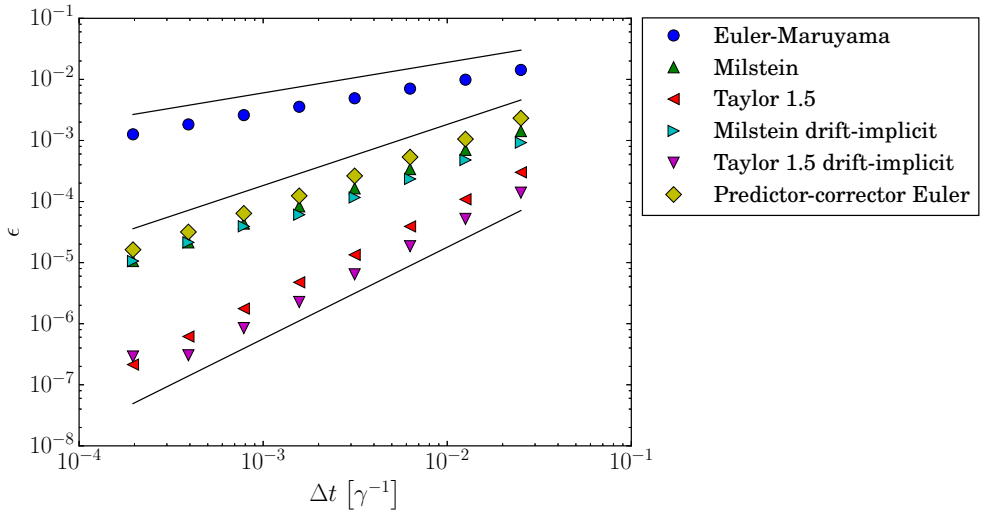

Figure 10.1.1: Oscillator squeezing. We plot the average absolute error ϵ of the variance V for each numerical method as a function of the step size Δt. We used 100 trajectories and 20 Fock states with the vacuum as initial state. The parameters are $g/\gamma = 1$, $\alpha = \cos(0.1)$, $\beta = \sin(0.1)$. The stochastic integrals were calculated with the Itô sum rule. The black solid lines have slopes 0.5, 1.0 and 1.5 (from top to bottom) to illustrate the convergence of the methods.

The Taylor 2.0 method with $p = 10$ is barely visible in the plot as its mark is covered by the method with $p = 50$ and the implicit Taylor 1.5 scheme. Note that the Taylor 2.0 scheme seems to only have convergence 1.5 here.

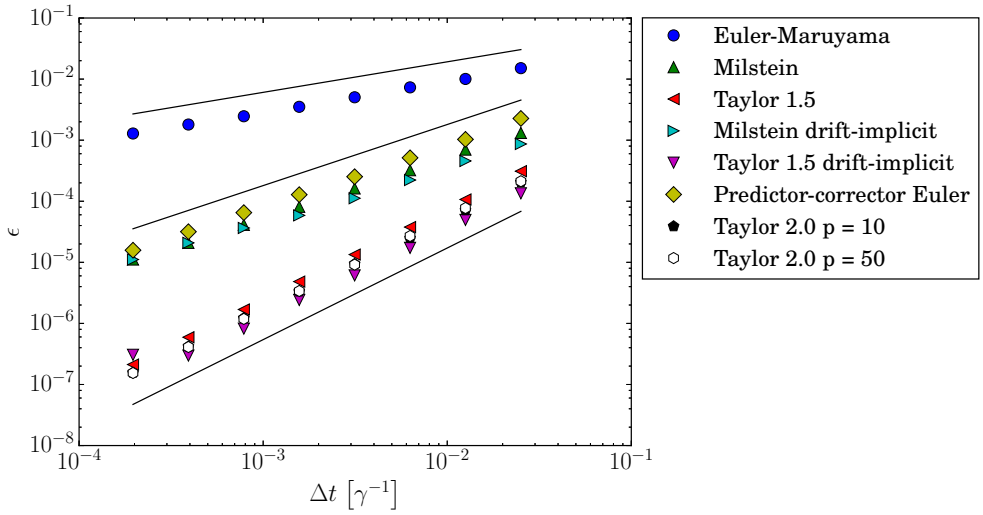

Figure 10.1.2: Oscillator squeezing. Average absolute error ϵ of the variance V for each numerical method as a function of the step size Δt. The stochastic integrals were calculated with normally distributed random numbers. The black solid lines have slopes 0.5, 1.0 and 1.5 (from top to bottom) to illustrate the convergence of the methods.

In Fig. 10.1.3 we plot the average computation time of each method compared to the Milstein scheme as a function of the step size. For small time steps the largest contribution to the

computation time is given by the framework of QuTiP. For small time steps we see that the implicit methods take much longer than their explicit counterparts. We did not optimize the implementation of the Taylor 1.5 and Taylor 2.0 method. A speed-up factor of $1.5 - 2$ might be realistically achievable.

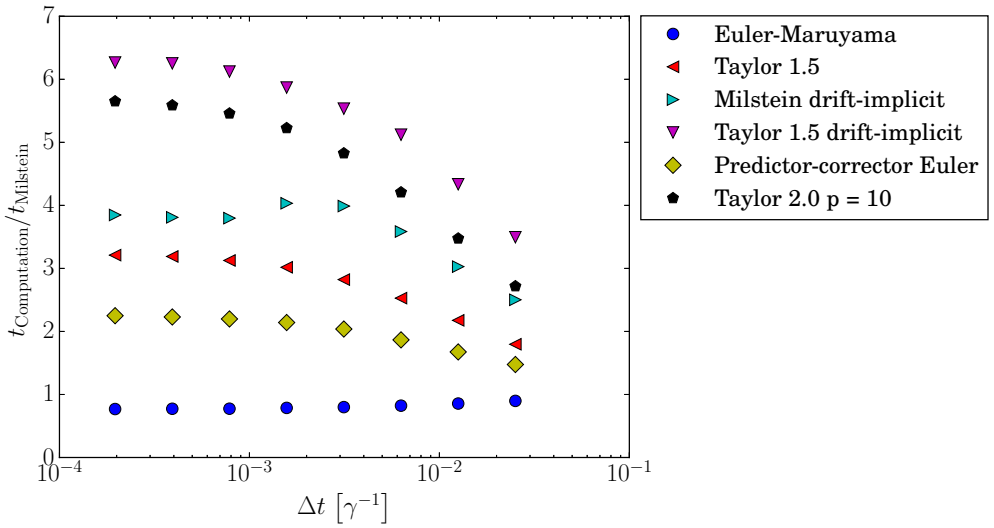

Figure 10.1.3: Oscillator squeezing. Computation time compared to the Milstein method as a function of the step size Δt. The computation time of the Milstein method t_{Milstein} is used as a reference.

10.2 Optomechanics

The next test problem we look at is the homodyne measurement of a standard optomechanical system (without Kerr-nonlinearity) as we introduced it in the first part of this thesis

$$\mathrm{d}\rho = -i[H,\rho]\mathrm{d}t + \Gamma_m(\bar{n}+1)\mathcal{D}[b]\rho\mathrm{d}t + \Gamma_m\bar{n}\mathcal{D}[b^\dagger]\rho\mathrm{d}t + \kappa\mathcal{D}[a]\rho\mathrm{d}t + \sqrt{\kappa}\mathcal{H}[a]\rho\mathrm{d}W, \tag{10.2.1}$$

with the Hamiltonian

$$H = \omega_m b^\dagger b + -\Delta a^\dagger a - g_0 a^\dagger a(b+b^\dagger) + E(a+a^\dagger). \tag{10.2.2}$$

This system is dominated by the deterministic part of the stochastic master equation. We test for which (approximate) time step the numerical methods diverge. The step size is doubled after each iteration. The parameters were chosen as $\Delta/\omega_m = 1$, $g_0/\omega_m = 0.8$, $E/\omega_m = 0.1$, $\kappa/\omega_m = 0.3$, $\Gamma_m/\omega_m = 0.002$, $\bar{n} = 0$. For the simulation we used 18 mechanical and 4 cavity states. The initial state of the system is its steady-state. Again we used 100 trajectories to show that the behaviour is not due to a specific Wiener path. We simulated the stochastic integrals with Gaussian random variables as we saw in the first test problem that this does not change the outcome. The Stratonovich integrals for the Taylor 2.0 method are approximated with the method of Kloeden/Platen using $p = 10$ and $p = 50$.

The explicit Euler-Maruyama and Milstein methods are the least numerically stable and diverge already for the step size $\Delta t/\omega_m \approx 0.012$. This was expected as both schemes include the deterministic drift term up to first order in $\mathrm{d}t$. The Taylor 1.5 and predictor-corrector method diverge both for the step size $\Delta t/\omega_m \approx 0.051$, which is four times as large as the time step of the Euler-Maruyama and Milstein method. The implicit methods are extremely stable. In fact

they do not diverge for any step size. As a demonstration we plot the expectation value $\langle b^\dagger b\rangle$ as a function of time for one trajectory in Fig. 10.2.1. We used the step size $\Delta t/\omega_m = 0.025$ such that both the Euler-Maruyama and Milstein method show divergence. Note that the Taylor 2.0 scheme does not have the same trajectory as we used a different method to calculate its multiple stochastic integrals which leads to a different Wiener path.

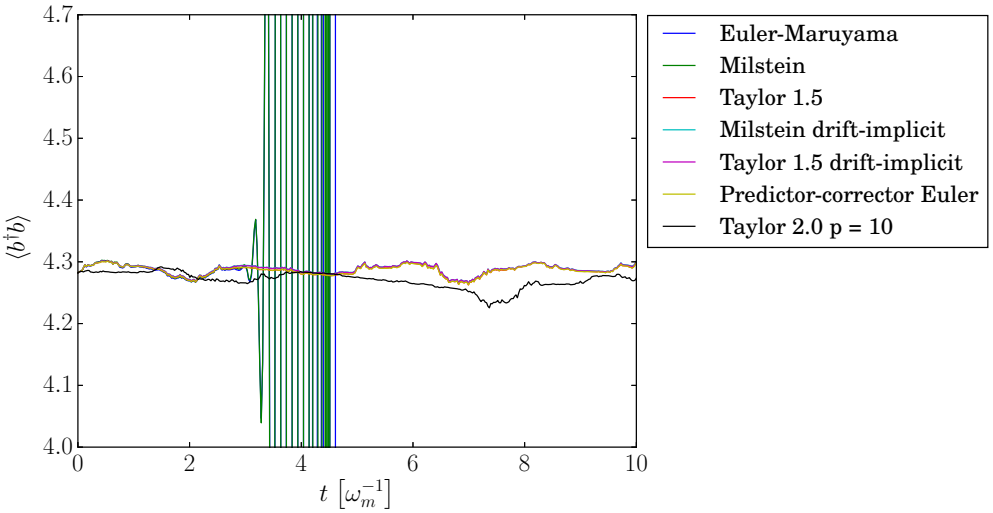

Figure 10.2.1: Optomechanics. We plot the expectation value $\langle b^\dagger b\rangle$ as a function of the time t/ω_m for one trajectory with 18 mechanical and 4 cavity states. The parameters are $\Delta/\omega_m = 1$, $g_0/\omega_m = 0.8$, $E/\omega_m = 0.1$, $\kappa/\omega_m = 0.3$, $\Gamma_m/\omega_m = 0.002$, $\bar{n} = 0$ with the step size $\Delta t/\omega_m = 0.025$.

10.3 Phonon jumps

The last test problem is phonon jumps. We use an effective stochastic master equation [49]

$$\mathrm{d}\rho = \Gamma_m(\bar{n}+1)\mathcal{D}[b]\rho\mathrm{d}t + \Gamma_m\bar{n}\mathcal{D}[b^\dagger]\rho\mathrm{d}t + \gamma\mathcal{D}[b^\dagger b]\rho\mathrm{d}t + \sqrt{\gamma}\mathcal{H}[b^\dagger b]\rho\mathrm{d}W, \tag{10.3.1}$$

where γ is much larger than Γ_m. This problem is then dominated by the stochastic part. We test for which time steps the different methods start to converge. The parameters used are $\gamma/\Gamma_m = 200$ and $\bar{n} = 1.5$ with 10 Fock states. The initial state of the system is a thermal state with $\bar{n}$ phonons. The stochastic integrals are approximated with Gaussian random variables. The Taylor 2.0 method uses the approximation by Kloeden/Platen with $p = 10$.

The implicit methods cannot be used here as their computation is extremely inefficient for this problem. Their computation time is too long for any practical purpose. The Euler-Maruyama method is again the least stable diverging at $\Delta t/\Gamma_m \approx 5.0 \cdot 10^{-5}$. The Milstein scheme diverges at $\Delta t/\Gamma_m \approx 7.5 \cdot 10^{-5}$. The (explicit) Taylor 1.5 and 2.0 method as well as the predictor corrector scheme seem to be the most suitable, diverging for time steps larger than $\Delta t/\Gamma_m \approx 1.0 \cdot 10^{-4}$. We demonstrate the behaviour of this system in Fig. 10.3.1. We plot the average value of $\langle b^\dagger b\rangle$ of one trajectory for step size $\Delta t/\Gamma_m = 2.5 \cdot 10^{-5}$. While the Euler method does not diverge for this step size it is less exact than the Milstein, Taylor 1.5 and predictor-corrector method. Once again the Taylor 2.0 scheme does not show the same trajectory as the other methods since we used a different method to calculate its multiple stochastic integrals.

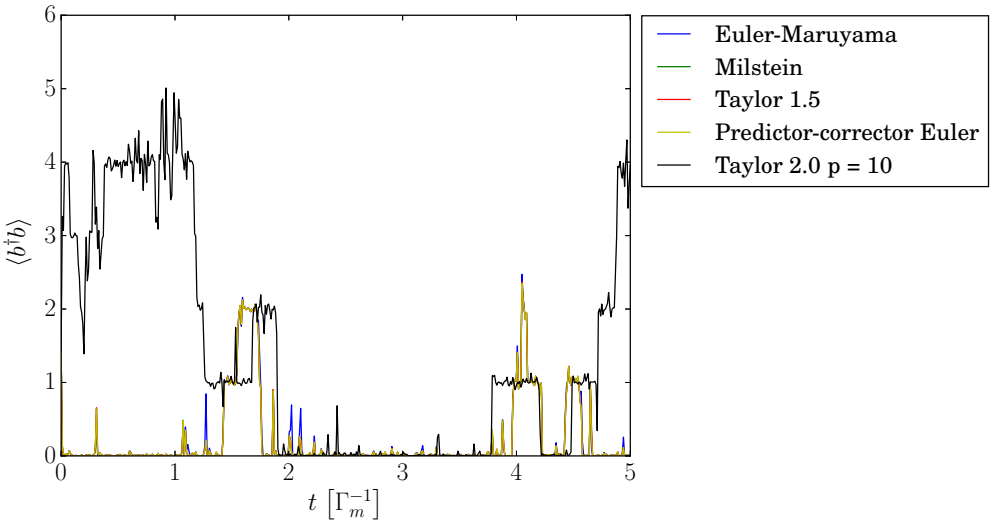

Figure 10.3.1: Phonon jumps. We plot the expectation value $\langle b^\dagger b \rangle$ as a function of the time t/Γ_m for one trajectory with 10 Fock states. The parameters are $\gamma/\Gamma_m = 200$ and $\bar{n} = 1.5$ with the step size $\Delta t/\Gamma_m = 2.5 \cdot 10^{-5}$. The Milstein and Taylor 1.5 method overlap with the the Predictor-corrector scheme and can therefore not be seen.

11 Conclusion

In the second part of this thesis we presented different numerical schemes to solve the stochastic master equation generated by homodyne detection. In particular we introduced the explicit Euler-Maruyama, Milstein, Taylor 1.5 and Taylor 2.0 methods, the first two of which are already implemented in QuTiP. As in most cases the implicit methods are numerically more stable, we presented the implicit Euler-Maruyama and Milstein as well as the predictor-corrector Euler method.

We tested these numerical schemes for three test problems. First we considered a system where an analytical solution for its variance exists. We showed the convergence of each method for this problem. The Taylor 1.5 and Taylor 2.0 scheme converge the fastest to the analytical solution and have the smallest absolute error for each time step.

For this problem we also compared the computation time of each method. We found that the implicit methods are slower than their explicit counterparts as they need to additionally solve a system of linear equations. The Taylor 1.5 and Taylor 2.0 scheme are slower by a factor of three and six compared to the Milstein scheme, respectively. It should be noted that we did not yet optimize our implementation for computation time but rather focused on readability.

To demonstrate the stability of each method we looked at a typical optomechanical setup where the deterministic part of the master equation dominates. The Taylor 1.5, Taylor 2.0 and predictor-corrector method were more stable than the already implemented (explicit) Euler-Maruyama and Milstein schemes. The implicit methods did not diverge for any time step, i.e. they are the most stable for this kind of problem.

As a last test we compared the numerical methods in the case of phonon jumps. In this system the stochastic part dominates the master equation. The implicit schemes cannot be used here as their computation time is too long for any practical purpose. The Taylor 1.5, Taylor 2.0 and predictor-corrector Euler method showed better stability than the Milstein scheme.

Depending on the problem a different numerical scheme should be used. As a general rule the implicit methods are the most suited for systems where the deterministic part might induce numerical instability. If the stochastic term of the master equation is large, either the Taylor 1.5 or predictor-corrector Euler scheme should be used. We recommend the Taylor 1.5 method as it has a smaller absolute error while its computation time is not much larger. The Taylor 2.0 method still needs testing, since one must find an appropriate parameter p such that the multiple Stratonovich integrals are approximated well enough.

Acknowledgements

I would like to thank Prof. Dr. Christoph Bruder for his time and support during my studies. A special thanks goes to Dr. Niels Lörch for the interesting discussions and for helping me whenever I had problems. I would also like to thank Dr. Denis Vasilyev for his help with the numerical implementations.

Appendices

A Terms for the numerical methods

A.1 Strong order Taylor 1.5 method

The additional terms for the strong order Taylor 1.5 method can be derived with the differentiation rules in Eqs. (9.2.3), (9.2.7). We find

$$\begin{aligned}
L^0\vec{a} =& \mathcal{L}\vec{a},\\
L^j\vec{a} =& \mathcal{L}\vec{b}_j,\\
L^0\vec{b}_j =& \left((c_j + c_j^\dagger - \mathrm{Tr}[c_j\rho + \rho c_j^\dagger]\right)\vec{a} - \mathrm{Tr}[c_j a + a c_j^\dagger]\vec{\rho} - \mathrm{Tr}[c_j b_j + b_j c_j^\dagger]\vec{b}_j,\\
L^{j_1}L^{j_2}\vec{b}_{j_3} =& \left(c_{j_3} + c_{j_3}^\dagger - \mathrm{Tr}[c_{j_3}\rho + \rho c_{j_3}^\dagger]\right) L^{j_1}\vec{b}_{j_2} - \mathrm{Tr}[c_{j_3} b_{j_1} + b_{j_1} c_{j_3}^\dagger]\vec{b}_{j_2} - \mathrm{Tr}[c_{j_3} b_{j_2} + b_{j_2} c_{j_3}^\dagger]\vec{b}_{j_1}\\
&- \mathrm{Tr}[c_{j_3}(L^{j_1} b_{j_2}) + (L^{j_1} b_{j_2}) c_{j_3}^\dagger]\vec{\rho},
\end{aligned} \tag{A.1}$$

where the vector $L^{j_2}\vec{b_{j_3}}$ is given in Eq. (9.4.6) and $(L^{j_2} b_{j_3})$ is the corresponding matrix. Note that we assumed the Hamiltonian of the system to be time-independent.

A.2 Strong order Taylor 2.0 method

The additional terms in the strong order Taylor 2.0 method are calculated as

$$\begin{aligned}
\underline{\vec{a}} =& \vec{a} - \frac{1}{2}L^1\vec{b},\\
\underline{L}^1\vec{b} =& L^1\vec{b},\\
\underline{L}^1\underline{\vec{a}} =& \mathcal{L}\vec{b} - \frac{1}{2}L^1L^1\vec{b},\\
\underline{L}^0\vec{b} =& (c + c^\dagger - \mathrm{Tr}[c\rho + \rho c^\dagger])\underline{\vec{a}} - \mathrm{Tr}[c\underline{a} + \underline{a}c^\dagger]\vec{\rho},\\
\underline{L}^0\underline{\vec{a}} =& \mathcal{L}\underline{\vec{a}} - \frac{1}{2}\underline{L}^0\underline{L}^1\vec{b},\\
\underline{L}^0\underline{L}^1\vec{b} =& (c + c^\dagger - \mathrm{Tr}[c\rho + \rho c^\dagger])\underline{L}^0\vec{b} - \mathrm{Tr}[c\underline{a} + \underline{a}c^\dagger]\vec{b} - \mathrm{Tr}[cb + bc^\dagger]\underline{\vec{a}} - \mathrm{Tr}[c(\underline{L}^0 b) + (\underline{L}^0 b)c^\dagger]\vec{\rho},\\
\underline{L}^1\underline{L}^1\vec{b} =& (c + c^\dagger - \mathrm{Tr}[c\rho + \rho c^\dagger])L^1\vec{b} - \mathrm{Tr}[c(L^1 b) + (L^1 b)c^\dagger]\vec{\rho} - 2\mathrm{Tr}[cb + bc^\dagger]\vec{b},\\
\underline{L}^1\underline{L}^0\vec{b} =& (c + c^\dagger - \mathrm{Tr}[c\rho + \rho c^\dagger])L^1\underline{\vec{a}} - \mathrm{Tr}[cb + bc^\dagger]\underline{\vec{a}} - \mathrm{Tr}[c\underline{a} + \underline{a}c^\dagger]\vec{b} - \mathrm{Tr}[c(L^1\underline{a}) + (L^1\underline{a})c^\dagger]\vec{\rho},\\
\underline{L}^1\underline{L}^1\underline{\vec{a}} =& \mathcal{L}L^1\vec{b} - \frac{1}{2}L^1L^1L^1\vec{b},\\
\underline{L}^1\underline{L}^1\underline{L}^1\vec{b} =& L^1L^1L^1\vec{b}\\
=& (c + c^\dagger - \mathrm{Tr}[c\rho + \rho c^\dagger])L^1L^1\vec{b} - \mathrm{Tr}[cb + bc^\dagger]L^1\vec{b} - (\mathrm{Tr}[c(L^1 b) + (L^1 b)c^\dagger]\\
&+ 2\mathrm{Tr}[cb + bc^\dagger])\vec{b} - (\mathrm{Tr}[c(L^1L^1 b) + (L^1L^1 b)c^\dagger] + 2\mathrm{Tr}[c(L^1 b) + (L^1 b)c^\dagger])\vec{\rho}.
\end{aligned} \tag{A.2}$$

B Commutative noise

B.1 Commutative noise of the first kind

Commutative noise of the first kind satisfies

$$L^{j_1} b^{k,j_2} = L^{j_2} b^{k,j_1}. \tag{B.1}$$

These terms were evaluated in the case of homodyne detection as (see Eq. (9.4.6))

$$L^{j_1} \vec{b}_{j_2} = \left(c_{j_2} + c_{j_2}^\dagger - \mathrm{Tr}[c_{j_2}\rho + \rho c_{j_2}^\dagger] \right) \vec{b}_{j_1} - \mathrm{Tr}[c_{j_2} b_{j_1} + b_{j_1} c_{j_2}^\dagger]\vec{\rho}, \tag{B.2}$$

where we left out the specifications pre(.), post(.). Subtracting the term on the right-hand side of Eq. (B.1) we find

$$\begin{aligned} 0 =& \{(c_{j_2} + c_{j_2}^\dagger)(c_{j_1} + c_{j_1}^\dagger) - (c_{j_1} + c_{j_1}^\dagger)(c_{j_2} + c_{j_2}^\dagger) \\ & - \mathrm{Tr}[c_{j_2}(c_{j_1}\rho + \rho c_{j_1}^\dagger) + (c_{j_1}\rho + \rho c_{j_1}^\dagger)c_{j_2}^\dagger] + \mathrm{Tr}[c_{j_1}(c_{j_2}\rho + \rho c_{j_2}^\dagger) + (c_{j_2}\rho + \rho c_{j_2}^\dagger)c_{j_1}^\dagger]\}\vec{\rho}. \end{aligned} \tag{B.3}$$

This can be equivalently written in matrix form

$$\begin{aligned} 0 =& c_{j_2}(c_{j_1}\rho + \rho c_{j_1}^\dagger) + (c_{j_1}\rho + \rho c_{j_1}^\dagger)c_{j_2}^\dagger - c_{j_1}(c_{j_2}\rho + \rho c_{j_2}^\dagger) - (c_{j_2}\rho + \rho c_{j_2}^\dagger)c_{j_1}^\dagger \\ & - \mathrm{Tr}[c_{j_2}(c_{j_1}\rho + \rho c_{j_1}^\dagger) + (c_{j_1}\rho + \rho c_{j_1}^\dagger)c_{j_2}]\rho + \mathrm{Tr}[c_{j_1}(c_{j_2}\rho + \rho c_{j_2}^\dagger) + (c_{j_2}\rho + \rho c_{j_2}^\dagger)c_{j_1}^\dagger]\rho \\ =& [c_{j_2}, c_{j_1}]\rho + \rho[c_{j_1}^\dagger, c_{j_2}^\dagger] - \mathrm{Tr}\left[[c_{j_2}, c_{j_1}]\rho + \rho[c_{j_1}^\dagger, c_{j_2}^\dagger]\right] \\ =& [c_{j_2}, c_{j_1}]\rho - \mathrm{Tr}\left[[c_{j_2}, c_{j_1}]\rho\right] + \mathrm{h.c.}, \end{aligned} \tag{B.4}$$

where we used the additivity of the trace and the fact that the density matrix is hermitian. It is obvious that if the stochastic operators c_{j_1}, c_{j_2} commute, this condition is satisfied.

B.2 Commutative noise of the second kind

Commutative noise of the second kind satisfies Eq. (B.1) as well as

$$L^{j_1} L^{j_2} b^{k,j_3} = L^{j_2} L^{j_1} b^{k,j_3}. \tag{B.5}$$

We define where we defined for simplicity

$$u = [c_{j_2}, c_{j_1}]\rho - \mathrm{Tr}\left[[c_{j_2}, c_{j_1}]\rho\right] + \mathrm{h.c.}, \tag{B.6}$$

such that Eq. (B.1) is satisfied for $u = 0$. Similarly as in Appendix B.1 we find after some calculations

$$\begin{aligned} 0 =& -2\mathrm{Tr}[c_{j_3}\rho + \rho c_{j_3}^\dagger]u + \left(c_{j_3}u + u c_{j_3}^\dagger\right) \\ & - \Bigg(\mathrm{Tr}\left[c_{j_3}\left(c_{j_2}(c_{j_1}\rho + \rho c_{j_1}^\dagger) + (c_{j_1}\rho + \rho c_{j_1}^\dagger)c_{j_2}^\dagger\right) + \left(c_{j_2}(c_{j_1}\rho + \rho c_{j_1}^\dagger) + (c_{j_1}\rho + \rho c_{j_1}^\dagger)c_{j_2}^\dagger\right) c_{j_3}^\dagger\right] \\ & - \mathrm{Tr}\left[c_{j_3}\left(c_{j_1}(c_{j_2}\rho + \rho c_{j_2}^\dagger) + (c_{j_2}\rho + \rho c_{j_2}^\dagger)c_{j_1}^\dagger\right) + \left(c_{j_1}(c_{j_2}\rho + \rho c_{j_2}^\dagger) + (c_{j_2}\rho + \rho c_{j_2}^\dagger)c_{j_1}^\dagger\right) c_{j_3}^\dagger\right] \Bigg) \\ =& -2\mathrm{Tr}[c_{j_3}\rho + \rho c_{j_3}^\dagger]u + \left(c_{j_3}u + u c_{j_3}^\dagger\right) \\ & - \mathrm{Tr}\left[c_{j_3}\left([c_{j_2}, c_{j_1}] + [c_{j_1}^\dagger, c_{j_2}^\dagger]\right) + \left([c_{j_2}, c_{j_1}] + [c_{j_1}^\dagger, c_{j_2}^\dagger]\right) c_{j_3}^\dagger\right]. \end{aligned} \tag{B.7}$$

For commuting stochastic operators c_{j_1}, c_{j_2} we have $u = 0$ and therefore this condition is satisfied.

C Source code for the numerical methods

C.1 Strong order Taylor 1.5 method

```
def _generate_rho_A_ops_simple(sc, L, dt):
    """
␣␣␣␣pre-compute␣superoperator␣operator␣combinations␣that␣are␣commonly
    ␣needed
␣␣␣␣when␣evaluating␣the␣RHS␣stochastic␣master␣equations,␣works␣for␣
    Taylor␣1.5
␣␣␣␣and␣Taylor␣2.0
␣␣␣␣"""

    A_len = len(sc)
    temp = [spre(c).data + spost(c.dag()).data for c in sc]
    tempL = (L + np.sum([lindblad_dissipator(c, data_only=True) for c
        in sc], axis=0)) # Lagrangian

    out = []
    out += temp
    out += [tempL]


    return out




def _generate_noise_Taylor_15(sc_len, N_store, N_substeps, d2_len, dt
    ):
    """
␣␣␣␣generate␣noise␣terms␣for␣the␣strong␣Taylor␣1.5␣scheme
␣␣␣␣"""

    U1 = np.random.randn(sc_len, N_store, N_substeps, 1)
    U2 = np.random.randn(sc_len, N_store, N_substeps, 1)

    dW = U1 * np.sqrt(dt)
    dZ = 0.5 * dt**(3./2) * (U1 + 1./np.sqrt(3) * U2)

    if sc_len == 1:
        noise = np.vstack([ dW, 0.5 * (dW * dW - dt), dZ, dW * dt -
            dZ, 0.5 * (1./3. * dW**2 - dt) * dW ])

    elif sc_len == 2:
        noise = np.vstack([ dW, 0.5 * (dW**2 - dt), dZ, dW * dt - dZ,
            0.5 * (1./3. * dW**2 - dt) * dW]
                + [[dW[n] * dW[m] for (n, m) in np.ndindex(sc_len
                    , sc_len) if n < m]]  # Milstein
```

```
                    + [[0.5 * dW[n] * (dW[m]**2 - dt) for (n, m) in
                        np.ndindex(sc_len, sc_len) if n != m]])

    else:
        noise = [] # needs to be written


    return noise




def _rhs_rho_Taylor_15_one_simple(L, rho_t, t, A, dt, ddW, d1, d2,
                                  args):


    dW = ddW[:, 0]   # this is needed such that the function works
        with the QuTiP framework

    #reusable operators and traces
    a = A[-1] * rho_t
    e0 = cy_expect_rho_vec(A[0], rho_t, 1)
    b = A[0] * rho_t - e0 * rho_t
    TrAb = cy_expect_rho_vec(A[0], b, 1)
    Lb = A[0] * b - TrAb * rho_t - e0 * b
    TrALb = cy_expect_rho_vec(A[0], Lb, 1)
    TrAa = cy_expect_rho_vec(A[0], a, 1)

    drho_t = a * dt
    drho_t += b * dW[0]
    drho_t += Lb * dW[1] # Milstein term

    # new terms:
    drho_t += A[-1] * b * dW[2]
    drho_t += (A[0] * a - TrAa * rho_t - e0 * a - TrAb * b) * dW[3]
    drho_t += A[-1] * a * (0.5 * dt*dt)
    drho_t += (A[0] * Lb - TrALb * rho_t - (2 * TrAb) * b - e0 * Lb)
        * dW[4]


    return rho_t + drho_t
```

C.2 Strong order Taylor 2.0 method

```
def _generate_noise_Taylor_2_approx(sc_len, N_store, N_substeps,
    d2_len, dt):
    """
    generate noise terms for the strong Taylor 2.0 scheme with
    approximate integrals
    see Kloeden/Platen "Numerical Solution of Stochastic Differential
    Equations" p.357
    """

    p = 10  # p value cannot be given as an argument because of QuTiP
        's framework

    zeta = np.random.randn(sc_len, N_store, N_substeps, 1)
    xi = np.random.randn(p, sc_len, N_store, N_substeps, 1)
    eta = np.random.randn(p, sc_len, N_store, N_substeps, 1)
    mu = np.random.randn(sc_len, N_store, N_substeps, 1)
    phi = np.random.randn(sc_len, N_store, N_substeps, 1)

    rho = 1./12. - 1./(2.*pi*pi) * np.sum([1./(r*r) for r in range(1,
        p + 1)], axis=0)
    a = -1./pi * np.sqrt(2 * dt) * np.sum([1./r * xi[r-1] for r in
        range(1,p + 1)], axis=0) - 2 * np.sqrt(dt * rho) * mu

    alpha = pi*pi/180. - 1./(2*pi*pi) *np.sum([1./(r*r*r*r) for r in
        range(1,p + 1)], axis=0)
    b = np.sqrt(.5 * dt) * np.sum([1./(r*r) * eta[r-1] for r in range
        (1,p + 1)], axis=0) + np.sqrt(dt * alpha) * phi

    B = 1./(4*pi*pi) * np.sum([1./(r*r) * (xi[r-1]*xi[r-1] + eta[r
        -1]*eta[r-1]) for r in range(1,p + 1)], axis=0)
    C = -1./(2*pi*pi) * np.sum([(1.0*(r+1))/((r+1)*(r+1) - (l+1)*(l
        +1)) * (1./(l+1) * xi[r]*xi[l] - (1.0*(l+1))/(r+1)
                            * eta[r]*eta[l]) for (r,l) in np.ndindex(
                                p,p) if r != l], axis=0)

    dW = zeta * np.sqrt(dt)
    dZ = 0.5 * dt * (np.sqrt(dt) * zeta + a)

    J101 = 1./6. * dt*dt * zeta*zeta - 0.25 * dt *a*a + 1./pi * dt*np
        .sqrt(dt) * zeta * b - dt*dt * B
    J011 = (1./6. * dt*dt * zeta*zeta - 1./(2*pi) * np.sqrt(dt)*dt *
        zeta * b  + dt*dt * B
          - 0.25 * dt*np.sqrt(dt) * a * zeta + dt*dt * C)
    J110 = (1./6. * dt*dt * zeta*zeta + 0.25 * dt * a*a - 1./(2*pi) *
         dt*np.sqrt(dt) * zeta * b
          + 0.25 * dt*np.sqrt(dt) * a * zeta - dt*dt * C)


    if sc_len == 1:
```

```
        noise = np.vstack([ dW, 0.5 * dW*dW, dZ, dW * dt - dZ, 1./6.
            * dW*dW*dW,
                           1./(4.*3.*2.) * dW*dW*dW*dW,
                           J011, J101, J110 ])

    else:
        noise = []  # needs to be written


    return noise




def _rhs_rho_Taylor_2_simple(L, rho_t, t, A, dt, ddW, d1, d2,
                                                    args):
    """
    strong order 2.0 Tylor scheme for homodyne detection with 1
        stochastic operator
    """

    dW = ddW[:, 0]

    #reusable operators and traces
    e0 = cy_expect_rho_vec(A[0], rho_t, 1)
    b = A[0] * rho_t - e0 * rho_t
    TrAb = cy_expect_rho_vec(A[0], b, 1)
    L1b = A[0] * b - TrAb * rho_t - e0 * b
    a = A[-1] * rho_t - 0.5 * L1b                    # drift term in
        Stratonovich form
    TrAL1b = cy_expect_rho_vec(A[0], L1b, 1)
    L1L1b =  A[0] * L1b - e0 * L1b - TrAL1b * rho_t - (2 * TrAb) * b
    TrAL1L1b = cy_expect_rho_vec(A[0], L1L1b, 1)
    L1a = A[-1] * b - 0.5 * L1L1b
    TrAa = cy_expect_rho_vec(A[0], a, 1)
    L0b = A[0] * a - e0 * a - TrAa * rho_t
    TrAL0b = cy_expect_rho_vec(A[0], L0b, 1)
    L0L1b = A[0] * L0b - e0 * L0b - TrAL0b * rho_t - TrAa * b - TrAb
        * a
    L0a = A[-1] * a - 0.5 * L0L1b
    TrAL1a = cy_expect_rho_vec(A[0], L1a, 1)
    L1L0b = A[0] * L1a - e0 * L1a - TrAb * a - TrAa * b - TrAL1a *
        rho_t
    L1L1L1b = A[0] * L1L1b - e0 * L1L1b - TrAb * L1b - (TrAL1b + 2 *
        TrAb) * b - (TrAL1L1b + 2 * TrAL1b) * rho_t
    L1L1a = A[-1] * L1b - 0.5 * L1L1L1b


    # Milstein terms:
    drho_t = a * dt
```

```
drho_t += b * dW[0]
drho_t += L1b * dW[1]

# Taylor 1.5:
drho_t += L1a * dW[2]
drho_t += L0b * dW[3]
drho_t += L0a * (0.5 * dt*dt)
drho_t += L1L1b * dW[4]

#Taylor 2.0:
drho_t += L1L1L1b * dW[5]
drho_t += L0L1b * dW[6]
drho_t += L1L0b * dW[7]
drho_t += L1L1a * dW[8]


return rho_t + drho_t
```

References

[1] P. Lebedew, "Untersuchungen über die Druckkräfte des Lichtes," *Ann. Phys.*, vol. 311, no. 11, pp. 433–458, 1901.

[2] B. P. Abbott *et al.*, "Observation of Gravitational Waves from a Binary Black Hole Merger," *Phys. Rev. Lett.*, vol. 116, no. 6, p. 61102, 2016.

[3] M. Aspelmeyer, T. J. Kippenberg, and F. Marquard, "Cavity optomechanics," *Rev. Mod. Phys.*, vol. 86, no. 4, pp. 1391–1452, 2014.

[4] T. J. Kippenberg and K. J. Vahala, "Cavity Optomechanics: Back-Action at the Mesoscale," *Science*, vol. 321, pp. 1172–1176, 2008.

[5] D. Kleckner and D. Bouwmeester, "Sub-kelvin optical cooling of a micromechanical resonator," *Nature*, vol. 444, no. 7115, pp. 75–78, 2006.

[6] J. D. Thompson, B. M. Zwickl, a. M. Jayich, F. Marquardt, S. M. Girvin, and J. G. E. Harris, "Strong dispersive coupling of a high-finesse cavity to a micromechanical membrane.," *Nature*, vol. 452, no. 7183, pp. 72–75, 2008.

[7] A. Schliesser, P. Del'Haye, N. Nooshi, K. J. Vahala, and T. J. Kippenberg, "Radiation pressure cooling of a micromechanical oscillator using dynamical backaction," *Phys. Rev. Lett.*, vol. 97, no. 24, pp. 1–4, 2006.

[8] T. Weiss, C. Bruder, and A. Nunnenkamp, "Strong-coupling effects in dissipatively coupled optomechanical systems," *New J. Phys.*, vol. 15, 2013.

[9] J. D. Teufel *et al.*, "Supplementary Sideband cooling of micromechanical motion to the quantum ground state.," *Nature*, vol. 475, no. 7356, pp. 359–363, 2011.

[10] J. Chan *et al.*, "Laser cooling of a nanomechanical oscillator into its quantum ground state," *Nature*, vol. 478, p. 18, 2011.

[11] D. J. Wilson *et al.*, "Measurement and control of a mechanical oscillator at its thermal decoherence rate," *Nature*, vol. 524, no. 7565, pp. 325–329, 2014.

[12] J. B. Khurgin, "Phonon lasers gain a sound foundation," *Physics*, vol. 3, p. 16, 2010.

[13] S. Mancini and P. Tombesi, "Quantum noise reduction by radiation pressure," *Phys. Rev. A*, vol. 49, no. 5, pp. 4055–4065, 1994.

[14] S. Bose, K. Jacobs, and P. L. Knight, "Preparation of nonclassical states in cavities with a moving mirror," *Phys. Rev. A*, vol. 56, no. 5, pp. 4175–4186, 1997.

[15] M. A. Nielsen and I. L. Chuang, *Quantum Computation and Quantum Information*. Cambridge University Press, 2010.

[16] A. Bassi, K. Lochan, S. Satin, T. P. Singh, and H. Ulbricht, "Models of wave-function collapse, underlying theories, and experimental tests," *Rev. Mod. Phys.*, vol. 85, no. 2, pp. 471–527, 2013.

[17] V. C. Vivoli, T. Barnea, C. Galland, and N. Sangouard, "Proposal for an Optomechanical Bell Test," *Phys. Rev. Lett.*, vol. 116, no. February, pp. 1–5, 2016.

[18] J.-M. Pirkkalainen, E. Damskägg, M. Brandt, F. Massel, and M. A. Sillanpää, "Squeezing of Quantum Noise of Motion in a Micromechanical Resonator," *Phys. Rev. Lett.*, vol. 115, no. 24, p. 243601, 2015.

[19] S. Rips, M. Kiffner, I. Wilson-Rae, and M. J. Hartmann, "Steady-state negative Wigner functions of nonlinear nanomechanical oscillators," *New J. Phys.*, vol. 14, no. 2, p. 023042, 2012.

[20] D. A. Rodrigues, J. Imbers, and A. D. Armour, "Quantum dynamics of a resonator driven by a superconducting single-electron transistor: A solid-state analogue of the micromaser," *Phys. Rev. Lett.*, vol. 98, no. 6, pp. 1–4, 2007.

[21] C. Gerry and P. L. Knight, *Introductory Quantum Optics*. Cambridge University Press, 2005.

[22] C. Gardiner and P. Zoller, *Quantum noise*. Springer Science & Business Media, 2004.

[23] H.-Y. Fan and C.-H. Lv, "s-Parameterized phase space distribution for describing no counts registered on a photonic detector," *Opt. Commun.*, vol. 282, no. 24, pp. 4741–4744, 2009.

[24] D. A. Rodrigues and A. D. Armour, "Amplitude Noise Suppression in Cavity-Driven Oscillations of a Mechanical Resonator," *Phys. Rev. Lett.*, vol. 104, p. 053601, 2010.

[25] A. D. Armour and D. A. Rodrigues, "Quantum dynamics of a mechanical resonator driven by a cavity," *Comptes Rendus Physique*, vol. 13, no. 5, pp. 440–453, 2012.

[26] H. P. Breuer and F. Petruccione, *The Theory of Open Quantum Systems*. Oxford University Press, 2002.

[27] N. Lörch, J. Qian, A. Clerk, F. Marquardt, and K. Hammerer, "Laser Theory for Optomechanics: Limit Cycles in the Quantum Regime," *Phys. Rev. X*, vol. 4, no. 1, p. 011015, 2014.

[28] H. Carmichael, *Statistical Methods in Quantum Optics 1: Master Equations and Fokker-Planck Equations*. Springer Science & Business Media, 1999.

[29] D. Walls and G. Milburn, *Quantum Optics*. Springer Science & Business Media, 1994.

[30] M. O. Scully and M. S. Zubairy, *Quantum Optics*. Cambridge University Press, 1997.

[31] A. Balanov, N. Janson, D. Postnov, and O. Sosnovtseva, *Synchronization: From Simple to Complex*. Springer Science & Business Media, 2010.

[32] J. R. Johansson, P. D. Nation, and F. Nori, "QuTiP 2: A Python framework for the dynamics of open quantum systems," *Comput. Phys. Commun.*, vol. 184, no. 4, pp. 1234–1240, 2013.

[33] A. Kraus and R. H. Blick, "Mechanical mixing in nonlinear nanomechanical resonators," *Appl. Phys. Lett.*, vol. 77, no. 19, pp. 3102–3104, 2000.

[34] A. Husain *et al.*, "Nanowire-based very-high-frequency electromechanical resonator," *Appl. Phys. Lett.*, vol. 83, no. 6, pp. 1240–1242, 2003.

[35] B. Witkamp, M. Poot, and H. S. J. Van Der Zant, "Bending-mode vibration of a suspended nanotube resonator," *Nano Lett.*, vol. 6, no. 12, pp. 2904–2908, 2006.

[36] H. Bruus and K. Flensberg, *Many-Body Quantum Theory in Condensed Matter Physics*. OUP Oxford, 2004.

[37] N. J. Kasdin, "Runge-Kutta Algorithm for the Numerical Integration of Stochastic Differential Equations," *J. Guid. Control Dyn.*, vol. 18, no. 1, pp. 114–120, 1995.

[38] G. Breitenbach, S. Schiller, and J. Mlynek, "Measurement of the quantum states of squeezed light," *Nature*, vol. 387, no. 6632, pp. 471–475, 1997.

[39] A. I. Lvovsky and M. G. Raymer, "Continuous-variable optical quantum-state tomography," *Rev. Mod. Phys.*, vol. 81, no. 1, pp. 299–332, 2009.

[40] M. Fuwa, S. Takeda, M. Zwierz, H. M. Wiseman, and A. Furusawa, "Experimental proof of nonlocal wavefunction collapse for a single particle using homodyne measurements," *Nature Communications*, vol. 6, p. 6665, 2015.

[41] T. Hirano, H. Yamanaka, M. Ashikaga, T. Konishi, and R. Namiki, "Quantum cryptography using pulsed homodyne detection," *Phys. Rev. A*, vol. 68, no. 4, p. 042331, 2003.

[42] R. Quadt, M. Collett, and D. F. Walls, "Measurement of Atomic Motion in a Standing Light Field by Homodyne Detection," *Phys. Rev. Lett.*, vol. 74, no. 3, pp. 351–354, 1995.

[43] C. W. Gardiner, *Handbook of Stochastic Methods for Physics, Chemistry, and the Natural Sciences*. Springer Science & Business Media, 2004.

[44] H. M. Wiseman and G. J. Milburn, *Quantum Measurement and Control*. Cambridge University Press, 2014.

[45] K. Jacobs, *Quantum Measurement Theory and its Applications*. Cambridge University Press, 2014.

[46] P. E. Kloeden and E. Platen, *Numerical Solution of Stochastic Differential Equations*. Springer Science & Business Media, 1992.

[47] E. Platen and N. Bruti-Liberati, *Numerical Solution of Stochastic Differential Equations with Jumps in Finance*. Springer Science & Business Media, 2010.

[48] D. V. Vasilyev, C. A. Muschik, and K. Hammerer, "Dissipative versus conditional generation of gaussian entanglement and spin squeezing," *Phys. Rev. A*, vol. 87, no. 5, pp. 1–10, 2013.

[49] A. A. Gangat, T. M. Stace, and G. J. Milburn, "Phonon number quantum jumps in an optomechanical system," *New J. Phys.*, vol. 13, pp. 1095–1096, 2011.